Ca' Foscari
University
of Venice

Master in Environmental Sciences

Final Thesis

Oceanic near-surface current variability induced by interior dynamics: experimental and numerical simulations

Supervisor
Angelo Rubino

Master candidate
Ricardo Viana Barreto
Matriculation Number: 864351

Academic Year
2017/2018

Abstract

Surface vorticity in the oceans is usually driven by wind dynamics. However, in semi-enclosed and stratified basins - like the Mediterranean - internal ocean processes may dominate the development of surface as well as interior vorticity. A possible scenario for this particular case is the Ionian Sea, the deepest sea of the Mediterranean Sea, in which the observed near-surface circulation periodic (decadal) reversals appear not to be entirely explained by wind vorticity, suggesting the predominance of interior dynamics over the wind forcing. The theory of the Adriatic-Ionian Bimodal Oscillating System (BiOS) proposes that the redistribution of water masses, related to variations in the thermohaline properties of the Southern Adriatic, is the main driver of those vorticity inversions. In order to investigate such phenomena, a set of experiments was performed at the Legi Coriolis Rotating Platform, a rotating tank with 13m diameter that allows reproducing ocean behavior under the influence of Earth rotation, within the European project CROPEX. Topography and water inlets representing the Ionian Sea were constructed in the tank and velocity fields were obtained and analyzed using, among other techniques, Particle Image Velocimetry (PIV). In this thesis, the experiments performed at the rotating tank are documented, analyzed and simulated using a multi-layer numerical model. Case studies comparing PIV measurements and model results were considered. In the physical as well as in the numerical simulations it was found that interior dynamics were able to trigger near-surface vorticity reversals.

Aknowledgements

In the preparation for this thesis, I was helped by people that I respect the most. Those people are worthy of my deepest gratitude. With the completion of this last goal, this cycle ends and I would like to take this opportunity to thank first and foremost Professor Angelo Rubino, my advisor in this course, for all the guidance, lectures, honest advices and for believing in my potential when provinding me the opportunity of this work, which I appreciated the most. I would also like to thank Professors Roberto Pasters and Fabio Pranovi for the passionate and valuable teaching and for the opportunities that went beyond the class room. I would also like to express my gratitude to Professor Davide Zanchettin, for his availabity and support during the development of this work.

In addition, I would like to express my most sicere gratitude to the team from OGS that welcomed me warmly during 6 weeks of experiment in Grenoble for the European Project CROPEX, in special Miroslav Gacic, Vanessa Cardin, Giuseppe Siena, Vedrana Kovacevic and Manuel Bensi for your trust and companionship. I also would like to expand my gratitude to Eletta Negretti, Joel Sommeria, Samuel Viboud and Thomas Valran from LEGI for the support, patience and availability in this critical phase of this work.

Finally, I would like to thank those who have been with me since long before the beggining of this course and have supported me in much more ways that I could express in this note. To my parents, brother and familly, thank you for all the love, care and advice. To Marilia, thank you for always being there for me. To Andrei Flores, Luiza Khorramchahi, Alexandre Costa, Andreia Caldas, Hugo Areas, Anesio de Leles, Renato Fontana, Alexandre Santos, Nicollas Milani and Thiago Nascimento, thank you for being part of this journey from the very beginning of it and also for all inspiration, good moments, beers and for a friendship that crossed the distance of an ocean.

Contents

List of Acronyms

AABW Antarctic Bottom Water

ADW Adriatic Deep Water

BiOS Adriatic-Ionian Bimodal Oscillating System

EMDW Eastern Mediterranean Deep Water

EMT Eastern Mediterranean Transient

LEGI Laboratoire des Écoulements Géophysiques et Industriels

LIW Levantine Intermediate Water

MAW Modified Atlantic Water

NADW North Atlantic Deep Water

NIG North Ionian Gyre

PIV Particle Image Velocimetry

1 Introduction

The objective of this thesis is to *investigate* the mechanism responsible for the periodic vorticity reversals observed in the North Ionian Gyre (NIG), as suggested by the theory of Adriatic-Ionian Bimodal Oscillating System (BiOS). In order to do so, two different simulations were performed: a) a physical simulation carried out in a rotating tank and b) a numerical simulation using a multi-layer model for ocean circulation. Results of both simulations were compared and discussed regarding the details of the theory of BiOS. The experimental simulation was performed at the Coriolis Platform, a rotating tank with 13 m diameter - the largest in the world - located at the Laboratoire des Écoulements Géophysiques et Industriels (LEGI), Grenoble, France. The computational model used for the numerical simulation is a multi-layer numerical model, adapted from a two-layer numerical model [15, 2].

On a first step, in order to introduce concepts approached in this thesis, this section briefly describes the oceanic thermohaline process, confronting it with wind-driven circulation and presenting its contributions to the understanding of ocean dynamics. Deep water formation and geostrophic currents are also detailed. Next, focus is placed on the Eastern Mediterranean Overturning Circulation and the recent events that allowed the scientific community to perceive its variations, including the periodic circulation reversals observed at the NIG surface. Moreover, it will approach the Theory of the BiOS, which intent to provide a concise explanation of the dynamics related to the circulation reversal of the NIG.

Finally, an introduction about the physical experiment, performed at the LEGI Coriolis platform is presented, followed by an introduction on the numerical model used.

In order to achieve the goals proposed by this thesis, the following activities were performed:

- A numerical model was converted from fixed format FORTRAN to free format FORTRAN in order to produce a more friendly environment for this and future researches, where compatibility with netCDF data format was implemented.
- Successive optimizations were implemented at the numerical model in order to allow a better use of the computational resources available.

- The numerical model was confronted against well know phenomena in order to verify its behavior.
- A set of 27 physical simulations were performed at LEGI laboratory, in Grenoble, France, during a period of six weeks. From the 27 experiments performed, 2 were used for the case studies produced in this thesis.
- A set of experiment reports was produced in order to document the simulations carried out in at LEGI. The reports are annexed to the end of this thesis.

1.1 Theoretical introduction

Most of the geographic sites referenced in this thesis belong to the Mediterranean region. In order to assist those who are not familiar with the features of the region, a map is provided on Figure 1 where seas, straits and relevant regions are labeled.

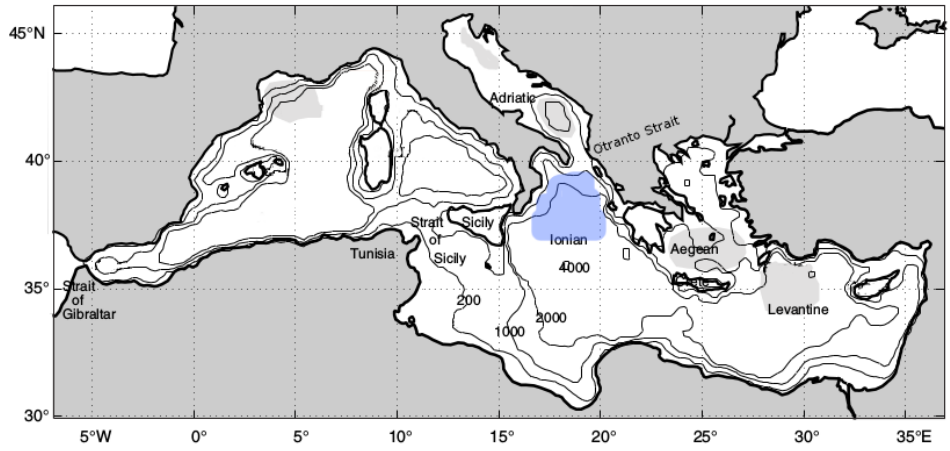

Figure 1: Map of the Mediterranean Sea indicating names of places mentioned in this thesis. The shaded gray areas in the Adriatic, Aegean and Levantine Seas correspond to known regions of water mass formation. The light blue area in the Ionian Sea correspond to the North Ionian Gyre (NIG). The 200, 1000, 2000 and 4000 m depth contours are also shown. - Credit for the image: [8] - Adapted

1.1.1 The Thermohaline Process

"*The thermohaline circulation is that part of the ocean circulation which is driven by fluxes of heat and freshwater across the sea surface and subsequent interior mixing of heat and salt.*" - Rahmstorf, 2015 [14]

During the late 19th century, scientist were discussing if the main driver of ocean currents was the wind, pushing water along the surface, or the convection of water masses, as a result of changes in their densities due to heating, cooling, evaporation and rainfall [14]. A few years later, in the beginning of the 20th century, a set of tank experiments was performed by Johan Sandström, in Sweden, in order to evaluate the contribution of each driver. In his experiments, Sandström used the terms wind-driven and thermal circulation. Later, in 1920, the term thermohaline was used by Albert

Defant in an oceanography textbook [14].

The historical developments described above can be used to point out a separation between two of the major circulation drivers: *wind-driven* and *thermohaline*. However, this separation may lead to erroneous interpretations of the dynamics governing water masses in the ocean. Although both drivers can be studied as independent forcing, it is not possible to experimentally measure their individual contribution over the transport of a water mass. In other words, variations in wind stress will also cause variations in the thermohaline circulation and variations in the forcing of the thermohaline circulation will also lead to changes in wind driven circulations [14]. Therefore, the global overturning circulation displayed in Figure 2, besides the thermohaline driver, is also influenced by wind stress and other drivers such as tidal and gravitational force. Moreover, the Coriolis effect should be taken into account once all ocean dynamics take place in a rotating frame [11].

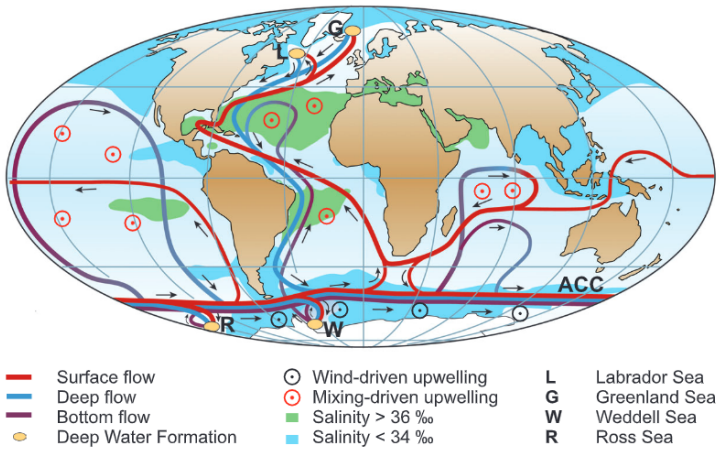

Figure 2: The global ocean overturning circulation is a representation of the large scale dynamics of the ocean, influenced by, among others, thermohaline and wind processes - Credit for the image: [14]

Thus, despite being originally called thermohaline *circulation*, nowadays the concept is preferably referred as thermohaline *process*[11, 14]. It shall be understood as a mechanism - a forcing - which transports water masses according to specific properties related to their temperature and salinity, contributing along with other mechanism to the actual resultant circula-

tion. The key concept to observe in thermohaline forcing is water density, which can be deduced as a function of temperature, salinity and pressure[19]. Once, in the ocean, pressure acts mostly as a direct function of depth, the relevant water properties regulating the thermohaline circulation are temperature and salinity. As density of water masses changes due to variation of these properties, denser waters will sink to its equilibrium depth, causing the rise of less dense water masses to shallower depths.

The strongest and most relevant forcing of ocean circulation - and of most climatic phenomena - is the solar radiation [11]. Solar radiation intensity will depend mainly on the latitude and on the cloudiness of the area, and will affect - among others - wind circulation, heat inflow and outflow to and from the ocean, evaporation and rainfall [11]. Thus, wind as well as thermohaline processes can have their energy tracked back to solar radiation [11].

The ocean is, hence, mostly forced from the surface with wind stress and thermohaline processes [11]. Periodicity of wind stress can be observed over different time scales, including the diurnal cycle, the seasons and longer time scales such as decadal and other multiannual cycles. When computing effects of wind stress on ocean circulation, wind stress data is usually composed of large scale records - both in time and space - as for instance, persistent winds and smoothed wind data [11]. Known currents dominated by wind stress include the Gulf Stream, the circumpolar current system in the Southern Ocean - one of the most relevant circulations for all oceans and for global weather - besides large scale anticyclonic gyres in subtropical basins and cyclonic gyres in sub-polar basins [11].

The thermohaline forcing is dominated by heat and freshwater fluxes at the interface with the air. Solar radiation provides heat inflow to the ocean, warming it and reducing its surface density. On the other hand, most of the heat leaving the ocean to the atmosphere is lost through evaporation - yielding an increase in salinity and density. The remaining heat in the ocean is transported through advection and diffusion. Solar radiation will also provide energy for precipitation and river run-off - resultant from evaporation in the ocean and precipitation on land - both contributing to decrease surface water salinity. In fact, freshwater flux is the key ingredient in controlling the salinity distribution in the oceans [11], as it is specially important for the thermohaline regulation due to its ability to change both salinity (evaporation and rainfall) and temperature (heat transported by wa-

ter vapor)[11]. However, despite the direct importance of solar radiation and freshwater flux for the local circulation, the most dominant forcing of the global thermohaline process is the thermal gradient between high and low latitudes, induced by differences in solar radiation according to latitude. In this manner, high-latitude cooling [14] produces high density water mostly by effect of low temperatures - Figure 3 - causing the newly formed water mass to sink, which displaces the old bottom water - when less dense - to shallower depths.

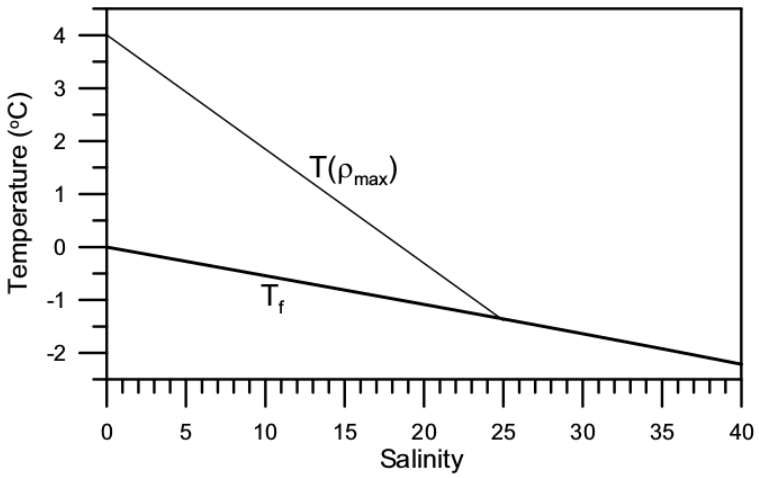

Figure 3: Freezing point of sea water (T_f) and maximum water density ($T_{\rho max}$) as a function of temperature (^oC) and salinity (psu) - Credit for the image: [19]

In this way, the study of the thermohaline process provides a better understandings of features such as deep water formation, spreading of deep waters partly through deep boundary currents, upwelling and near-surface currents, each of them contributing to a large-scale deep overturning motion of the oceans [14], already shown in Figure 2. Of all those features, two require a more detailed description due to their importance to global climate, ocean life and to the very subject of this thesis: the *deep water formation* and the *geostrophic currents*.

Deep water formation and its importance to climate and ocean life

Oceans, as well as other water bodies, are stratified. This means that ocean vertical density profiles can be conceived as a superimposition of different layers containing different water masses with a density gradient pointing to the bottom - i.e. each layer is denser than the layer above. Once formed, water masses may remain recognizable by their intrinsic characteristics for centuries - Figure 4. In this manner, a dense water layer lying on the bottom of the ocean is practically isolated from the surface, which largely prevents gas and nutrients exchanges between the oxygen-rich surface waters and the nutrient-rich bottom water. In fact, due to the restriction of oxygen production to the near-surface euphotic layer and oxygen consumption in most biological processes, low oxygen concentration is one of the signatures of an old age water mass - a parcel of water that has for long being secluded from the surface [11].

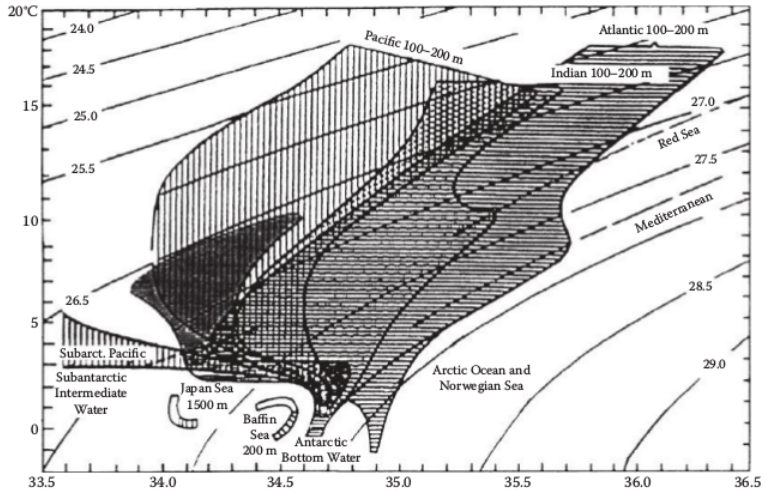

Figure 4: Ocean water masses signatures identified at a temperature salinity (T-S) diagram - Credit for the image: [19]

Apart from the prevailing stratified ocean, a *vertical channel* between the surface and the bottom can be found in regions were deep water formation occurs - and only when it occurs. Deep water formation is a phenomenon that takes place where the stratification is destroyed (preconditioning) and vertical convection dominates in the water column. Roughly, as surface water cools and evaporate, it gets denser and sinks to the bottom. Figure 5 shows two density profiles from the Labrador Sea, one of the rare spots where open-ocean deep water formation takes place. The profile on the

left, taken during autumn '96, shows a clear stratification of the sea, with all layers separated and horizontally displaced while, on the other hand, in the profile on the right, taken in winter 97, the water column is largely unstratified due to a density increase of surface water, which produces a convective transport resulting in intermediate water formation. Under more severe conditions, this convection could extend to the bottom of the sea, forming deep water.

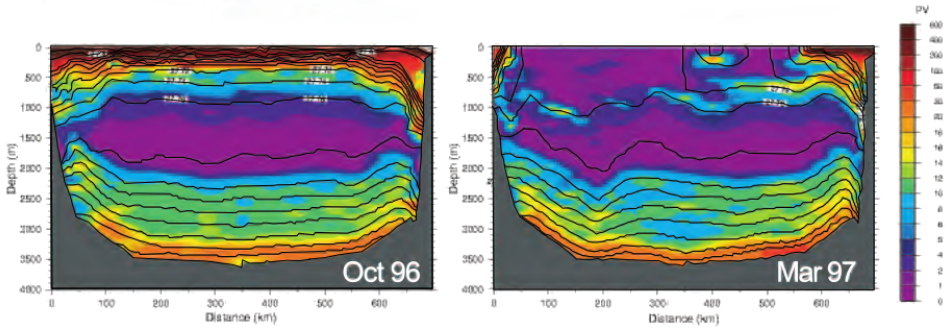

Figure 5: Ocean stratification at the Labrador Sea showing two different seasons: Autumn (left) and Winter (right). The black line are isopycnics, marking the path drawn by water masses with the same density. In Autumn, ocean stratification is clear as the layers are horizontally disposed. However, in Winter, the stratification is broken by the increase in surface water density and convection takes place. Credit for the image: [12]

High oxygen concentration found in deep water masses - about 200 $\mu mol/kg$ - indicates they were recently formed [11]. Not surprisingly, the very downward transport - which is a consequence of convective activity - is also responsible for displacing the old bottom water to different locations. This is the main process behind the before approached large-scale thermohaline process [14]. The displaced bottom water, due to its contact with the floor, contains nutrients which are carried along, eventually reaching the surface through upwelling in a process that may take centuries [11]. Figure 6 illustrates a simplified scheme of the process described above. It ranges from south Atlantic, on the left, to North Atlantic, on the right, representing the formation of two water masses: the Antarctic Bottom Water (AABW) and the North Atlantic Deep Water (NADW), as well as their changes in oxygen, carbon dioxide and nutrient supply.

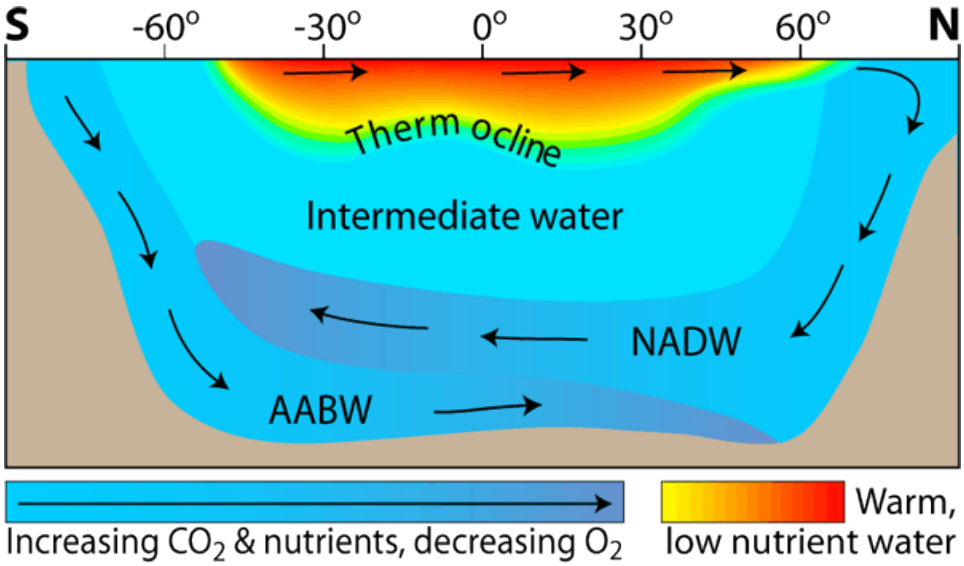

Figure 6: Atlantic deep water formation at the poles. Water cooled at the poles sinks taking oxygen to the bottom of the ocean. At the bottom, it increases its nutrient content, which is later (maybe centuries later) transported to the surface through a process called upwelling. Credit for the image: `http://www.seos-project.eu/modules/oceancurrents/oceancurrents-c03-p03.html`

The processes described above have a large impact on climate regulation. One of its most known effects is called the *carbon physical pump*. The surface water is the only interface between the atmosphere and the ocean, acting as a bottleneck for gas exchange. However, as water temperature decreases, gas solubility in water increases. In this way, gases such as oxygen, but also carbon dioxide, are transferred to the water, which later sinks due to convection, carrying along the gases within it. The ocean act, thus, as a sink for natural and anthropogenic carbon emissions - or more generally stating - as a buffer for climate changes [9]. Deep water formation takes place in very limited regions and only under specific conditions. Those are, hence, regions of critical importance for the ocean life and for global climate.

Geostrophic currents

Ocean surface is not regular, but composed of hills and valleys that may form and vanish as a result of different ocean processes. A common process known to participate in the formation of hills is the Coriolis effect. Coriolis deviates water currents to the right in the Northern Hemisphere, and to the

left in the Southern Hemisphere. Thus, an anti-cyclonic circulation develops in the ocean basis, with water always being deviated towards the center of the basin, causing the water to literally pile up [1]. This phenomena can be observed in all subtropical gyres of the ocean, but the hill of water is not visible while navigating the region: they are hardly higher than 2 meter over an area of thousands of square kilometers.

However, the small slope formed is enough to create a water flow downhill - due to gravity. The Coriolis effect acts again over this flow, deviating it and opposing to the force of gravity which pulls the water down. The balance between the two forces, ideally, describes a closed path anti-cyclonically oriented and centered at the center of the hill, as shown in Figure 7. However, due to energy losses, the actual path described is an spiral that gradually approaches the base of the hill [1]. Those currents that exist as the result of the balance between the gravity force and the Coriolis effect are known as Geostrophic currents.

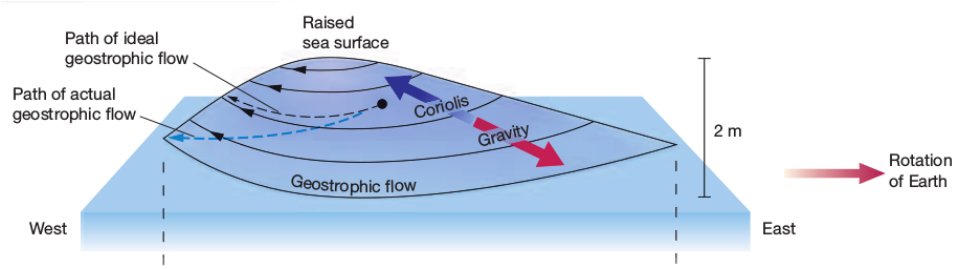

Figure 7: Geostrophic currents as a result of the balance between gravity force and Coriolis effect. Ideal currents describe a closed path around the center, but real currents - in light blue - fall towards the base as they lose energy due to friction. - Credit for the image: [1]

The same dynamic is observed when a *valley* if formed. Water flow to the center of the valley due to gravity, being opposed by the Coriolis effect and resulting in a geostrophic current. However, in this case, instead of inducing an anti-cyclone, the result is a cyclone. Thanks to this property, it is possible to observe local ocean vortices in satellite altimetry readings, also called sea surface height. Ocean areas where readings indicate a higher height will present an anti-cyclonic geostrophic circulation, while in ocean areas with a lower height, a cyclonic geostrophic circulation will be found.

Another byproduct of ocean surface topography are the local changes in

pycnoclines. As water pile up, mass is concentrated over that area, which causes a depression in the pycnocline right below the hill due to the increase in the local weight - Figure 8. In a *valley*, the opposite happens. As the surface layer becomes lighter, the dooming of the pycnoclines below is observed.

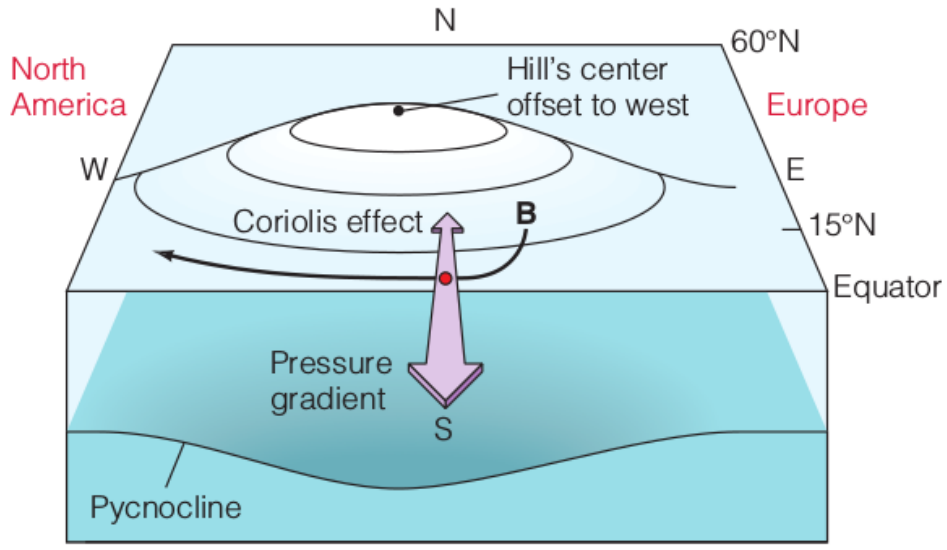

Figure 8: Local changes in pycnoclines due to a local change of surface layer mass, as water pile up in to form a hill - Credit for the image: [6]

The hills and valleys in the subtropical gyres are maintained by wind energy [6]. As wind blows, water moves in the surface and is deflected by the Coriolis effect, as already described. In the absence of wind, friction would slowly consume the energy maintaining such gyres, converting it into heat [6]. Although most of the gyres are sustained by wind energy, the theory of BiOS - as explained further - describes a situation which may lead to the formation of a gyre not by the wind, but by the change in pycnoclines and in the horizontal gradient of density.

1.2 The Eastern Mediterranean Overturning Circulation

The Mediterranean Sea is a semi-closed basin which, as well as the global ocean, has its own overturning circulation. In fact, the Mediterranean Sea

is frequently described as a reduced scale laboratory for studying the phenomena characterizing of the open ocean on a smaller temporal and spatial scale. Features of the open ocean, such as gyres, deep water formation and an overturning circulation can be found along the Mediterranean Sea. Despite the similarities, the Mediterranean is saltier and has its nutrients input limited by inputs from the North Atlantic and rivers [13].

Most of the inlet water in the Mediterranean Sea is provided by the Atlantic Ocean. When Atlantic surface water crosses the Strait of Gibraltar, it gradually mixes with existent Mediterranean water, becoming saltier as it moves towards the Eastern Mediterranean. This slightly saltier surface water is called the Modified Atlantic Water (MAW) - Figure 9. The MAW is known to cross the Western Mediterranean, passing trough the Strait of Sicily, to reach the Levantine basin. As it covers its journey, its density increases as a result of evaporation and mixing with the saltier Mediterranean water. [17].

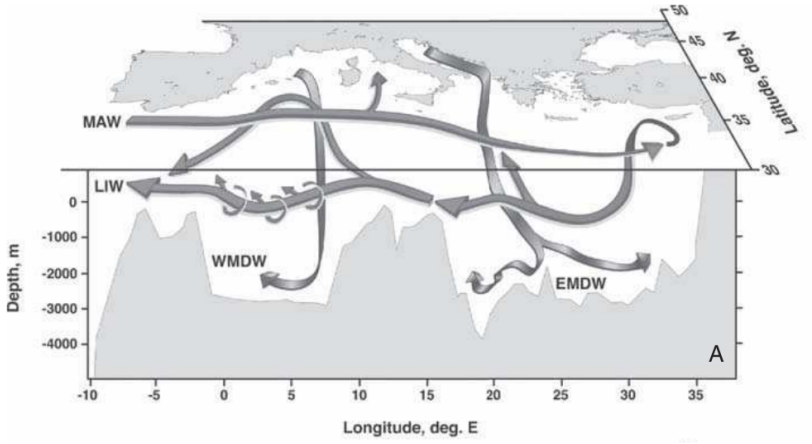

Figure 9: Mediterranean overturning circulation. MAW crosses the Mediterranean Sea eastwards from the Strait of Gibraltar, increasing its density along the way to finally sink at the Levantine Sea to become LIW. LIW crosses back the Mediterranean Sea westwards, also deviating to the north after entering the Ionian Sea. Credit for image: [17] - Adapted

Along this path, salinity may not be the only factor to contribute to an increase in MAW density. As water temperature drops in winter season, the portion of MAW which arrived at the Levantine becomes dense enough to sink and form Levantine Intermediate Water (LIW). The LIW is one of the most important water masses of the Mediterranean and usually occupies

depths between 200 and 500 meters [17]. In its most common path, it moves westward from the Levantine to fill the intermediate depths of the Ionian Sea further moving into the Western Mediterranean. However, while still in the Ionian Sea, a fraction of the LIW separates from the current, moving northward along the west coast of Greece to later enter the Adriatic Sea.

The dynamic described above - and illustrated at Figure 9 - covers the basic relationship between surface and intermediate water masses in the Eastern Mediterranean. Nevertheless, one of the most notable features of the Eastern Mediterranean was yet not introduced: the Eastern Mediterranean also has different regions where deep water formation occurs. As already stated in the previous section, deep water formation is one of the most prominent phenomena powering the thermohaline process. In the same fashion as it happens in the global ocean, the Eastern Mediterranean Deep Water (EMDW) is formed as a consequence of an increase in water density due to both cooling and evaporation of surface water. These phenomena takes place in the Adriatic Sea. Persistent cold and dry northeastern winds cool the coastal shallow water of the northern Adriatic, which sinks to the bottom of the Adriatic basin, being pushed southward by the bottom topography, further mixing with another deep water mass formed in the Southern Adriatic. However, instead of forming in the shelf - as described for the northern Adriatic - deep water in the Southern Adriatic is formed in the open sea in a process called open-ocean convection - the same which is observed at the deep water formation regions in the ocean (e.g., Greenland, Labrador and Ross Sea). In this process, a persistent cyclonic circulation causes the pycnoclines to dome - see 1.1.1: Geostrophic Currents - weakening of the vertical density stratification. This is a precondition for convection, which will require - as already mentioned - an intense cooling and evaporation in order to occur and form deep water.

The deep water mass resultant from both processes is known as Adriatic Deep Water (ADW). It accumulates in the southern Adriatic, eventually leaking through the Strait of Otranto and moving down the oceanic shelf to reach the bottom of the Ionian Sea to later become EMDW.

Historically, the Adriatic Sea was considered to be the only relevant area of deep water formation in the Eastern Mediterranean [17] however, a comparison between the observations made by the F/S Meteor cruise in 1987 and in 1995, at south of Crete, surprised the scientific community by revealing a dramatic change of Eastern Mediterranean vertical structure [17]. A

new deep water mass, saltier and richer in oxygen than the ADW, was filling the bottom of the Ionian Sea, pushing the old EMDW upwards. This water mass was verified to originate not in the Adriatic, but in Aegean Sea, from where it moved south, reaching the bottom of the Levantine through the straits of the Cretan Arc, afterwards spreading into the Ionian basin. Along with this change in deep water formation, other changes in the overturning circulation were also observed: the MAW no longer drew a straight path to the Levantine as part of its water was now deviated to the north right after passing the Sicily Strait - Figure 10.

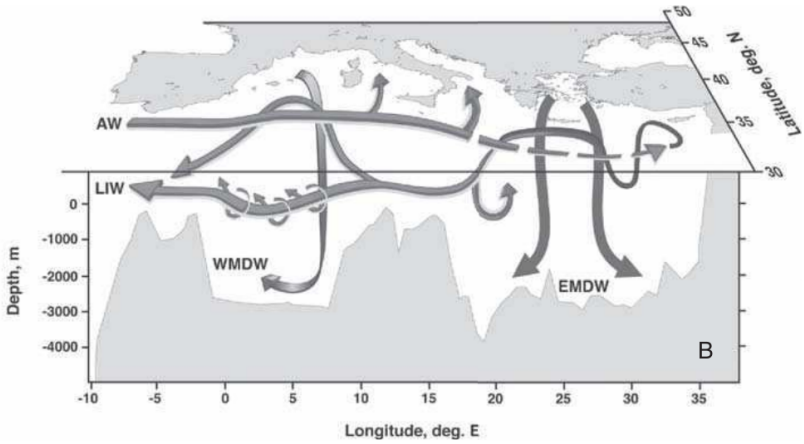

Figure 10: Overturning circulation in the Mediterranean Sea as observed during the EMT. Part of the MAW now deviates to the north after passing the Sicily Strait, later entering the Adriatic. Deep water was observed to form in the Aegean Sea, overcoming the deep water contribution coming from the Adriatic Sea in both volume and density. Credit for the image: [17]

This was a remarkable event for the scientific community for producing such a significant change in the overturning circulation over a short period [17], becoming known as the Eastern Mediterranean Transient (EMT). The EMT took place in the early 1990's and extended up to 1997, when a relaxation of is characteristics was observed, also leading the overturning circulation to return to its previous configuration [3]. During the EMT, the change in the MAW path was observed to be part of a complete reversal in the circulation of the North Ionian Gyre (NIG) - from cyclonic to anticyclonic - consequently leading to a change in the characteristics of the Adriatic, Ionian and Levantine water masses.

Such changes in vorticity may affect production in the Eastern Mediterranean. When the NIG presents a cyclonic circulation, a decrease in nutrient content of water entering the Adriatic is observed due to a deepening of the *nitracline* along the borders of the gyre [4]. Moreover, the usually oligotrophic central region of the Ionian experiences annual blooms only under cyclonic vorticity of the NIG [4]. Biodiversity was also observed to change according to the vorticity of the NIG. During the more productive cyclonic vorticity, the food web diversifies and exhibits the classic levels (phytoplankton, copepods and predators), while in the anti-cyclonic circulation, the food chain is not productive enough to sustain all the trophic levels [4].

While hypothesis for the causes and effects of the EMT were still being discussed, a group of scientists found evidences of another phenomena driving changes into the eastern Mediterranean overturning circulation. Using satellite altimetry measurements - Figure 12 - they observed a periodic change in the circulation of the Ionian basin, more specifically at the NIG. Circulation reversals in the NIG were observed every 5 years - composing a decadal period - producing changes in the direction of the MAW and of the LIW which - similarly to the EMT - resulted in changes in the composition of the Eastern Mediterranean Seas. Among the theories formulated to explain this behavior are wind driven changes in surface circulation, balancing between water volumes of the Eastern Mediterranean Seas and a feedback mechanism between the Adriatic and Ionian Sea - also known as Adriatic-Ionian Bimodal Oscillating System (BiOS) - which is the topic of the next section in this thesis.

1.2.1 The Theory of the Adriatic-Ionian Bimodal Oscillating System (BiOS)

The change in NIG vorticity observed in 1997 - back to cyclonic - due to the weakening of the EMT had a peculiarity that has been noticed only a few years after the event: contrary to most variations in the surface circulation, this one could not be explained by considering wind stress [3]. In fact, wind stress data shows a negative average wind vorticity in the region from 1995 to 1999, favoring the persistence of the anti-cyclonic circulation instead of a reversal - Figure 11. This suggests the predominance of the thermohaline process over wind stress, with baroclinic vorticity production determining the NIG circulation inversion [3].

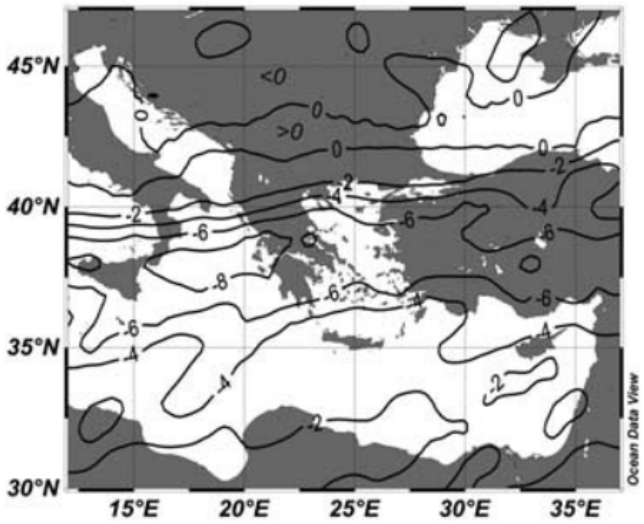

Figure 11: Average wind vorticity over the Eastern Mediterranean from 1995 to 1999. The negative vorticity over the NIG would induce an anti-cyclonic circulation in the gyre. However, an inversion to cyclonic circulation was observed instead. Credit for the image: [3]

This concept of baroclinic vorticity production as driver of the NIG inversion in 1997 was then extended to also explain the periodic reversals of the gyre observed in the altimetry data - Figure 12. However, this generalization also included an additional hypothesis: such inversions would be possible even in the absence of the Aegean Deep water influence, suggesting that the EMT was not the main actor in the change of the Eastern Mediterranean overturning circulation. This hypothesis is corroborated by decadal variations in salinity and density of the Southern Adriatic, coherent with anomalies in the altimetry data [7]. The set of physical features that describe this hypothesis form the so called theory of Adriatic-Ionian Bimodal Oscillating System (BiOS).

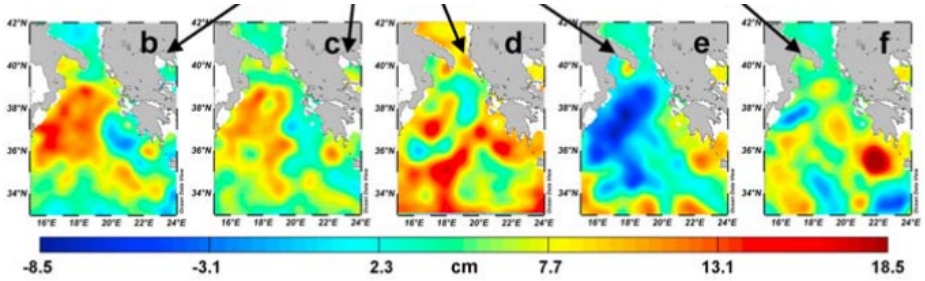

Figure 12: Sea level anomalies for b) 1994, c) 1995, d) 1997, e) 1998 and f) 2006. Positive anomalies in 1994 indicate an anti-cyclonic circulation, as a consequence of the EMT. The weakening of the circulation is observed at the reduction in positive anomaly up to a strong negative anomaly observed at 1997, characterizing a reversal to a cyclonic circulation. Credit for the image: [7]

The theory of BiOS focuses on the existence of a feedback mechanism between the density of the outflowing ADW and the inversions of Ionian circulation themselves. The main concept is that while NIG vorticity determines which water mass enters the Adriatic Sea, increasing or decreasing Adriatic's density, ADW density entering the north Ionian would determine the NIG vorticity, describing a feedback mechanism [7].

As ADW flows through the Strait of Sicily to the Ionian Sea, it follows a path along the topography, resembling a waterfall. As Coriolis effect deviates the path to the right, the downward flow describes a circular path in the bottom shelf, contouring the NIG region, which lies right above. In the case where the NIG circulation is cyclonic, saltier water from the Levantine Sea and from the Aegean Sea are driven inside the Adriatic - Figure 13 b). This slowly increases Adriatic's density, subsequently increasing ADW density, causing the flow to reach the bottom of the Ionian Sea. The circular path of dense water described by this flow has two main effects: a) it produces a density gradient in the bottom, pointing from the center of the basing to the coast and b) it locally affects the pycnoclines above the flow, dooming them and causing the formation of a local depression in the surface right above the dense flow path [7].

In the bottom of the Ionian Sea, the density gradient pointing to the coast induces a flow to the center of the basin, which in turn induces a cyclonic geostrophic current in the bottom layer. However, the depression in sea surface right above induces an anti-cyclonic geostrophic current in the surface layer. As ADW gets denser, the two phenomena intensifies and a

cyclonic circulation establishes in the bottom, while a anti-cyclonic circulation takes place in the surface, overcoming the previous cyclonic circulation - an inversion of the surface circulation of the NIG [7].

The now anti-cyclonic circulation of the NIG deviates the relatively fresh MAW into the Adriatic Sea, gradually reducing its density and thus, the density of the later formed ADW - Figure 13 a). This causes the ADW flow to no longer sink to the bottom, but to occupy an intermediate layer in the Ionian basin [7]. In its path, it will locally bend the pycnoclines down. As seen in Figure 8, this depression in pycnoclines associates with a local rise in sea surface level. As a consequence, the boarders of the NIG rises, inducing a cyclonic circulation and eventually tipping the balance and reverting the circulation to start the cycle all over again.

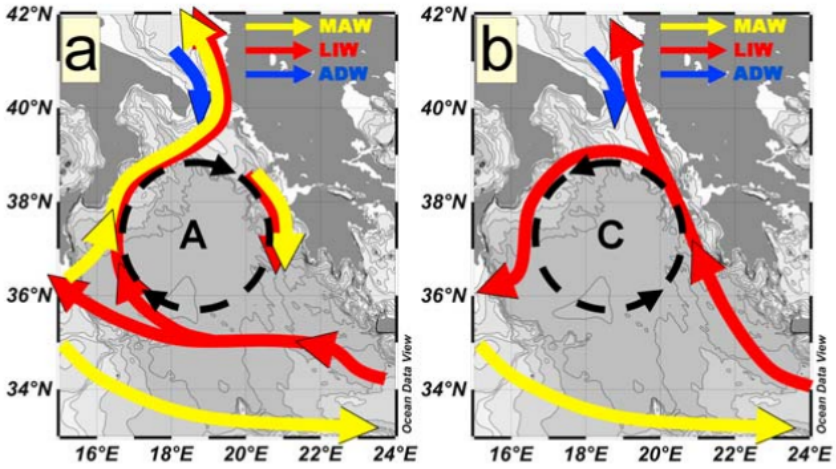

Figure 13: The two phases of the NIG periodic reversals and the feedback mechanism described by the theory of the BiOS. Credit for the image: [7]

1.3 Physical simulation

The physical simulation executed on this thesis was performed at the LEGI Coriolis platform, located in Grenoble, France. The platform is the largest rotating platform dedicated to fluid dynamics in the world[1] - with a 13 m diameter - and it is used to study fluid behavior in a rotational framework - including Earth rotation. Due to its large dimensions, the platform is ideal

[1] http://www.legi.grenoble-inp.fr/web/spip.php?rubrique10&lang=en

for simulating large scale dynamics with reduced interference of viscosity.

Figure 14: Photography of the LEGI Coriolis platform while prepared for another different experiment. Configuration for the experiment performed in this thesis is detailed below in 2 - Methodology.

The platform is equipped with ultrasonic velocity meters, profilers for salinity and temperature, and cameras and lasers for PIV analysis. For the scope of this thesis, only the velocity field obtained with PIV was considered. 27 experiments were executed using the setup further described in 2 - Methodology, and the experiment notes for each experiment can be found annexed in the end of this thesis. For the scope of this thesis, two experiments were chosen - experiments 24 and 25 - to be more detailed in case studies due to its relevance for the theory of BiOS and the EMT.

1.3.1 Particle Image Velocimetry (PIV)

Particle Image Velocimetry (PIV) is a technique used to analyze velocities inside transparent fluids using reflective tracers, lasers and photo cameras. The basic concept behind the technique is to illuminate tracer particles - usually added to the fluid - and then capture images of the fluid, each of them separated by a short time interval, allowing to analyze the movement

of particles - as illustrated in Figure 15 and 16.

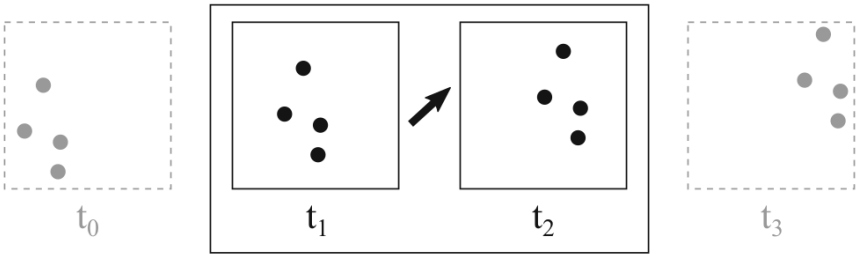

Figure 15: Displacement of a group of particles from $t = t_0$ to $t = t_3$, where two images were acquired in $t = t_1$ and $t = t_2$. The motion of tracer particles captured in the two images allows an estimate of a local velocity vector [5].

PIV can be described as the union of several other techniques [5]:

- **Seeding** In most applications tracer particles have to be added to the flow. Particles should have density similar to the fluid's in order to prevent sinking. The addition of surfactants to avoid agglutination of particles may also be necessary.
- **Illumination** These tracer particles have to be illuminated in a plane or volume of the flow at least twice within a short and known time interval. An usual choice is a laser sheet crossing a section of a fluid so that all particles passing along that section will reflect the laser light, clearly revealing the position and movement of the particle.
- **Recording** The light scattered by the tracer particles has to be recorded either on two separate frames or on a sequence of frames of a camera.
- **Calibration** In order to determine the relation between the particle image displacement in the image plane and the tracer particle displacement in the flow, a calibration is required. Usually pictures are taken before or after the experiments including rules, grids and measurement tapes over the captured area.
- **Evaluation** The displacement of the particle images between the light pulses has to be determined through evaluation of the PIV recordings. This step will use differences between two or more images to build the velocity vector in each region of the fluid.

- **Post-Processing** In order to detect and remove invalid measurements and to extract complex flow quantities of interest, sophisticated post-processing is required.

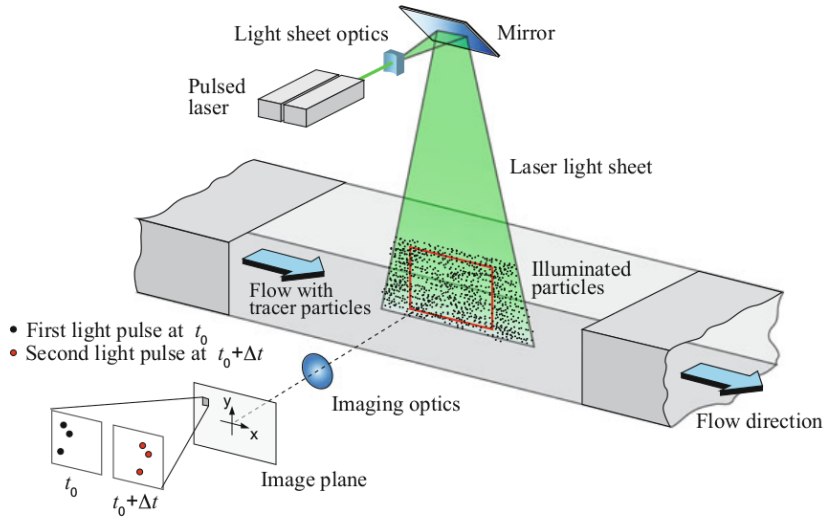

Figure 16: Image acquisition for PIV analysis over a plane in a fluid. Particles are added to the fluid and a lasers sheet is built to illuminate the particles. A camera is positioned perpendicular to light sheet formed in the fluid in order to capture the movement of the particles [5].

1.4 Numerical simulation

The model used for the numerical simulation is a multi-layer model. Layer models have a fixed horizontal grid which represents a discretization of the horizontal plane where the simulation takes place. On the other hand, the vertical grid does not represent a discretization of the vertical structure of the ocean, but an index for each layer instead. The depth and thickness of each layer is then described as variables associated to those indexes. Another characteristic of the model used is that all cells in a layer have the same density and density is constant along the simulation, meaning no mixing between the layers. Nevertheless, one of the most remarkable features of this model is the use of Boolean logic to compute the evolution of layer fronts. A state variable of dry and wet cells take part in the computations allowing layer fronts to expand and retract. Figure 17 shows - as an example - the expansion of a bottom layer front computed in one of the simulations

performed for this thesis.

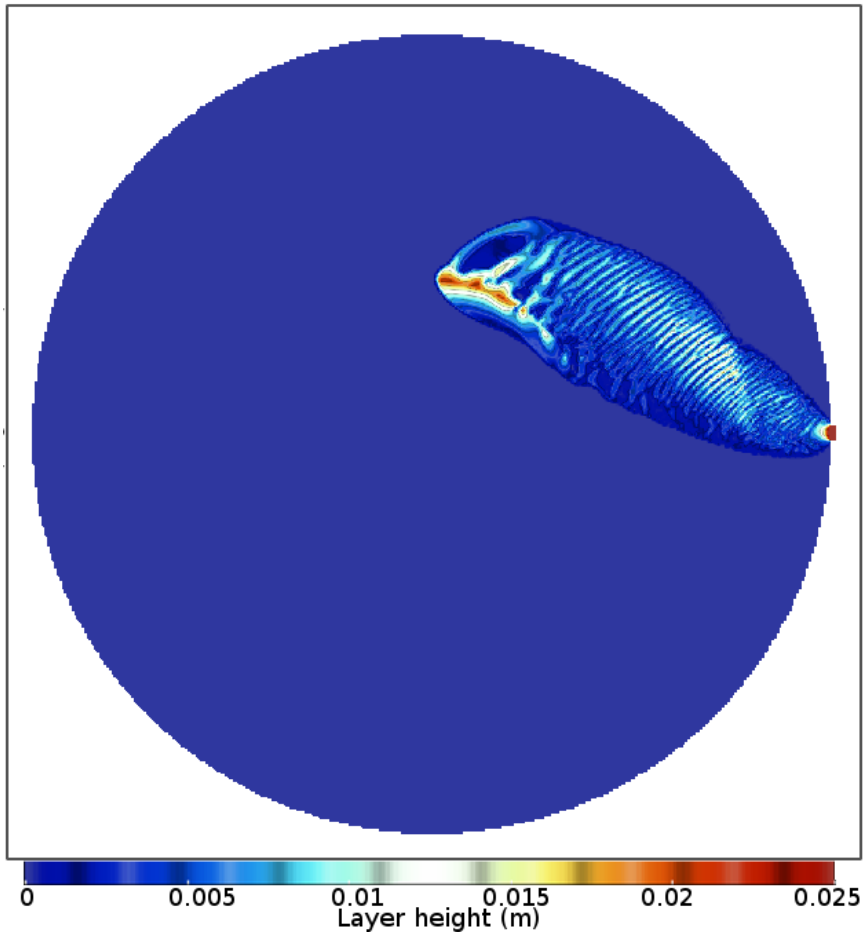

Figure 17: Evolution of a layer front following the topography. Deep water outflows from a source in the right of the circular tank, moving downward along the topography, deviated by the Coriolis effect. The deep water layer is set for all plane, but a Boolean state variable determines whether the cells are dry or wet, thus controlling the evolution of the layer front.

The equations that constitute the model are the non-stationary, non-linear, hydrostatic shallow-water equations for a multi-layer system on a f-plane. The momentum equation includes terms for horizontal momentum diffusion, advection and friction adapted from a 2-layer case [10], as shown at Equations 1 and 2:

$$\frac{\partial \vec{U}_i}{\partial t} + \nabla_h \cdot (\vec{u}_i \times \vec{U}_i) + F_h \cdot \vec{U}_i = -gh_i \nabla_h \eta_1 - \sum_{j=2}^{n} g' h_i \nabla_h \eta_j - \frac{\tau_{i,i'}}{\bar{\rho}} + A_h \nabla_h^2 \vec{U}_i \quad (1)$$

$$\frac{\partial \eta_i}{\partial t} + \sum_{j=1}^{n} \nabla_h \cdot \vec{U}_j = 0 \quad (2)$$

where i is the index of the layer, with $i = 1$ being the surface layer, n is the total number of layers, h_i is the thickness of the *i-th* layer, $\vec{U}_i$ and $\vec{u_i} = \vec{U}_i/h_i$ are, respectively, the transport and vertically averaged velocity vectors for the *i-th* layer, ∇_h is the horizontal Nabla operator, η_i represents the displacement of the *i-th* layer and F_h is the two-dimensional Coriolis matrix:

$$\begin{pmatrix} 0 & -f \\ f & 0 \end{pmatrix} \quad (3)$$

where f is the Coriolis parameter. $\bar{\rho} = (\rho_i + \rho_{i+1})/2$ is the mean water density among two successive layers and $g' = g(\rho_{i+1} - \rho_i)/\bar{\rho}$ is the reduced gravity, with g denoting the acceleration of gravity. A_h is the eddy diffusion coefficient and $\tau_{i,i'}$ is shear stress at the interface between layers i and i'. The shear stress is considered to be quadratically dependent on the horizontal velocity:

$$\frac{\tau_{i,i'}}{\bar{\rho}} = c\vec{u}_i|\vec{u}_i| \quad (4)$$

where c denotes the drag coefficient at the interface.

1.4.1 The Arakawa c-grid

The grid used in the model is the Arakawa C-grid[16] - Figure 18. In this grid, properties of each cell such as density or depth are stored in a position in the grid (blue) which is different from the position where transports are stored (red and green). In this manner, when a new value for - for instance - depth is computed, all properties used in the calculations of the new value must be located at the same grid location, in this case, a location with the blue color. This means that transport data U and V, stored in other

locations, must be moved to the desired location:

$$Ub_{(i,j)} = 0.5(U_{(i,j)} + U_{(i-1,j)}) \tag{5}$$
$$Vb_{(i,j)} = 0.5(V_{(i,j)} + V_{(i,j-1)}) \tag{6}$$

where Uc and Vc are the transports U and V moved to the location where depth is stored - marked with blue. In the same manner, to compute the value of a transport to the next time-step, all used data must be transported to the transport location. For instance, to move both the depth z, from the blue grid point and the transport V, from the green grid point, to a red grid point in order to compute the value of U in the next time-step, those should be computed as

$$zr_{(i,j)} = 0.5(z_{i,j} + z_{i+1,j}) \tag{7}$$
$$Vr_{(i,j)} = 0.25(V_{i,j} + V_{i,j-1} + V_{i+1,j} + V_{i+1,j-1}) \tag{8}$$

where zr and Vr are the depth and V transport, respectively, moved to the U transport location, in red.

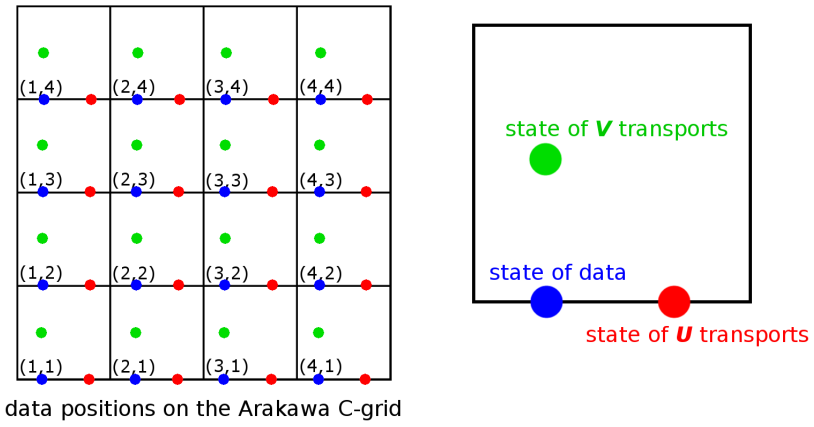

Figure 18: The Arakawa c-grid. Transports V and U are stored in different locations from the rest of the data belonging to the same grid cell.

2 Methodology

Two case studies were performed with the first one simulating the mechanism proposed by the theory of the BiOS and the second one simulating the conditions observed at the EMT. Both case studies are similar and share most of their specifications such as bottom topography, water inlet layout and data acquisition methods. Before describing the particularities of the methodology used in each case study, the methodology shared between both studies is detailed.

2.1 General specifications and methodologies

2.1.1 Bottom topography

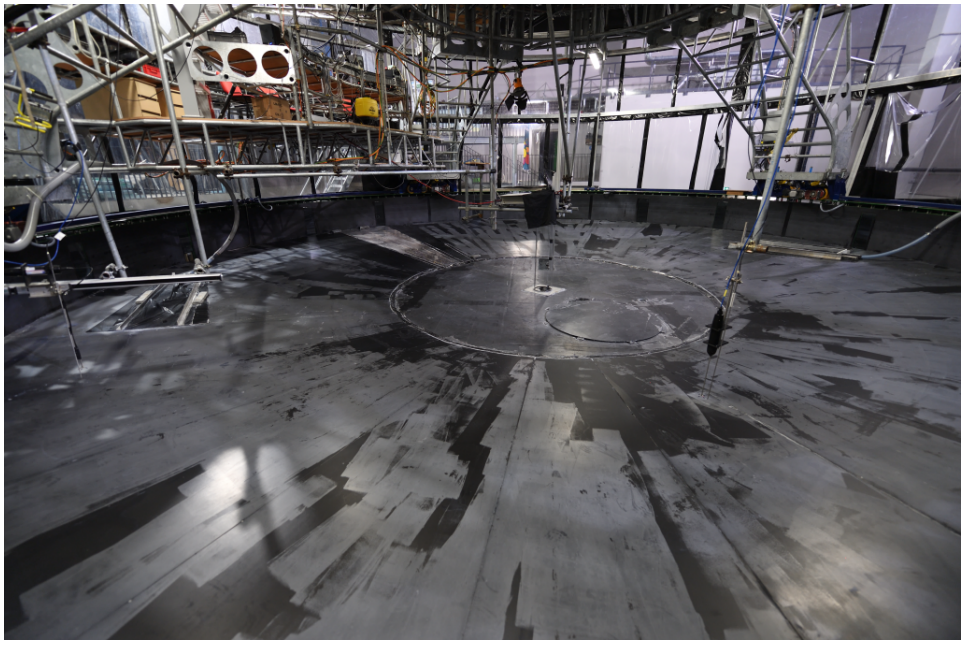

Figure 19: Photography of the empty tank with the topography installed and two sources in place. Credit for the image: Samuel Viboud.

As stressed before, the *Coriolis Platform* consists of a 13 m diameter tank, shaped as a right circular cylinder. In order to simulate the bathmetric conditions observed in the Ionian Sea, the tank bottom topography was modified by placing wooden plates in a manner to form a slope with a 10% inclination. Wooden plates were fixed along the border of the tank at a

height of 40cm from the bottom. Their height decreased as the wooden plates approached the center, finally touching the bottom to form a 5 m diameter circle in the center - where the bottom was no longer constituted by wooden plates, but by the actual tank bottom instead. The volume bellow the plates was empty. Figure 20 shows a 3D representation of the tank, while Figure 19 shown a photography of the tank.

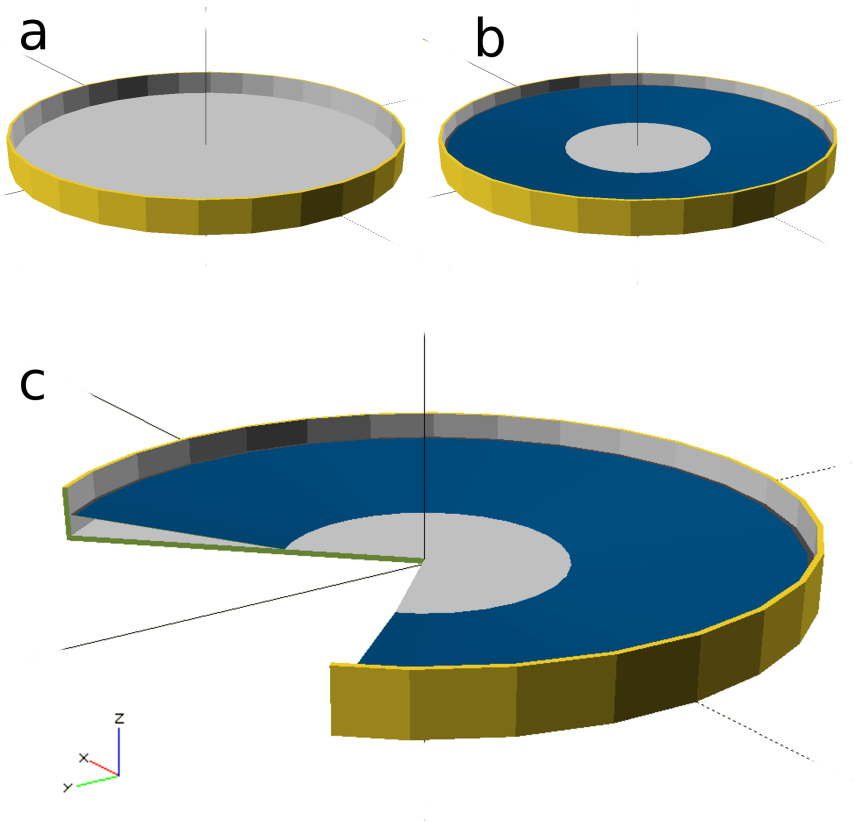

Figure 20: 3D representation of the tank bottom topography used for the experiment performed at the Coriolis Platform - LEGI. **a)** shows the original tank - a right circular cylinder - represented in gray. **b)** shows the wooden plates, in blue, added to form a slope with height decreasing from the border to the center. **c)** shows a cut where both the original and the modified bottom topography can be seen.

Despite the colors presented at Figure 20, both the wooden plates and the actual interior of the tank were painted in black to favor the PIV as

later detailed in this section. During the experiment, the region under the wooden plates was also filled with water in order to avoid stress over the plates. The junctions between the plates were sealed to prevent communication between water over and below the topography however, an opening were the wooden plates touch the wall was let in order to allow surface water to be removed by draining water under the slope.

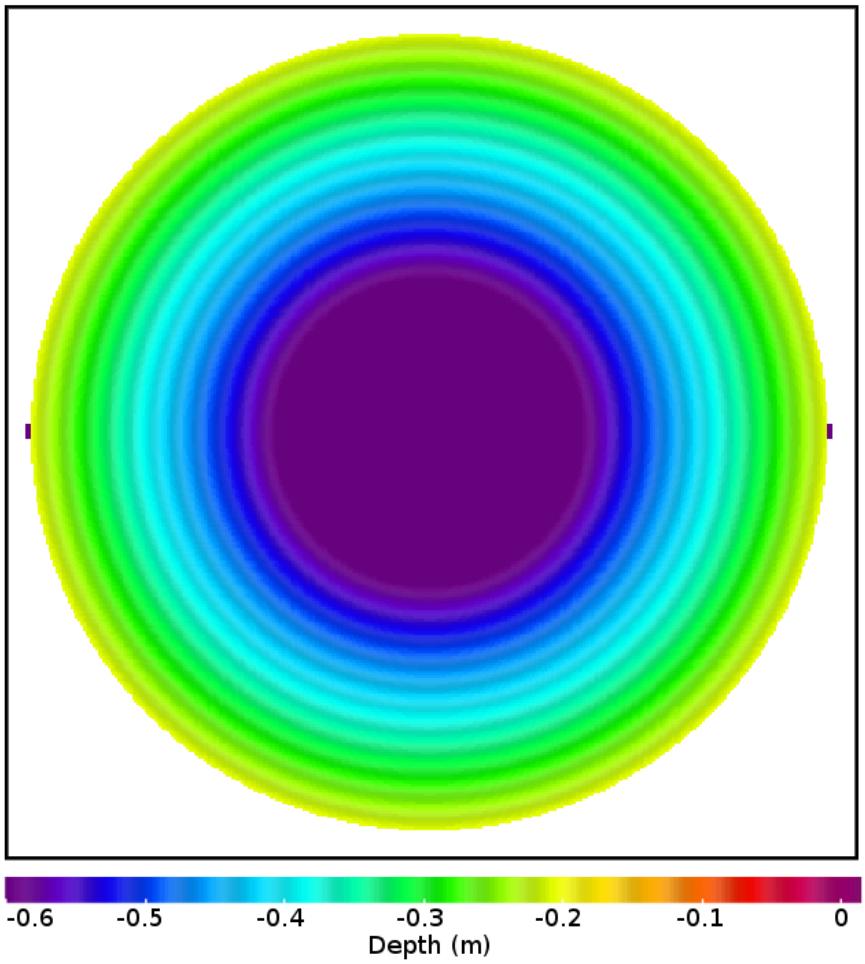

Figure 21: Bottom topography for the numerical model. Horizontal resolution is $16cm^2$, constituted by squared cells with $4cm$ on each side. The two darker rectangles on the left and right extremities over the central axis represent the position for water inlets.

The same topography used in the tank was reproduced in the computational model and discretized with a resolution of $16cm^2$ - squared cells with $4cm$ on each side. The volume bellow the wooden plates was not represented in the computational model once it considered that the bottom sealing was ideal and no transport took place between both volumes in the physical simulation. Figure 21 shows a contour plot of the bottom topography used in the computational model.

2.1.2 Procedure for building a solid body rotation stratified fluid

Prior to initiate the water injection procedure, the empty tank was set to rotate at the speed in which the experiment would be performed. A plastic plate was installed above the bottom inlet - as seen in the central circular area formed by the actual tank bottom in Figure 19 - in order to prevent abrupt vertical currents to break the 2 layer interface.

The stratification was then built by first injecting fresh water in the tank with a flow small enough to prevent the development of strong currents. Fresh water was also added in the volume under the wooden plates, keeping the same water level as the water injected in the open volume. Injection stopped after achieving the volume computed to obtain the desired layer height and the tank was left to rotate for 2 hours so the water inside the tank would achieve solid body rotation. Then, salt water with a density of about 1015 kgm^{-3} was injected. This process was initially done with a very small flow in order to prevent disturbances, creating an interface between the new bottom layer that slowly forms and the already built fresh water layer - which now becomes the surface layer. As the bottom layer increases its height, the injection flow is also increased back again to the same flow used when previously injecting fresh water.

The stratified system rested for the night until next day in order to achieve solid body rotation. Microscopic particles were added at the surface in different moments of this stage in order to permeate the fluid and reflect the laser used for PIV analysis, as later shown in this section.

In the computational model, solid body rotation is achieved by using the rotating frame as the frame of reference - a *f-plane*. The rotating period is the same as the one used in the practical simulation. Due to this feature, setting a solid body rotation fluid in the model requires only defining the

layers depth. However, a note on how the layers are displaced at the initial state is necessary. Although the system starts from a two-layers configuration - as in the physical simulation - it already has the 4 layers that will be observed in the end of the experiment. A layer with infinitesimal thickness lies between the initial bottom layer and the ground (layer 1 at Figure 22). It shall keep its infinitesimal thickness until denser water is injected, filling it and letting it become the new bottom layer. The same concept applies for a layer that lies between the bottom and the surface layer (layer 3 at Figure 22), which also remains with infinitesimal thickness until water with intermediate density is provided to the system. Figure 22 details the layer configuration in the initial condition and at a moment after intermediate and bottom water were injected.

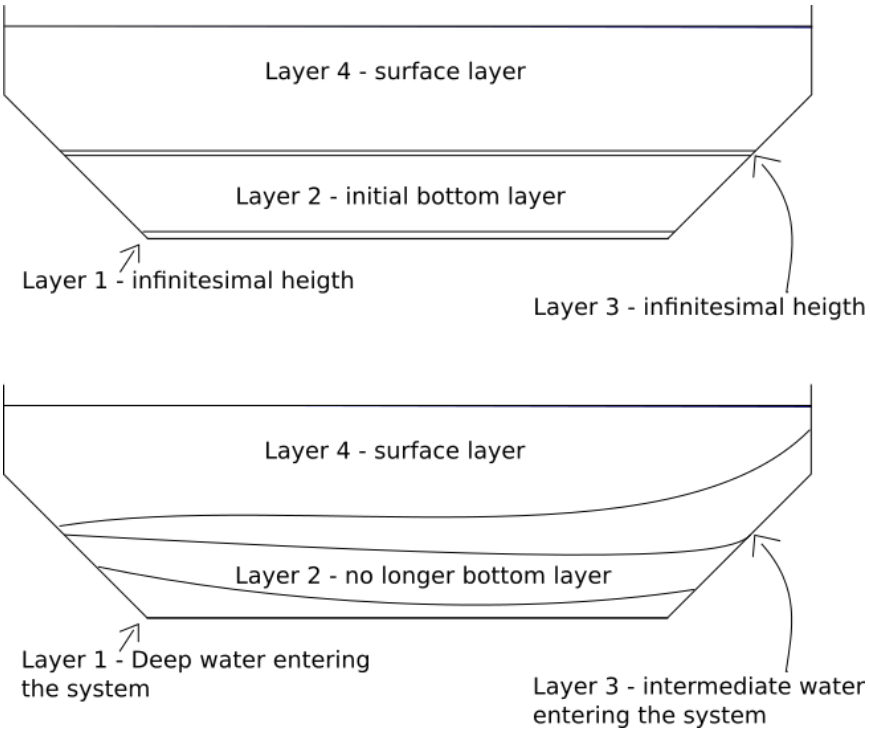

Figure 22: Vertical profile of the tank with **top image)** the initial condition for layer configuration in the numerical model with layers 1 and 3 starting with no water, and **bottom image)** the layer configuration after injection of intermediate - layer 3 - and deep water - layer 1.

2.1.3 Water inlet layout

For the physical experiment, a geostrophically adjusted water inlet was used in order to prevent effects of centrifugal forces over the water entering the tank. The concept used to impose this adjustment was to add a chamber right at the tube outlet with a length such that the water would take at least 1 rotation period to go through. Figure 23 shows a scheme for the apparel.

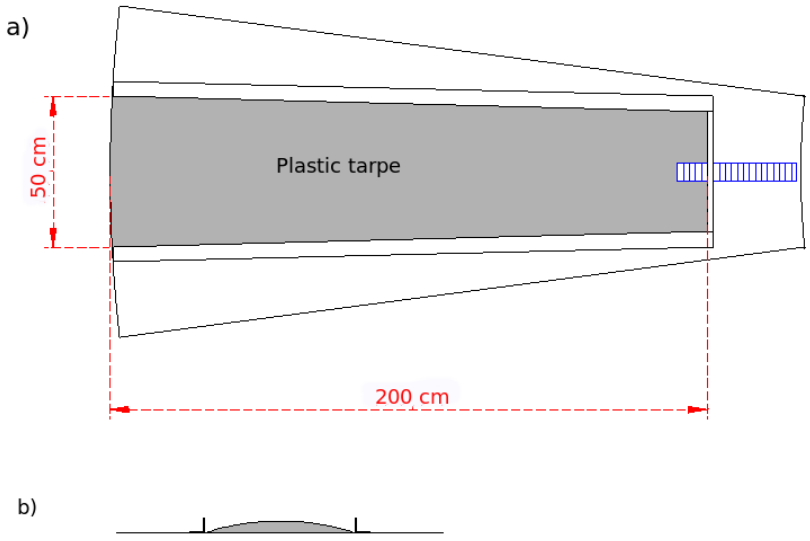

Figure 23: Geostrophically adjusted water inlet. **a)** shows a top view of the inlet. A corrugated tube - marked in blue - transported water to the inlet. Water exits the tube under a plastic tarpe - in gray - which has to be crossed in order to leave the inlet through the opposite extremity, covering a total of 2 meters under the tarpe. Along this course, water becomes geostrophically adjusted. **b)** shows a front view front the source illustrating the tarpe bulge where the water goes under. The bulge measures 4 cm height in the center and the volume where the water passes is marked in gray. Not all structures seen in the top view are illustrated in this cut.

As water is injected through the source, the equivalent volume is removed from the surface layer maintaining the volume during the experiment. Figure 24 shows a photography of the water inlet assembled in the tank.

The numerical simulation was not conceived using an adjusted water inlet. The sources in the model are represented by increments in the height of the layer which receives the water and all the layers above. This can be understood as a discrete increment Δh in the continuity equation for

incompressible flows:

$$\nabla \cdot \vec{u} + \frac{\Delta h}{\Delta t} = 0 \tag{9}$$

There is no removal of water from the system, thus the volume of water in the numerical simulation increases as water is supplied.

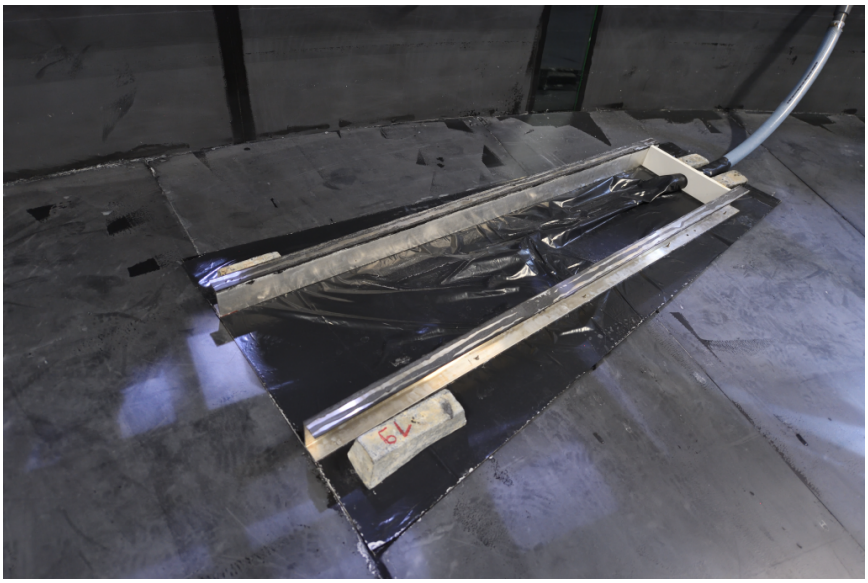

Figure 24: Photo of the water inlet assembled in the tank. Credit for the image: Samuel Viboud.

2.1.4 Data gathering - Particle Image Velocimetry (PIV)

Microscopic tracers - organic particles - were added to the water in order to track fluid movements. Those particles entered the system through the inlet water as well as through the free surface while it was resting and waiting to achieve solid body rotation. For being organic, the particles decompose after a few days in water, leaving no detritus in the discarded water. This fact also required the use of bleach in the water in order to avoid the proliferation of micro organism, which would reduce the transparency of the fluid.

A laser sheet was formed by pointing a laser beam to a rotating mirror in the center of the tank. The whole structure was protected from water by a glass cylinder. The laser beam was first emitted pointing towards the

bottom, then it was deviated by a set of two mirrors so it would point up, finally reaching a last mirror which, when rotating fast enough, produced a laser sheet in the whole tank. Figure 25 show a 3D model for the described apparatus.

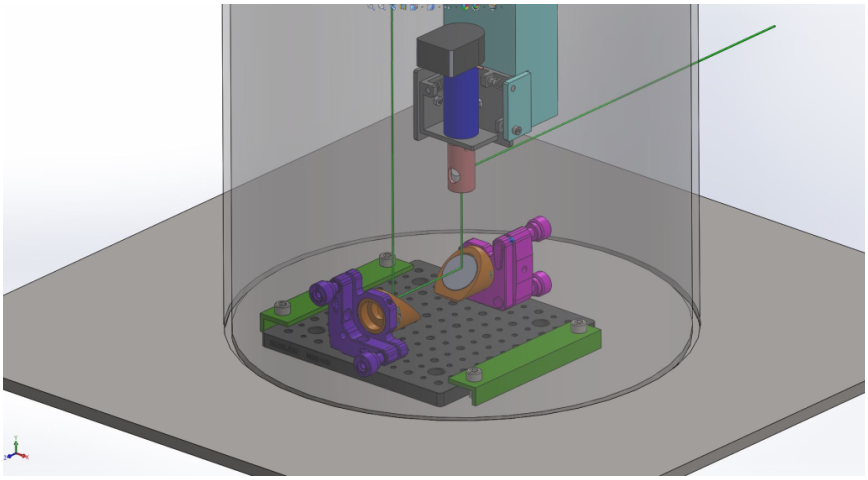

Figure 25: Mirror set used to produce the laser sheet used for PIV analysis. The laser is emitted towards the bottom where it is deviated by two mirrors, pointing up to reach a rotating mirror that rotates fast enough to produce an horizontal laser sheet. Credit for the image: LEGI

Images were taken by a camera positioned above the tank. It was possible to move the rotating mirror shown at Figure 25 up and down, allowing to select the depth which the laser sheet would illuminate. For each experiment, a total of 12 depth were used spaced by 4 cm each and starting 13.8 cm from the bottom. The laser sheet would move down, stopping on each level for long enough so 3 images could be captured with a time interval of 1 second between each. When reaching the last level, the laser then moved up continuously to stop again in the first position, repeating this cycle up to the end of the experiment.

Figure 26 shows a photography of the laser sheet while activated. The shutter was set to be slow enough so a complete turn of the rotating mirror could produce the sheet. The photography taken for PIV analysis during the experiments were taken with a shutter speed of 1/100 seconds. In the photography, tracers are also visible, drawing paths over the illuminated level.

Figure 26: Laser sheet over the rotating tank. The shutter was set to be slow enough so a complete turn of the rotating mirror could produce the sheet. Traces are visible drawing path over the illuminates level.

2.1.5 Data storage

All data, both from physical and numerical simulations, are stored in netCDF files [18]. According to the developers website[2], netCDF files are:

- **Self-Describing**. A netCDF file includes information about the data it contains.
- **Portable**. A netCDF file can be accessed by computers with different ways of storing integers, characters, and floating-point numbers.
- **Scalable**. A small subset of a large dataset may be accessed efficiently.
- **Appendable**. Data may be appended to a properly structured netCDF file without copying the dataset or redefining its structure.
- **Sharable**. One writer and multiple readers may simultaneously access the same netCDF file.

[2] `https://www.unidata.ucar.edu/software/netcdf/docs/faq.html`

- **Archivable**. Access to all earlier forms of netCDF data will be supported by current and future versions of the software.

Data from the physical simulation is stored in the serves at LEGI and will be publicly available in December 2020 - two years after the experiment. Data from the numerical simulations are stored in a private server but can be shared under request.

2.2 Case study 1 - The theory of the BiOS

This experiment was designed to reproduce the mesoscale features observed in the Ionian Sea overturning circulation during the 2012 winter, know for being an specially cold winter with strong winds. Figure 27 shows the temperature anomaly observed between Jan. 29 and Feb. 4 of 2012.

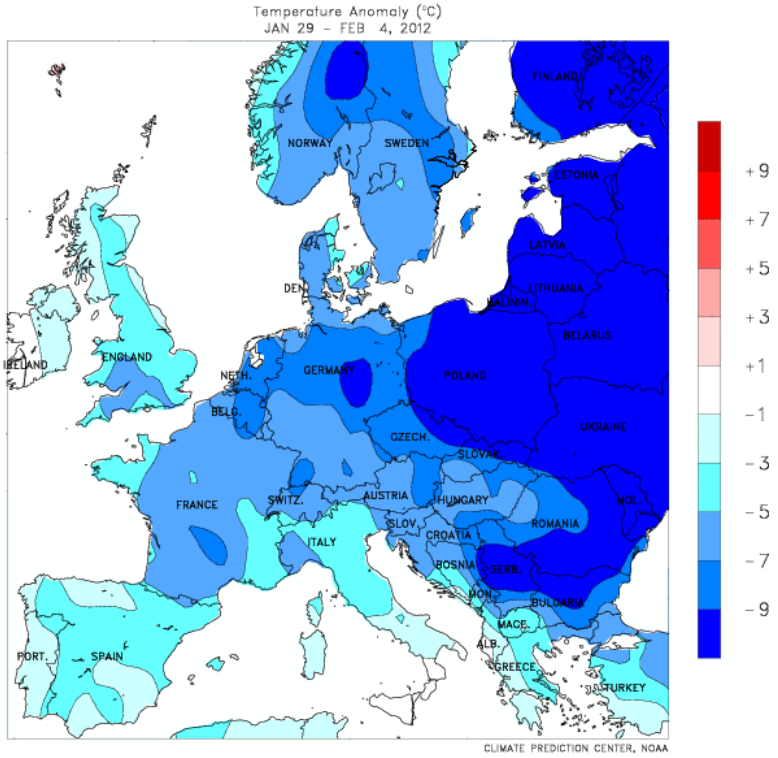

Figure 27: Temperature anomaly in Europe at winter 2012, Jan. 29 to Feb. 4. Credit for the image: NOAA

The excessive cold increased the volume and density of deep water formed

in the Adriatic, which according to the theory of BiOS favored an observed posterior inversion of the previously cyclonic circulation into an anti-cyclonic circulation.

A water inlet was used to simulate the water disposal from the Adriatic and a stratified two layer system in solid body rotation is set as initial condition. During the first phase of the experiment, intermediate water was injected, which was expected to induce a cyclonic surface circulation - according to the Theory of the BiOS. Later, the intermediate water injection ceased and deep water injection took place. This change in the inflow density was expected to weaken the previously established cyclonic gyre, eventually reversing its circulation to anti-cyclonic. Afterwards, by ceasing the injection of dense water and restarting the injection of intermediate water, the circulation is expect to weaken again and the intensification of a cyclonic gyre shall be observed.

Those variations in water inlet density intended to simulate the variations in ADW observed to enter the Ionian Sea as a consequence of this intense winter. Thus, this experiment should demonstrate the interaction among the layers as predicted by the theory of BiOS. Figure 28 shows the configuration for the injection of water versus time. Planned values - used in the numerical simulation - are drawn in a solid line while the values used in the physical simulation are drawn with a dashed line.

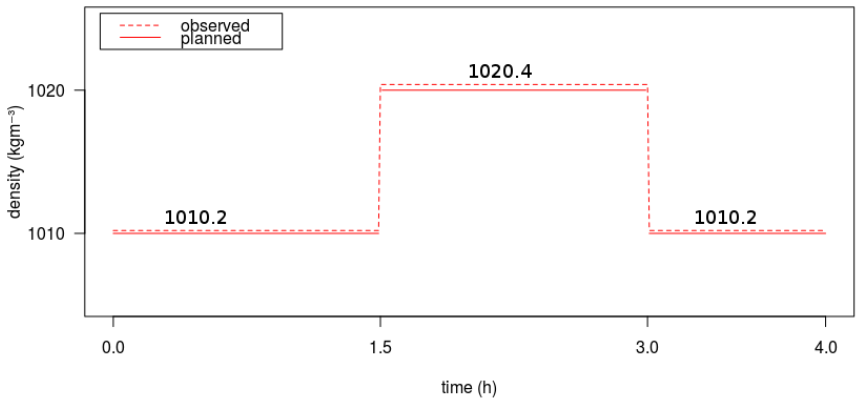

Figure 28: Case Study 1: Configuration of inlet water density versus time. Planned values - used in the numerical simulation - are drawn in a solid line while the values used in the physical simulation are drawn with a dashed line.

Parameter	unit	planned value	observed value
Rotation period	s	120	120
Flow rate	$l\ s^{-1}$	0.8	0.8
$\rho_{surface}$	$kg\ m^{-3}$	1000	999.2
ρ_{bottom}	$kg\ m^{-3}$	1015	1014.5
h_{bottom}	m	.30	0.162
$h_{surface}$	m	.30	0.411
h_{total}	m	.60	0.573

Table 1: Initial conditions for the experiment and used conditions in the physical simulation. $\rho_{surface}$ and ρ_{bottom} are the densities for the surface and bottom layers, respectively, at the initial condition. In the same manner, $h_{surface}$, h_{bottom} and h_{total} are the thickness of the surface, bottom and total water column.

2.3 Case study 2 - The EMT

This experiment was designed to reproduce the mechanism believed to induce the circulation reversals observed in the overturning circulation of the Eastern Mediterranean during the EMT [3].

Two water sources were used in order to simulate the inflow from the Aegean Sea and from the Adriatic Sea. Although not corresponding to the disposition in the Ionian basin, the sources were positioned at the same level and 180^o one from the other in order to avoid interference from water outflowing from one source into water outflowing from the other source. A stratified two layer system in solid body rotation is set as initial condition. In the beginning, the source corresponding to the Adriatic Sea pumps intermediate water inside the tank. This was expected to produce a cyclonic circulation over the surface. On a second stage, water was injected from the other inlet - corresponding to the Aegean Sea - while water from the Adriatic keeps being pumped and an inversion of the surface circulation was expected to develop.

The configuration planned (solid line) and executed (dashed line) for the water injection is shown on Figure 29. Blue indicates water outflowing from the inlet corresponding to the Aegean Sea while red corresponds to the inlet representing the Adriatic Sea.

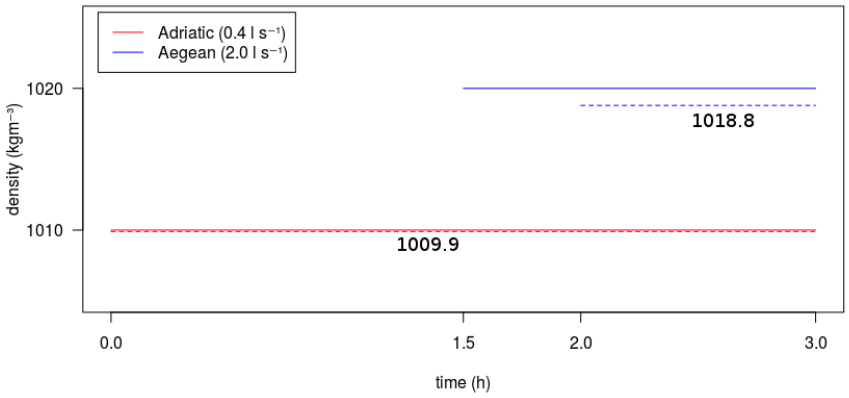

Figure 29: Blue indicates water outflowing from the inlet corresponding to the Aegean Sea while red corresponds to the inlet corresponding to the Adriatic Sea.

Parameter	unit	planned value	observed value
Rotation period	s	120	120
ρ_{amb}	$kg\ m^{-3}$	1000	999.4
ρ_{bottom}	$kg\ m^{-3}$	1015	1013.6
h_{botom}	m	.30	0.201
h_{amb}	m	.30	0.368
h_i	m	.60	0.569

Table 2: Initial conditions for the experiment and used conditions in the physical simulation. $\rho_{surface}$ and ρ_{bottom} are the densities for the surface and bottom layers, respectively, at the initial condition. In the same manner, $h_{surface}$, h_{bottom} and h_{total} are the thickness of the surface, bottom and total water column.

3 Analysis and Discussion

3.1 Case study 1 - The theory of the BiOS

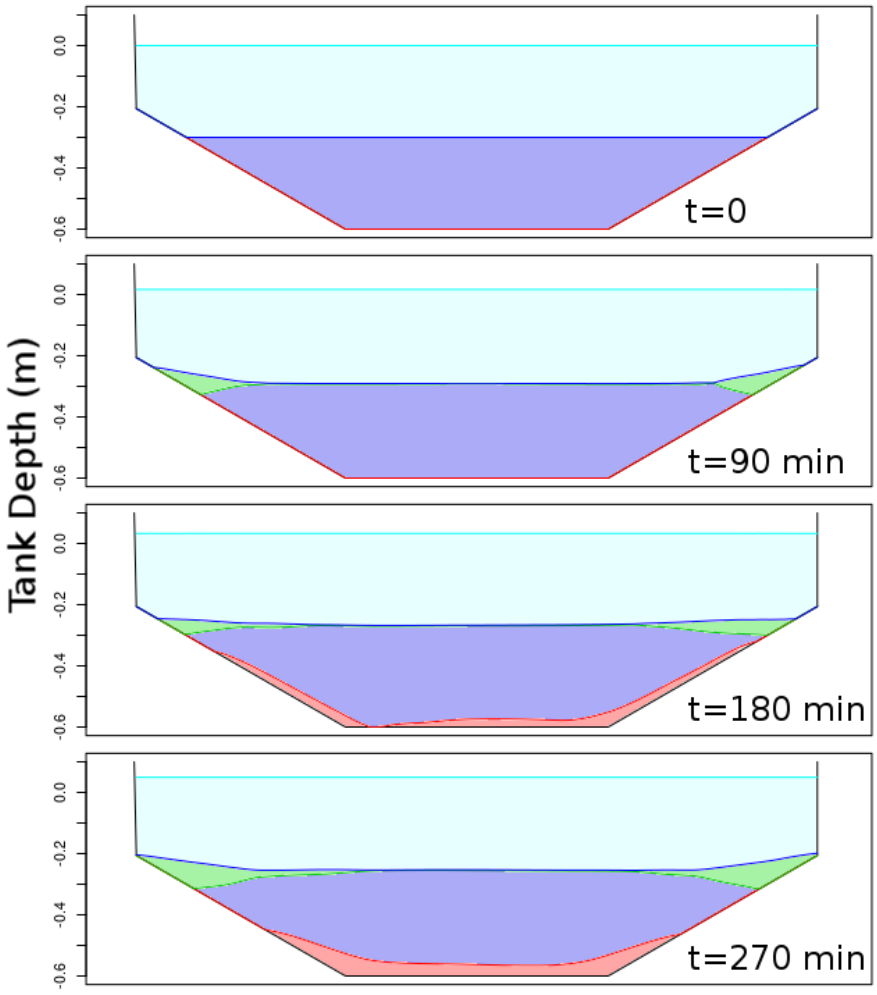

Figure 30: Numerical simulation: Evolution of water over the layers according to time. Initial surface and bottom layers are shown in light-blue and violet, respectively. Injected intermediate water is shown in green, while injected deep water is shown in red.

The numerical simulation ran up to 270 minutes. The evolution of water displacement over the layers is shown at figure 30 - a profile view of the tank width the layers separated by color. At $t = 0$, the tank is in its initial con-

figuration, a stratified two-layers system, with the surface layer represented in light-blue and the bottom layer in violet. Intermediate water is injected in the tank at the beginning of the experiment. At $t = 90\ min$, intermediate water has filled the border of the tank - in green - displacing water from the other layers. Deep water injection starts right after, injecting deep water - as seen in red at $t = 180\ min$ when it already fills part of the bottom, compressing the layer above. Deep water injection cease and intermediate water is injected again, enhancing the displacement of water in the intermediate levels.

Surface also reacts to the layer dynamics below it. However, due to the scale of the simulation, such reaction is very subtle. Although its variations cannot be perceived at Figure 30, the signal for the surface altimetry contains information about the currents in the surface. Surface altimetry was extracted from the numerical simulation data - Figure 31 - where the increase in surface level due to water entering the tank was removed from the signal by subtracting the average surface value for each instant. The remaining signal was then filtered for high frequencies using a binomial filter of $4th$ order. This procedure placed all curves centered at zero and smoothed the signal in order to highlight the general curvature of the surface.

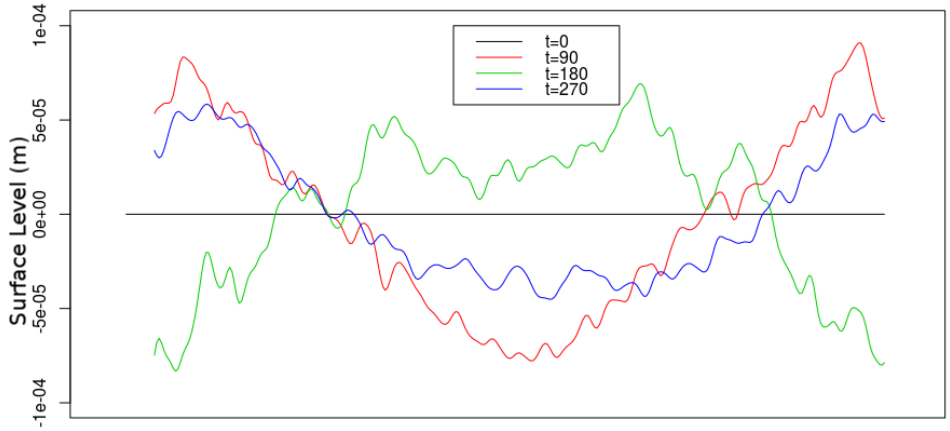

Figure 31: Normalized surface level profile for the numerical simulation at 4 different instants: $t = 0,\ 90,\ 180$ and $270\ min$. y-axis shows the depth in meters.

The *depression* in the central area shown at $t = 90\ min$, induces a cyclonic circulation, followed by a *hill* at $t = 180\ min$, which then induces an anti-cyclonic circulation and finally, at $270\ min$, a *depression* is

established again. This suggests that circulation at $t < 90'$ was cyclonic and also that two vorticity inversions took place during the experiment: one at $90' < t < 180'$ - from cyclonic to anti-cyclonic - and the other at $180' < t < 270'$ - back to cyclonic.

More information about the events in the surface can be obtained by observing its vorticity field - displayed at Figure 32. The field on the left portrays the moment right before the increase in inlet water density, while the one in the right describes the moment before the decrease in inlet water density back to its previous value - see Figure 28 for details on inlet density evolution in time. Both plots are coherent with the information displayed at Figure 31, describing a cyclonic circulation in the beginning of the experiment followed by a reversal to anti-cyclonic after the injection of Deep water.

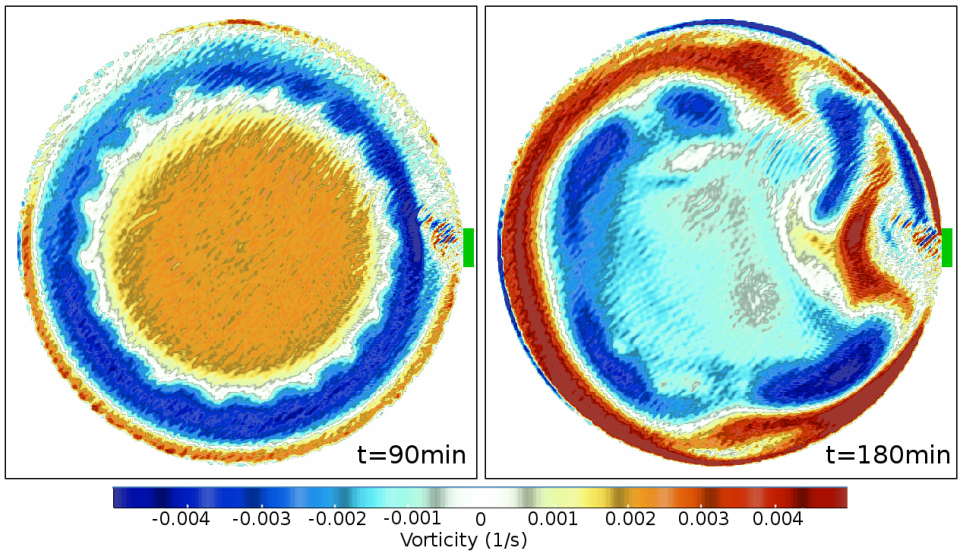

Figure 32: Vorticity fields on the surface of the tank for the *numerical* simulation. **Left**) was captured instants before the increase in inlet water density (injecting deep water) while **right**) was taken a moment before the decrease in inlet water density back to its previous value (intermediate water).

This results support a part of the dynamics described by the theory of the BiOS, showing surface circulation reversals as depending on baroclinic conditions in the layers below.

A vorticity plot was also produced for the physical simulation, generated with the velocities obtained using PIV analysis - as shown in Figure 33. Again, on the left, the capture retracts the instant before the increase in inlet water density, and on the right, it shows the moment before the reduce in inlet water density back to its previous value. It is possible to observe that both plots show an anti-cyclonic circulation in the center, contradicting the result of the simulation.

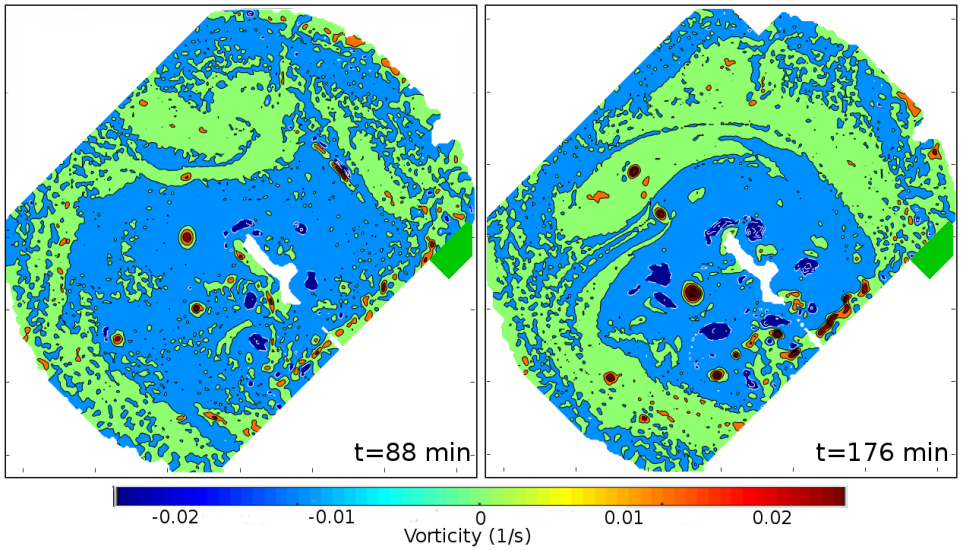

Figure 33: Vorticity fields on the surface of the tank for the *physical* simulation based on velocities measured using PIV analysis. **Left**) was captured instants before the increase in inlet water density (injecting deep water) while **right**) was taken a moment before the reduce in inlet water density back to its previous value (intermediate water).

This result is surprising, once the same procedure produced a cyclonic circulation in the beginning of the simulation presented in the case study 2 - Figure 38. This fact might indicate a failure in controlling all the parameters of the physical setup and simulation, leading to untraceable interference. The reports of the experiments in Grenoble indicates a possible leaking in the topography which may have played a role in this result.

A direct comparison between physical and numerical simulations is shown at Figure 34 - comparing vortices in the central gyre of the tank obtained with both the numerical and the physical simulations for the complete du-

ration of the experiment. A residual cyclonic circulation is observed in the beginning of the physical simulation, in red. Nevertheless, the circulation reversed to anti-cyclonic much before the dense water was injected and remained so up to the end of the experiment, clearly showing no trend to a cyclonic vorticity. As previously displayed in Figure 33, no relevant changes in vorticity were observed during the injection of deep water.

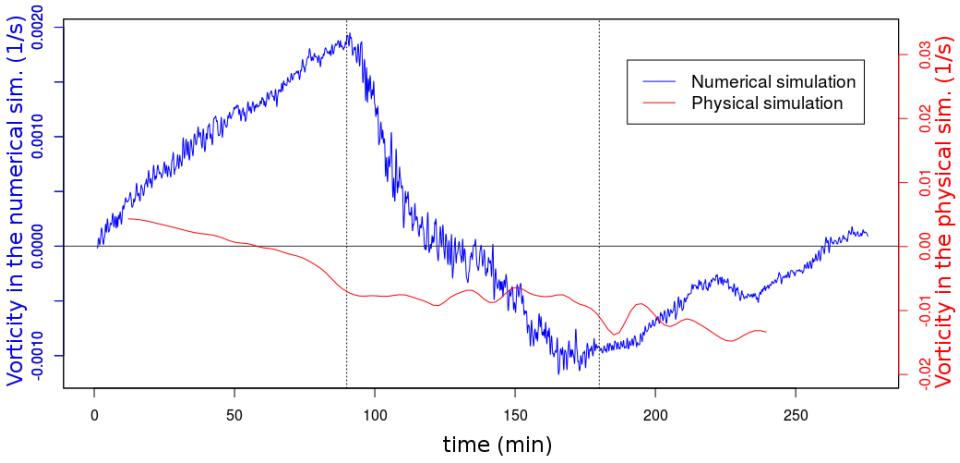

Figure 34: Evolution in time of surface vorticity in the central area of the tank for **red)** the physical simulation and for **blue**) the numerical simulation.

It is possible to see again that the numerical simulation responded as expected according to the theory of BiOS, presenting a sharp change in the *rate of change* of vorticity right at the moment where deep water injection started. Another sharp change in vorticity variation was observed after intermediate water was pumped in the tank again, although this change was not strong enough to build a cyclone in the tank again.

Although Figure 34 does not show a clear cyclonic vorticity formed at $t = 270\ min$, the curve observed for this time instant at Figure 31 shows a depression comparable to $t = 90\ min$, when a well defined cyclonic vorticity was established and confirmed by Figure 34. A possible explanation for this difference is that the depression in the surface layer, created after the displacement of intermediate water in the layer below, was inducing a cyclonic vorticity as a result of a geostrophic current, but the previous anti-cyclonic circulation was still to be overcome. It is possible that a cyclonic circulation

would be observed if the simulation had continued for a few more minutes.

3.2 Case study 2 - The Eastern Mediterranean Transient (EMT)

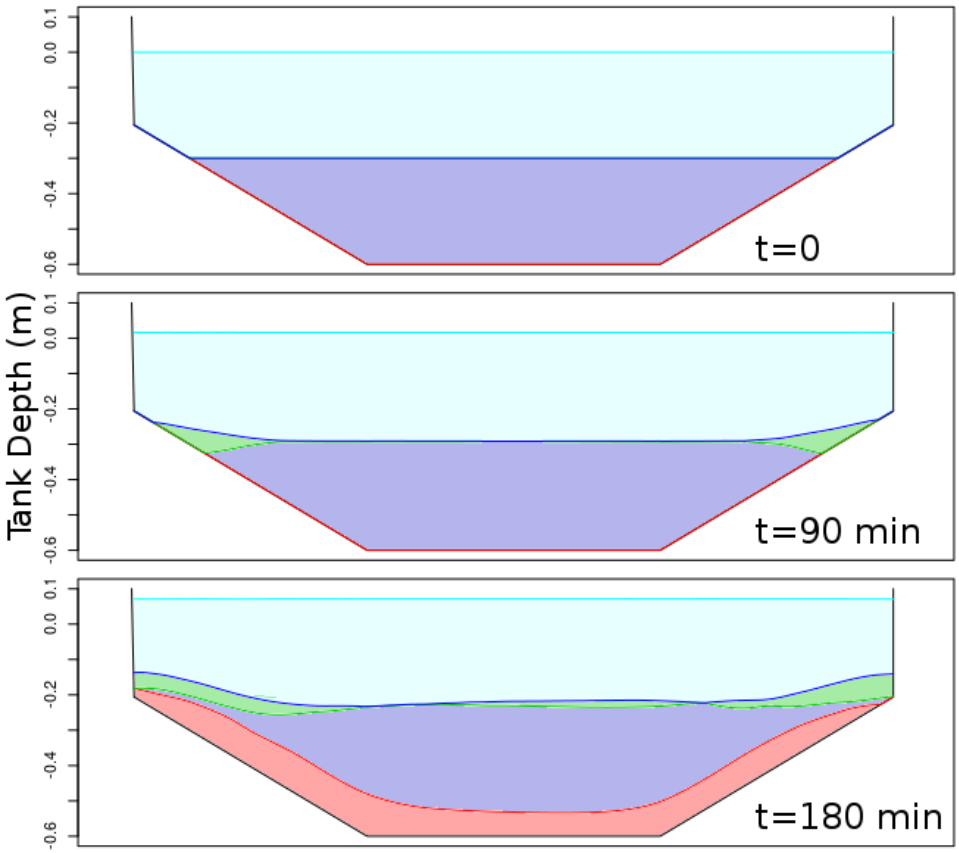

Figure 35: Numerical simulation: Evolution of water over the layers according to time. Initial surface and bottom layers are shown in light-blue and violet, respectively. Injected intermediate water is shown in green, while injected deep water is shown in red.

The total simulation time for the numerical simulation was 180 minutes. Figure 35 shows a vertical profile of the tank, detailing layer displacement over time with each layer marked by colors in the same fashion as in Case Study 1 - Figure 35. At $t = 0$, intermediate water from the Adriatic source (in green) started to be injected in the tank. Later, at $t = 90\ min$, the path

of intermediate water along the topography has caused a local dooming of the layers above - as expected - leading to a rise of surface level in the borders of the tank - as better seen in Figure 35. At this very moment, deep water started to be injected from the Aegean source (in red) without stopping to inject intermediate water from the Adriatic source. This led to the appearance of a deep water layer with a relatively large volume due to the high amount of injected water, as seen in $t = 180\ min$.

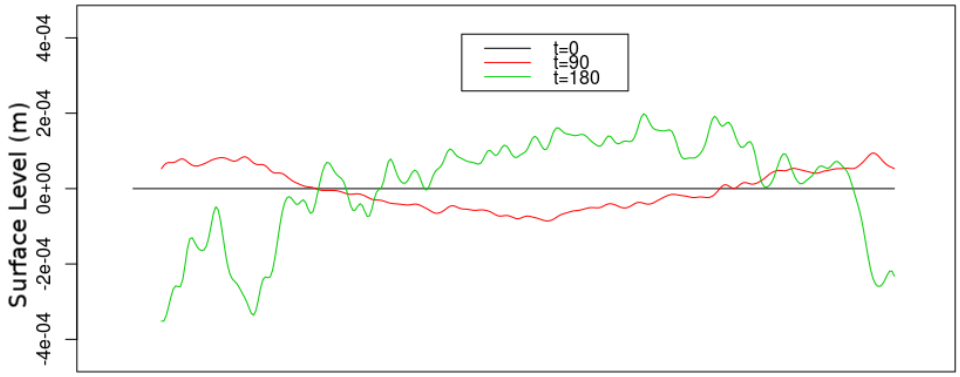

Figure 36: Normalized surface level profile for the numerical simulation at 3 different instants: $t = 0,\ 90$ and $180\ min$. y-axis shows the depth in meters.

The expected *hill* was observed at $t = 180\,\text{min}$, as shown in the green curve in Figure 36. Figure 37 confirms these observations by showing a clear cyclonic circulating at the left - $t = 90\,\text{min}$ - which agrees with the depression shown at Figure 36 for the same instant. Also, for $t = 180\ min$, a predominantly negative vorticity can be observed, meaning an anti-cyclonic circulation, although weak and small cyclonic eddies are still present in the central region o the tank. The vortices observed under intermediate and deep water injection agree with the expected for this experiment and thus, with the observed during the EMT.

The physical simulation results - Figure 38 - show a noisy signal for the cyclonic circulation at $t = 86\ min$, as a consequence of intermediate water injection and also an anti-cyclonic circulation at $= 172\ min$, after the deep water injection. These results agree with the obtained by the numerical simulation, as well as the observed at the Eastern Mediterranean Transient (EMT).

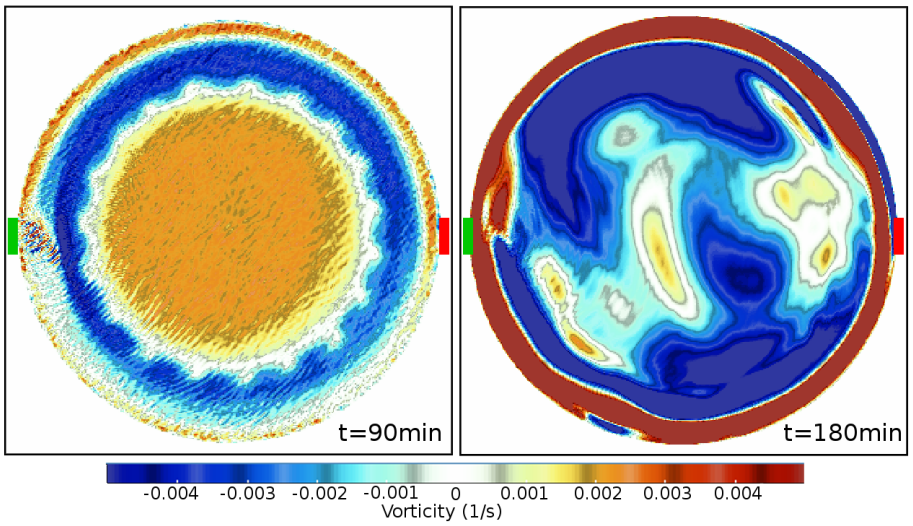

Figure 37: Vorticity fields on the surface of the tank for the *numerical* simulation. **Left**) was captured instants before the increase in inlet water density (injecting deep water) while **right**) was taken a moment before the decrease in inlet water density back to its previous value (intermediate water).

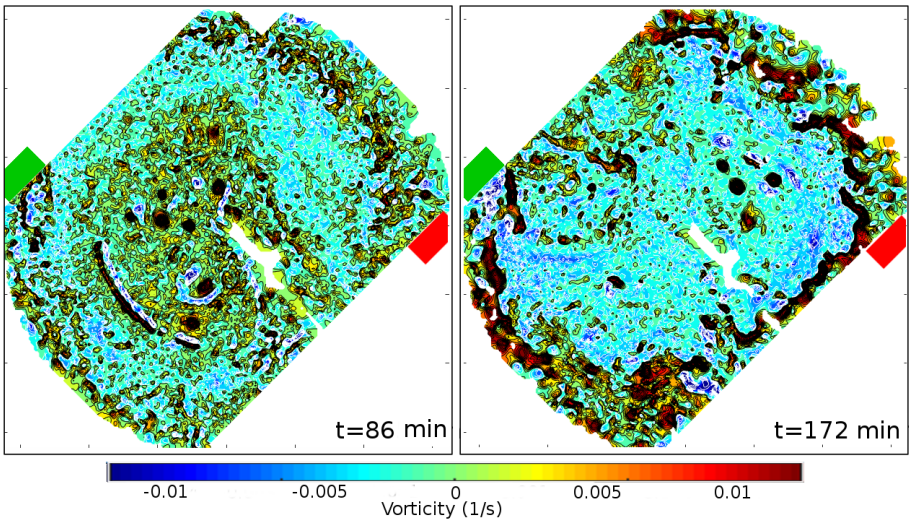

Figure 38: Vorticity fields on the surface of the tank for the *physical* simulation using velocities measured with PIV analysis. **Left**) was captured instants before starting to inject deep water while **right**) was taken a moment before the decrease in inlet water density back to inject intermediate water.

4 Conclusion

Regarding the numerical simulations, both case study 1 and 2 presented coherent results with the observations made in the Ionian Sea during 2012's winter and during the EMT, suggesting that vorticity inversions can be produced by internal baroclinic variations, and also being consistent with the core concept of the theory of the BiOS: the decadal vorticities inversions observed at NIG are due to a feedback mechanism between the Adriatic Sea and the current vorticity of the NIG

The results obtained from the physical simulation are also coherent to those observed in the EMT, producing a clear vorticity reversal from baroclinic internal changes only. However, when regarding the theory of the BiOS, the obtained results did not allow a conclusion to support or deny the hypothesis formulated by the theory: in fact, it is important to consider that the two physical experiments, although with similar initial conditions, did not present the same response to intermediate water injection in the first phase. This may indicate that a non-controlled factor might have taken place, producing a systematic error than requires investigation and possibly a repetition of the experiments.

Apart from the results obtained in this thesis, more research is required in order to provide a better understatement of the causes behind phenomena approached: the EMT and the decadal vorticity inversions at the NIG. Suggestion for further works include:

- To considerate layer mixing by adding an entrainment term to the equations governing the model.
- To deeper investigate and reproduce the physical simulations performed in order to identify and isolate possible sources of systematic errors.

References

[1] Harold V. Thurman Alan P. Trujillo. *Essentials of Oceanography*. Pearson, 12 edition, 2016.

[2] W. Alpers, P. Brandt, A. Rubino, and J. O. Backhaus. Recent contributions of remote sensing to the study of internal waves in the straits of Gibraltar and Messina. *Recent contributions of remote sensing to the study of internal waves in the straits of Gibraltar and Messina*, 17:21–40, 1996.

[3] G. L. E. Borzelli, M. Gačić, V. Cardin, and G. Civitarese. Eastern Mediterranean Transient and reversal of the Ionian Sea circulation. *Geophysical Research Letters*, 36:L15108, August 2009.

[4] G. Civitarese, M. Gačić, M. Lipizer, and G. L. E. Borzelli. On the impact of the bimodal oscillating system (BiOS) on the biogeochemistry and biology of the adriatic and ionian seas (eastern mediterranean). *Biogeosciences Discussions*, 7(5):6971–6995, sep 2010.

[5] Markus Raffel et al. *Particle Image Velocimetry: A Practical Guide*. Experimental Fluid Mechanics. Springer, 3rd edition, 2018.

[6] Tom S. Garrison. *Essentials of Oceanography*. Cengage Learning, 6 edition, 2011.

[7] M. Gačić, G. L. Eusebi Borzelli, G. Civitarese, V. Cardin, and S. Yari. Can internal processes sustain reversals of the ocean upper circulation? the ionian sea example. *Geophysical Research Letters*, 37(9), 2010.

[8] John Church Gerold Siedler and John Gould (Eds.). *Ocean Circulation and Climate: Observing and Modelling the Global Ocean*. International Geophysics 77. Academic Press, 1 edition, 2001.

[9] John Gould Gerold Siedler, Stephen M. Griffies and John A. Church (Eds.). *Ocean Circulation and Climate: A 21 Century Perspective*. International Geophysics 103. Academic Press, Elsevier, 2 edition, 2013.

[10] K. Hessner, A. Rubino, P. Brandt, and W. Alpers. The Rhine Outflow Plume Studied by the Analysis of Synthetic Aperture Radar Data and Numerical Simulations. *Journal of Physical Oceanography*, 31:3030–3044, October 2001.

[11] R. X. Huang. *Ocean Circulation - Wind-Driven and Thermohaline Processes*. Cambridge University Press, 2010.

[12] R. Alan Plumb John Marshall. *Atmosphere, Ocean and Climate Dynamics: An Introductory Text*. International Geophysics 93. Elsevier, Academic Press, 1 edition, 2007.

[13] P. Malanotte-Rizzoli and V.N. Eremeev. *The Eastern Mediterranean as a Laboratory Basin for the Assessment of Contrasting Ecosystems*. Nato Science Partnership Subseries: 2. Springer Netherlands, 1999.

[14] S. Rahmstorf. Thermohaline circulation. In *Reference Module in Earth Systems and Environmental Sciences*. Elsevier, 2015.

[15] A. Rubino. *Anregung und Ausbreitung von Tsunami-Wellen, die durch untermeerische Erdrutsche verursacht werden*. Berichte aus dem Zentrum fr Meeres- und Klimaforschung, 1994.

[16] A. Rubino, K. Hessner, and P. Brandt. Decay of Stable Warm-Core Eddies in a Layered Frontal Model. *Journal of Physical Oceanography*, 32:188–201, January 2002.

[17] Michael N. Tsimplis, Vassilis Zervakis, Simon A. Josey, Elissaveta L. Peneva, Maria Vittoria Struglia, Emil V. Stanev, Alex Theocharis, Piero Lionello, Paola Malanotte-Rizzoli, Vincenzo Artale, Elina Tragou, and Temel Oguz. Chapter 4 changes in the oceanography of the mediterranean sea and their link to climate variability. In P. Lionello, P. Malanotte-Rizzoli, and R. Boscolo, editors, *Mediterranean*, volume 4 of *Developments in Earth and Environmental Sciences*, pages 227 – 282. Elsevier, 2006.

[18] Unidata. Network common data form (netcdf). https://doi.org/10.5065/D6H70CW6, Mar 2018.

[19] van Aken H.M. *The Oceanic Thermohaline Circulation: An Introduction*. Springer, 2006.

Cropex 2018 Grenoble
Experiment Reports

November 27, 2018

Version 1
Revision A

Table of experiments

Experiments without laser for PIV analysis

Name	Date	$T(s)$	$Q(l/s)$	ρ_0	ρ_1	$h_i(m)$	$h_f(m)$	layers	Objective
TEST01	06.11	180	1.0	-	-	-	-	1	Testing the ink color and the choice for T and $\Delta\rho$.(*)(**)
TEST02	06.11	180	2.8	-	-	-	-	1	Testing the flow.(*)(**)
TEST03	06.11	180	3.7	-	-	-	-	1	Testing the flow.(*)(**)
EXP01	07.11	120	3.7	999.0	1010.1	0.595	0.618	1	Testing yellow ink jet flux and rectangular diffusor position.(*)
EXP02	07.11	120	3.7	999.0	1009.0	0.610	0.625	1	Testing red ink jet flux and rectangular diffusor position.(*)
EXP03	12.11	120	1.0	998.9	1008.9	0.593	0.617	1	Testing the COUGARinlet (plastic tunnel) with geostrophic adjustment and white TiO2 particles. FROM THIS EXPERIMENT ON ONLY THE PLASTIC TUNNEL INLET IS USED!Flow rate was too large, we reduce on 0.8l/s. Anticyclonic circulation in the Ionian basin from GOPRO2.
EXP04	13.11	120	0.8	998.9	1008.9	0.587	0.604	1	Cyclones formation at the outlet, weak cyclonic circulation in the Ionian basin from GOPRO2. Experimental duration too low.
EXP05	13.11	120	0.8	999.0	1008.6	0.604	0.614	2	Cyclones formation at the outlet. No circulation in the Ionian basin.
EXP06	14.11	120	0.8	999.1	1008.6	0.396	0.425	1	Increase to 60 inertial cycles.Decrease the total water depth to 41 cm. Cyclones formation at the outlet. Intermittent cyclonic and anticyclonic circulation (simultaneous, no long term lasting in the Ionian basin.
EXP07	14.11	120	0.8	999.0	see diary	0.425	0.430	2	Problem with salt injection, very high and non constant. Interruption of experiment.
EXP08	15.11	120	0.8	999.2	1018.6	0.404	0.452	1	Doubled density difference. Intense cyclones formation at the outlet. Initial residual ancicyclonic circulation due to tank drainage. Anticyclone persisted initially but died out due to collapse of satellite cyclones into the Ionian basin, that induced a global cyclonic circulation at the basin scale.
EXP09	16.11	60	0.8	999.9	1010.1	0.406	0.438	1	
EXP10	16.11	60	0.4	999.7	1010.1	0.438	0.454	2	

Table 1: All densities are expressed in ($kg\ m^{-3}$). (*)no data collected (**)no video collected

Experiments with laser for PIV analysis and homogeneous initial configuration

Name	Date	$T(s)$	$Q(l/s)$	ρ_0	ρ_1	h_i	h_f	Dur.(min)	Observations
EXP11	23.11	60	0.4	999.7	1010.1	0.438	0.454	-	This experiment was the first done using the laser for PIV. Laser was not working properly and there was a strong residual motion. No data was acquired.
EXP12	23.11	120	0.8	999.1	1010.3	0.574	0.578	120	Image quality for PIV was not satisfactory due to water turbidity. Conductivity probe cp 0 was observed not to work properly and its measurements should not be considered for this experiment.
EXP13	27.11	60	0.8	999.0	1021.1	0.577	0.577	120	
EXP14	28.11	120	0.8	999.2	1010.4	0.575	0.575	134	Repetition of Exp 12 with good conditions for capturing images for PIV. Strong residual motion observed at the beginning of the experiment.
EXP15	28.11	130	0.8	999.3	1010.4	0.39	0.39	134	Weak residual motion at the beginning of the experiment.
EXP16	29.11	60	0.8	999.5	1020	0.39	0.39	132	
EXP18	30.11	120	0.8	999.0	1020.0	0.390	0.391	132	
EXP23	10.12	120	0.8	999.0	1020.3	0.400	0.402	132	There was a failure in the aquisition of images, conductivity and probes position data in the end of experiment.

Table 2: All densities are expressed in ($kg\ m^{-3}$) and lengths in (m).

Experiments with laser for PIV analysis and stratified two-layers initial configuration.

Name	Date	$T(s)$	$Q(l/s)$	ρ_{bottom}	ρ_{amb}	ρ_{inlet}	h_{bottom}	h_{total}	Dur.(min)	Observations
EXP17	29.11	60	0.8	999.5	1009.8	1020.0	0.159	0.39	132	Used final state of Experiment 16 as initial condition. Particles added at the surface layer were not uniformly distributed over the fluid.
EXP19	30.11	110	0.8	999.5	1006.2	1004.2	0.25	0.39	132	Used final state of previous experiment as initial condition
EXP20	05.12	120	0.8	999.0	1009.1	1018.7	0.16	0.398	130	we observed the bottom layer was static, but the surface layer had a very strong cyclone with a triangular shape formed by three smaller cyclones. We believe the triangular shape was generated by the removal of the three floating inlets added to increase the thickness of the top layer.
EXP21	06.12	120	0.8	998.8	1009.0	1019.0	0.12	0.567	138	
EXP22	07.12	120	0.8	998.8	1018.0	1008.7	0.108	0.399	132	

Table 3: All densities are expressed in ($kg\ m^{-3}$) and lengths in (m). Q=$0.8 l/s$ for all experiments

Experiments that simulate the conditions observed at 2012 winter

Name	Date	$T(s)$	h_{bottom}	h_{total}	Dur.(min)	Observations
EXP24	11.12	120	0.162	0.573	242	No inversion was visually noticeable
EXP26	13.12	120	0.221	0.572	253	No inversion was visually noticeable

Table 4: All densities are expressed in $(kg\ m^{-3})$ and lengths in (m).

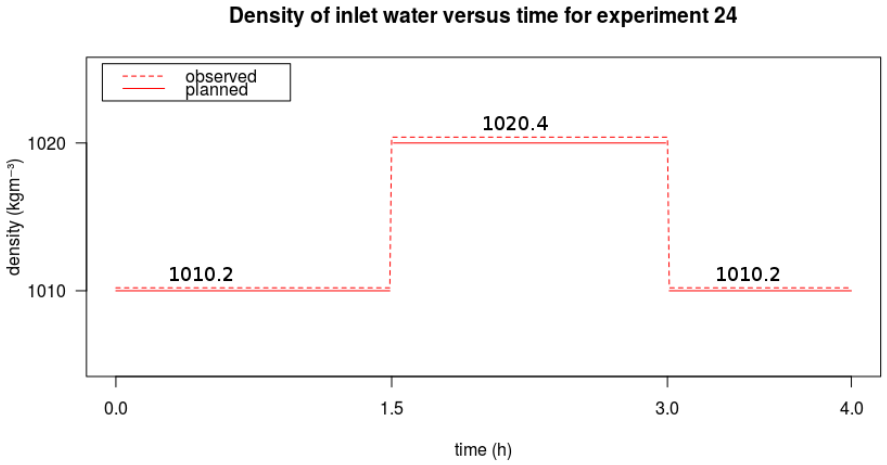

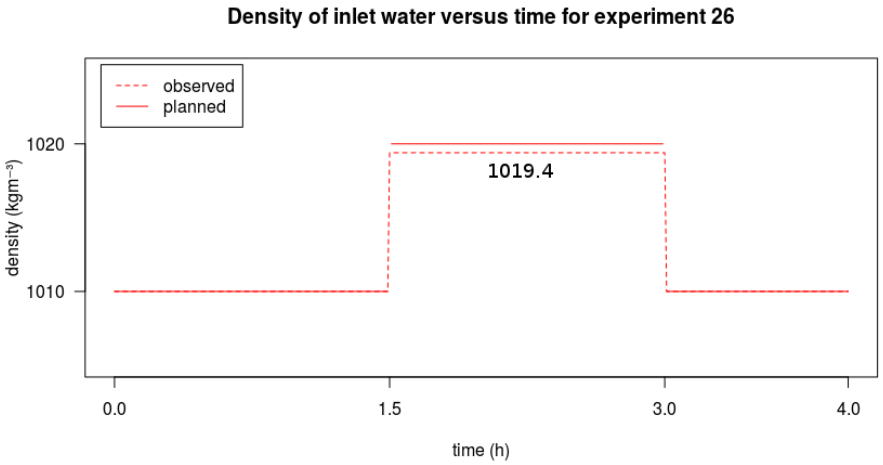

Experiments that simulate the EMT

Name	Date	$T(s)$	h_{bottom}	h_{total}	Dur.(min)	Observations
EXP25	12.12	120	0.201	0.569	192	An inversion was visually noticeable
EXP27	14.12	120	0.209	0.574	279	An inversion was visually noticeable

Table 5: All densities are expressed in $(kg\ m^{-3})$ and lengths in (m).

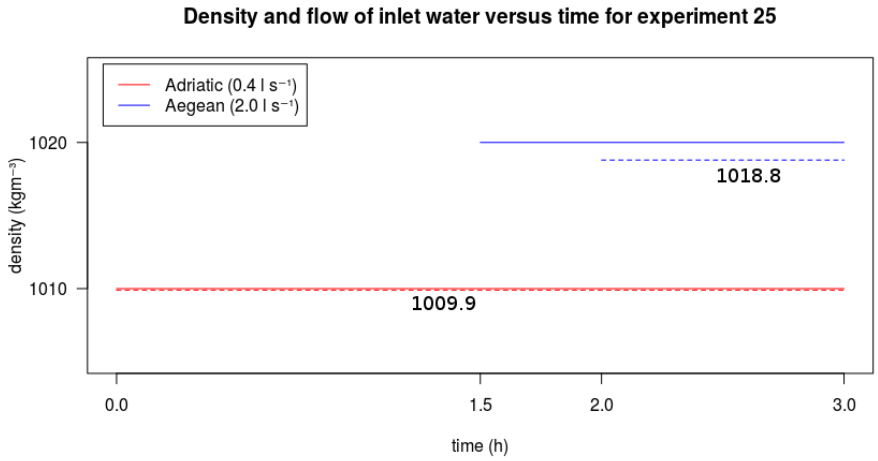

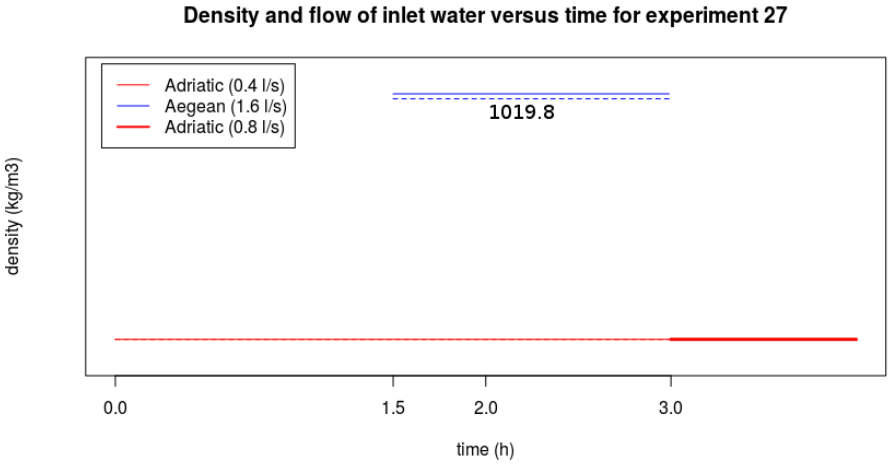

Cropex 2018 Grenoble
Daily report: Experiment 08

November 15, 2018

1 Initial conditions

The initial conditions used at the experiment are displayed at table 1.

Parameter	unit	value
Rotation period	s	120
Flow rate	$l\ s^{-1}$	0.8
ρ_{amb}	$kg\ m^{-3}$	999.2
ρ_{inlet}	$kg\ m^{-3}$	1018.6
h_i	m	0.404
Stratus		1 layer

Table 1: Initial conditions for the experiment

2 Objectives

In this experiment, we expect an earlier and more frequent formation of both the gyres near to the source and in the center of the basin. We also expect them to move faster. Due to the dynamics observed in the center of the basin during yesterday's experiments, we also expect to see the formation of an anti-cyclonic gyre in the center of the basin.

3 Methodology

The tank was drained before the experiment and filled with fresh water. White particles were added to the inlet flow in order to improve the visualization of bottom structures and dynamics. Floaters were added to the surface to allow a brief visualization of the surface flow. When the movement of the floaters allowed the identification of a surface gyre, a fillet of red ink mixed with ethanol was thrown over it to reveal its behavior.

Data was collected using 3 conductivity probes (cp0, cp1 and cp3), one ADV profiler, one ADV and 2 gopro cameras tied to the metal structure on the top of the rotating table - see Figure 1. More details about the tank configuration are documented at the file *one_geostrophic_source.dxf*.

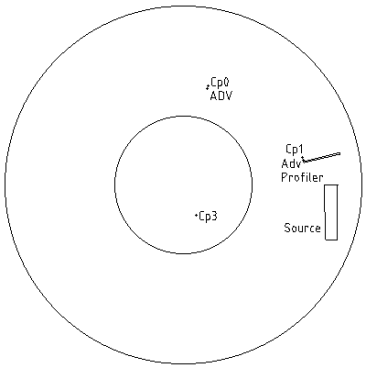

Figure 1: Experiment configuration.

4 Field Observations

Cyclonic eddies were observed to form close to the inlet. Those were larger than previously observed with lower values of $\Delta\rho$. The expected anti-cyclonic gyre in the center was not observed.

The addition of ethanol to the red ink was observed to be very efficient for revealing surface dynamics.

Data obtained at the end of the experiment is shown at table 2:

Parameter	unit	value
h_f	m	0.452
Duration	min	130

Table 2: Data collected at the end of the experiment.

5 Discussion and notes for next experiments

We think the anti-cyclonic gyre in the center was not observed because it might have been destroyed by the large eddies that entered the center of the basin. Thus, for the next experiment we decided to reduce the rotation period to 60 s in order to decrease the radius of deformation by half. We expect this modification will reduce the radius of the eddies and prevent - at least for some time - the destruction of the anti-cyclonic gyre in the center.

Cropex 2018 Grenoble
Daily report: Experiment 09

November 16, 2018

1 Initial conditions

The initial conditions used at the experiment are displayed at table 1.

Parameter	unit	value
Rotation period	s	60
Flow rate	$l\ s^{-1}$	0.8
ρ_{amb}	$kg\ m^{-3}$	999.9
ρ_{inlet}	$kg\ m^{-3}$	1010.1
h_i	m	0.406
Stratus		1 layer

Table 1: Initial conditions for the experiment

2 Objectives

We expect the decrease in the rotation period will reduce the size of the eddies and prevent - at least for some time - the destruction of the anti-cyclonic gyre in the center, allowing us to observe it for longer.

3 Methodology

The remaining dense water from the previous experiment was drained leaving a bottom layer of negligible height and density $\rho = 1000.0\ kg\ m^{-3}$. White particles and titanium dioxide were added to the inlet flow to allow ADV measurements and visualization of the inflow dynamics. Floaters were added to the surface to allow a brief visualization of the surface flow. When the movement of the floaters allowed the identification of a surface gyre, a fillet of red ink mixed with ethanol was thrown over it to reveal its behavior.

Rotation period was reduced to $60s$ - half of its previous value - in order to reduce the radius of deformation by half.

Data was collected using 3 conductivity probes (cp0, cp1 and cp3), one ADV profiler, one ADV and 2 gopro cameras tied to the metal structure on the top of the rotating table - see Figure 1. More details about the tank configuration are documented at the file *one_geostrophic_source.dxf*.

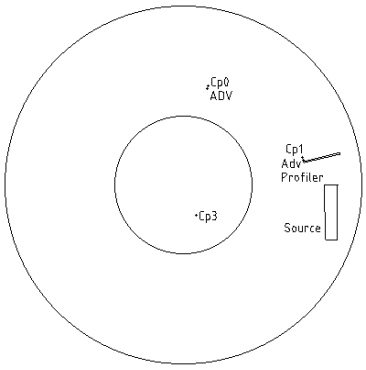

Figure 1: Experiment configuration.

4 Field Observations

As expected, when concerning the previous experiment, the eddies formed close to the inlet were smaller and to moved closer to the border. A weak, but persistent, anti-cyclonic circulation was observed in the center. In contrast to the previous experiment, eddies were not observed to have entered the center.

Data obtained at the end of the experiment is shown at table 2:

Parameter	unit	value
h_f	m	0.438
Duration	min	86

Table 2: Data collected at the end of the experiment.

5 Discussion and notes for next experiments

Although the experiment has produced the expected behavior, we believe a rotation period of 120 s provides better conditions to study the eddies that forms close to the source. Another experiment shall be performed in the afternoon with a lower flow rate in order increase the distance of eddies from the border of the tank. A two layers configuration will be used in order to verify possible changes at the formation of the central gyre.

Cropex 2018 Grenoble
Daily report: Experiment 10

November 16, 2018

1 Initial conditions

The initial conditions used at the experiment are displayed at table 1.

Parameter	unit	value
Rotation period	s	60
Flow rate	$l\ s^{-1}$	0.4
ρ_{amb}	$kg\ m^{-3}$	999.7
ρ_{bottom}	$kg\ m^{-3}$	1007.1
ρ_{inlet}	$kg\ m^{-3}$	1010.1
h_i	m	0.438
h_{bottom}	m	0.14
Stratus		2 layers

Table 1: Initial conditions for the experiment

2 Objectives

Regarding the last experiment, we expect the satellite eddied to form further from the border. We used a 2 layers configuration because we had not enough time to prepare and homogeneous configuration for this experiment.

3 Methodology

Water from the previous experiment was let to rest until solid body rotation was achieved. Bottom layer height was measured by knowing the vertical speed of the central conductivity probe - *Cp3* and the pulse width of the peak of salinity.

White particles and titanium dioxide were added to the inlet flow to allow ADV measurements and visualization of the inflow dynamics. Floaters were added to the surface to allow a brief visualization of the surface flow. When the movement of the floaters allowed the identification of a surface gyre, a fillet of red ink mixed with ethanol was thrown over it to reveal its behavior.

Data was collected using 3 conductivity probes (cp0, cp1 and cp3), one ADV profiler, one ADV - see Figure 1 - and 2 gopro cameras tied to the metal structure on the top

of the rotating table. More details about the tank configuration are documented at the file *one_geostrophic_source.dxf*.

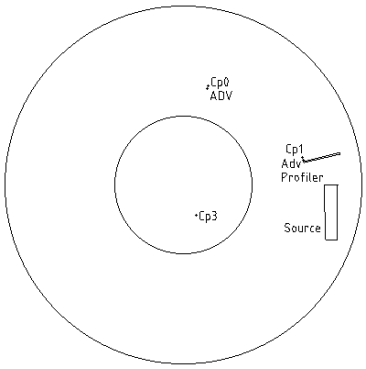

Figure 1: Experiment configuration.

4 Field Observations

Cyclonic satellite eddies were observed to form close to the inlet. As expected, by decreasing the input flow rate, the eddies path moved further from the border when regarding the path observed in the previous experiment. No clear gyre was observed to form in the surface of the central basin, but anti-cyclonic eddies were observed to form in the bottom. We are not sure if this anti-cyclonic eddies were formed in the interface between the tank bottom and the bottom layer or in the interface between the bottom layer and the ambient layer.

Data obtained at the end of the experiment is shown at table 2:

Parameter	unit	value
h_f	m	0.454
Duration	min	78

Table 2: Data collected at the end of the experiment.

5 Discussion and notes for next experiments

We decided the observations from this experiment are not enough to draw any conclusions. We might replicate this experiment changing some conditions and using PIV to get more detailed data. Nevertheless, the reduction in the inlet flow was observed to produced dynamic that may be too slow or too weak for our proposes.

Cropex 2018 Grenoble
Daily report: Experiment 12

November 23, 2018

1 Initial conditions

The initial conditions used for the experiment are displayed in table 1.

Parameter	unit	value
Rotation period	s	120
Flow rate	$l\ s^{-1}$	0.8
ρ_{amb}	$kg\ m^{-3}$	999.1
ρ_{inlet}	$kg\ m^{-3}$	1010.3
h_i	m	0.574
Stratus		1 layer

Table 1: Initial conditions for the experiment

Table 2 shows the adimensional numbers computed for the experiment:

Rossby number	0.0763944
Rossby radius (R_D)	0.5182455
Burger number (Bu)	0.0518245
Nof	1.3053652
Γ	0.2634045

Table 2: Adimensional numbers for the experiment

2 Objectives

We expect to observe the formation of satellite cyclonic eddies close to the dense water inlet and the appearance of an anti-cyclonic gyre at the surface of the cental basin. Moreover, regarding the computed values for R_D and Γ, we expect the dynamics in the central gyre to develop, predominantly, as a result from the ambient layer compression with limited influence of the satellite eddies due to their size. Satellite eddies are expected to move far from the center and to have a low shedding frequency when compared to experiments performed in shallower conditions ($h_i \approx 0.4\ m$).

3 Methodology

Data was collected using 3 conductivity probes (cp0, cp1 and cp3), one ADV profiler, one ADV - see Figure 2 - 2 gopro cameras tied to the metal structure on the top of the rotating table and 4 high resolution cameras for PIV analysis. More details about the tank configuration are documented in the file *one_geostrophic_source.dxf*.

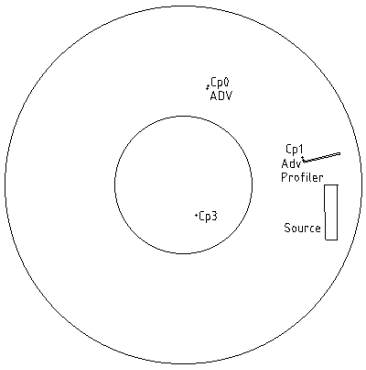

Figure 1: Experiment configuration.

Fluid motion was registered with a laser and high resolution cameras for posterior PIV analysis. The laser was configured to illuminate 11 layers, covering a total height of 40 cm with 4 cm gap between each level, as detailed at Table 3. This table - along with Figure 2 - also documents an inclination of the laser sheet. The deepest level was located at 13.8 cm from the bottom in the center. The laser started from the higher level and moved downwards in $660s$, stopping at each level to allow pictures to be taken. The laser is slightly inclined downwards. The laser rotating motor was powered with 2.97 V.

h_c (cm)	h_s (cm)	L_{motor} (mm)
13.8	7	1000
17.8	11	960
21.8	15	920
25.8	19	880
29.8	23	840
33.8	27	800
37.8	31	760
41.8	35	720
45.8	39	680
49.8	43	640
53.8	47	600

Table 3: Positions used for laser layers

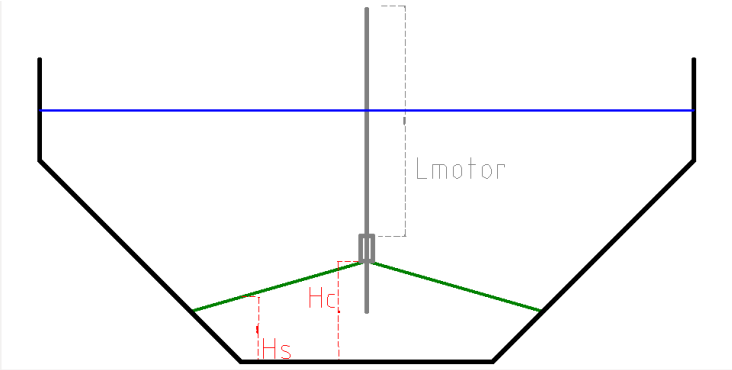

Figure 2: Heights used on Table 3.

A solution with nanoscopic particles was added to the fluid in order to provide information for the PIV analysis.

Among the high resolution cameras are two PCO, 1 JAI and 1 Nikon D850. The Nikon was positioned pointing to the center of the tank with a 14mm lens in order to cover most of the tank surface. Table 4 display the shooting frequency for each camera. Nikon images were compressed to jpg format in order to decrease dimensions of each image, and thus enable storing more images (5 times more) on the memory card.

Camera	Freq (Hz)
PCO 1	2
PCO 2	2
JAI	2
Nikon D850	0.5

Table 4: Shooting frequency for each camera.

Surface water was removed at a similar rate as dense water was injected.

4 Field Observations

We observed that the particles at the surface are not as abundant as the particles close to the bottom. To prevent this, we suggest to mix the water 2 hours before the start of the experiment. Conductivity probe *cp 0* was observed not to work properly and its measurements should not be considered for this experiment.

Data obtained at the end of the experiment is shown in table 5:

Parameter	unit	value
h_f	m	0.578
Duration	min	120

Table 5: Data collected at the end of the experiment.

5 Discussion and notes for next experiments

The results of the PIV analysis were not satisfactory. We observed that the estimated circulation patterns were noisy and with a lot of spurious velocity vectors. We believe the bad quality of data may result from image compression, lack of scatters in the observed layer or low shooting frequency. To better understand the role played by each of those factors, we will acquire images - for a short duration - changing each of the factors and compare the results. We will then use the best setting on next experiment.

Cropex 2018 Grenoble
Daily report: Experiment 13

November 27, 2018

1 Initial conditions

The initial conditions used for the experiment are displayed in table 1.

Parameter	unit	value
Rotation period	s	60
Flow rate	$l\ s^{-1}$	0.8
ρ_{amb}	$kg\ m^{-3}$	999
ρ_{inlet}	$kg\ m^{-3}$	1021.1
h_i	m	0.577
Stratus		1 layer

Table 1: Initial conditions for the experiment

Table 2 shows the adimensional numbers computed for the experiment:

Rossby number	0.0381972
Rossby radius (R_D)	0.3632366
Burger number (Bu)	0.0363237
Nof	1.281061
Γ	0.2664045

Table 2: Adimensional numbers for the experiment

2 Objectives

We expect to observe the formation of satellite cyclonic eddies close to the dense water inlet and the appearance of an anti-cyclonic gyre at the surface of the cental basin. Moreover, regarding the computed values for R_D and Γ, we expect the dynamics in the central gyre to develop, predominantly, as a result from the ambient layer compression with very low influence of the satellite eddies due to their reduced size. Satellite eddies are expected to move far from the center and to have a low shedding frequency when compared to experiments performed in shallower conditions ($h_i \approx 0.4\ m$).

3 Methodology

Data was collected using 3 conductivity probes (cp0, cp1 and cp3), one ADV profiler, one ADV - see Figure 2 - 2 gopro cameras tied to the metal structure on the top of the rotating table and 4 high resolution cameras for PIV analysis. More details about the tank configuration are documented in the file *one_geostrophic_source.dxf*.

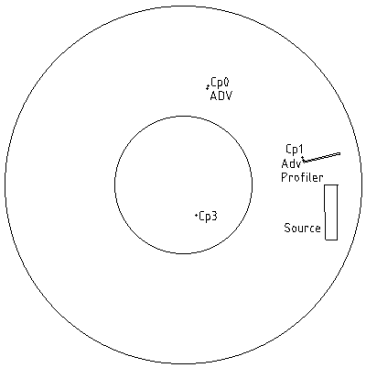

Figure 1: Experiment configuration.

Fluid motion was registered with a laser and high resolution cameras for posterior PIV analysis. The laser was configured to illuminate 12 layers, covering a total height of 44 *cm* with 4 *cm* gap between each level, as detailed at Table 3. This table - along with Figure 2 - also documents an inclination of the laser sheet. The deepest level was located at 13.8 *cm* from the bottom in the center. The laser started from the higher level and moved downwards in 60s, stopping at each level to allow pictures to be taken. It took 30s to position the laser in the upper layer again and restart the acquisition. Four pictures were taken for each level. The laser rotating motor was powered with 3.04 V.

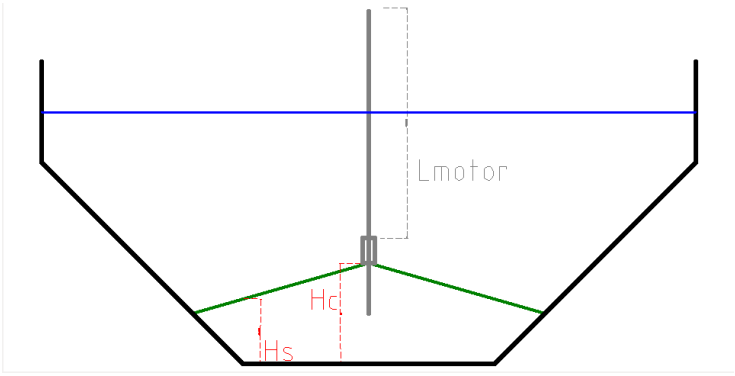

Figure 2: Heights used on Table 3.

A solution with nanoscopic particles was added to the ambient and to the inlet fluid

h_c (cm)	h_s (cm)	L_{motor} (mm)
13.8	7	1000
17.8	11	960
21.8	15	920
25.8	19	880
29.8	23	840
33.8	27	800
37.8	31	760
41.8	35	720
45.8	39	680
49.8	43	640
53.8	47	600
57.8	51	560

Table 3: Positions used for laser layers

in order to provide information for the PIV analysis. Bleach was dissolved in the solution before introducing it to the tank in order to prevent the late appearance of organism in the water, which compromises visibility and the quality of further experiments.

Among the high resolution cameras are 2 PCO, 1 JAI and 1 Nikon D850. The Nikon was positioned pointing to the center of the tank with a 14mm lens in order to cover most of the tank surface. Table 4 display the shooting frequency for each camera. Nikon images were compressed to jpg format in order to decrease dimensions of each image, and thus enable storing more images (5 times more) on the memory card.

Before starting injecting water, the layers were scanned once in order to register the initial conditions of the fluid.

Camera	Freq (Hz)
PCO 1	1
PCO 2	1
JAI	1
Nikon D850	1

Table 4: Shooting frequency for each camera.

Surface water was removed at a similar rate as dense water was injected.

4 Field Observations

Data obtained at the end of the experiment is shown in table 5:

Density measured at the end of the experiment, close to cp3, was 1014.4 $kg\ m^{-3}$.

Parameter	unit	value
h_f	m	0.577
Duration	min	120

Table 5: Data collected at the end of the experiment.

5 Discussion and notes for next experiments

We observed a notable difference of particles abundance and water transparency when compare to the last experiment. The main factor compromising the quality of the previous experiment was discovered to be a decrease in water visibility due to the development of organisms. Image compression was not observed to have significant implications of the final result of PIV analysis.

Cropex 2018 Grenoble
Daily report: Experiment 14

November 28, 2018

1 Initial conditions

The initial conditions used for the experiment are displayed in table 1.

Parameter	unit	value
Rotation period	s	120
Flow rate	$l\ s^{-1}$	0.8
ρ_{amb}	$kg\ m^{-3}$	999.2
ρ_{inlet}	$kg\ m^{-3}$	1010.4
h_i	m	0.575
Stratus		1 layer

Table 1: Initial conditions for the experiment

Table 2 shows the adimensional numbers computed for the experiment:

Rossby number	0.0763944
Rossby radius (R_D)	0.5183199
Burger number (Bu)	0.051832
Nof	1.3052353
Γ	0.2644045

Table 2: Adimensional numbers for the experiment

2 Objectives

This experiment intents to repeat experiment 12 within conditions that allow PIV analysis with the captured images.

We expect to observe the formation of satellite cyclonic eddies close to the dense water inlet and the appearance of an anti-cyclonic gyre at the surface of the cental basin. Moreover, regarding the computed values for R_D and Γ, we expect the dynamics in the central gyre to develop, predominantly, as a result from the ambient layer compression with limited influence of the satellite eddies due to their size. Satellite eddies are expected to move far from the center and to have a low shedding frequency when compared to experiments performed in shallower conditions ($h_i \approx 0.4\ m$).

3 Methodology

Data was collected using 3 conductivity probes (cp0, cp1 and cp3), one ADV profiler, one ADV - see Figure 2 - 2 gopro cameras tied to the metal structure on the top of the rotating table and 4 high resolution cameras for PIV analysis. More details about the tank configuration are documented in the file *one_geostrophic_source.dxf*.

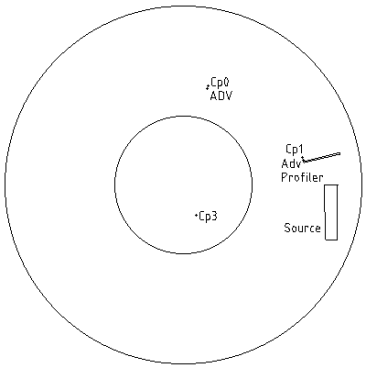

Figure 1: Experiment configuration.

Fluid motion was registered with a laser and high resolution cameras for posterior PIV analysis. The laser was configured to illuminate 12 layers, covering a total height of 44 *cm* with 4 *cm* gap between each level, as detailed at Table 3. This table - along with Figure 2 - also documents an inclination of the laser sheet. The deepest level was located at 13.8 *cm* from the bottom in the center. The laser started from the higher level and moved downwards in 60s, stopping at each level to allow pictures to be taken. It took 30s to position the laser in the upper layer again and restart the acquisition. Three pictures are taken for each level. The laser rotating motor was powered with 3.00 V.

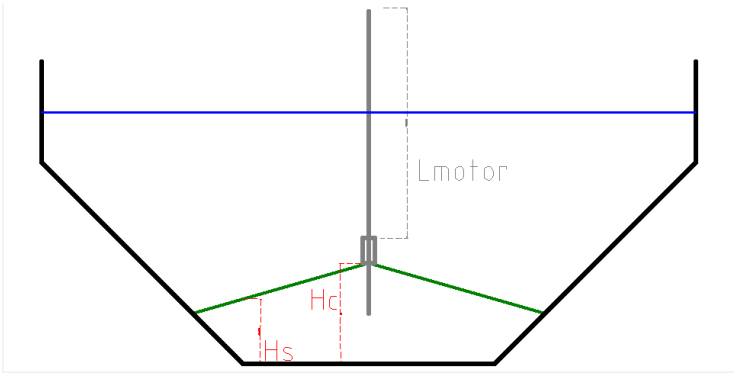

Figure 2: Heights used on Table 3.

The water was shaken two hours before the experiment in order to spread the

h_c (cm)	h_s (cm)	L_{motor} (mm)
13.8	7	1000
17.8	11	960
21.8	15	920
25.8	19	880
29.8	23	840
33.8	27	800
37.8	31	760
41.8	35	720
45.8	39	680
49.8	43	640
53.8	47	600
57.8	51	560

Table 3: Positions used for laser layers

nanoscopic particles that remained from the previous experiment. No particles were added at the ambient water since the last experiment, but the inlet flow was mixed with particles. Bleach was dissolved in the solution before introducing it to the tank in order to prevent the late appearance of organism in the water, which compromises visibility and the quality of further experiments.

Among the high resolution cameras are 2 PCO, 1 JAI and 1 Nikon D850. The Nikon was positioned pointing to the center of the tank with a 14mm lens in order to cover most of the tank surface. Table 4 display the shooting frequency for each camera. Nikon images were compressed to jpg format in order to decrease dimensions of each image, and thus enable storing more images (5 times more) on the memory card.

Before starting injecting water, the layers were scanned twice in order to register the initial conditions of the fluid.

Camera	Freq (Hz)
PCO 1	1
PCO 2	1
JAI	1
Nikon D850	1

Table 4: Shooting frequency for each camera.

Surface water was removed at a similar rate as dense water was injected.

4 Field Observations

Data obtained at the end of the experiment is shown in table 5:

Parameter	unit	value
h_f	m	0.575
Duration	min	134

Table 5: Data collected at the end of the experiment.

We observed a strong residual motion present in the beginning of the experiment. This residual motion is documented in the first two set of layer images. Density measured at the bottom in the end of the experiment, close to cp3, was 1006.4 $kg\ m^{-3}$.

5 Discussion and notes for next experiments

We believe the strong and persistent residual motion observed before the start of the experiment originates from the events of emptying and refilling the tank. For next experiment, the water will be leveled in the day before and left to rest at night.

Cropex 2018 Grenoble
Daily report: Experiment 15

November 28, 2018

1 Initial conditions

The initial conditions used for the experiment are displayed in table 1.

Parameter	unit	value
Rotation period	s	130
Flow rate	$l\ s^{-1}$	0.8
ρ_{amb}	$kg\ m^{-3}$	999.3
ρ_{inlet}	$kg\ m^{-3}$	1010.4
h_i	m	0.39
Stratus		1 layer

Table 1: Initial conditions for the experiment

Table 2 shows the adimensional numbers computed for the experiment:

Rossby number	0.0827606
Rossby radius (R_D)	0.5025097
Burger number (Bu)	0.050251
Nof	1.4013101
Γ	0.0794045

Table 2: Adimensional numbers for the experiment

2 Objectives

We expect to observe the formation of satellite cyclonic eddies close to the dense water inlet and the appearance of an anti-cyclonic gyre at the surface of the cental basin. Moreover, regarding the computed values for R_D and Γ, we expect the dynamics in the central gyre to suffer a noticeable influence from satellite gyres due to the increase in their shedding frequency and intensity when compared to experiments performed with a deeper basin - $h_i \approx 0.6\ m$.

3 Methodology

Data was collected using 3 conductivity probes (cp0, cp1 and cp3), one ADV profiler, one ADV - see Figure 2 - 2 gopro cameras tied to the metal structure on the top of the rotating table and 4 high resolution cameras for PIV analysis. More details about the tank configuration are documented in the file *one_geostrophic_source.dxf*.

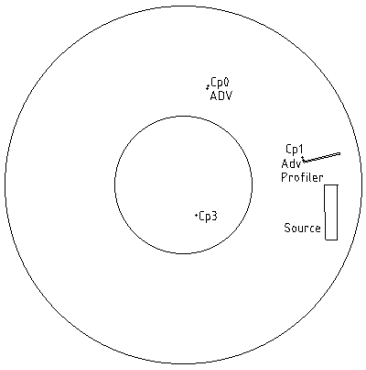

Figure 1: Experiment configuration.

Fluid motion was registered with a laser and high resolution cameras for posterior PIV analysis. The laser was configured to illuminate 12 layers, covering a total height of 24 cm with 2 cm gap between each level - except by the deeper gat which has a height of 4 cm - as detailed at Table 3. This table - along with Figure 2 - also documents an inclination of the laser sheet. The deepest level was located at 13.8 cm from the bottom in the center. The laser started from the higher level and moved downwards in 60s, stopping at each level to allow pictures to be taken. It took 30s to position the laser in the upper layer again and restart the acquisition. Three pictures are taken for each level. The laser rotating motor was powered with 3.00 V.

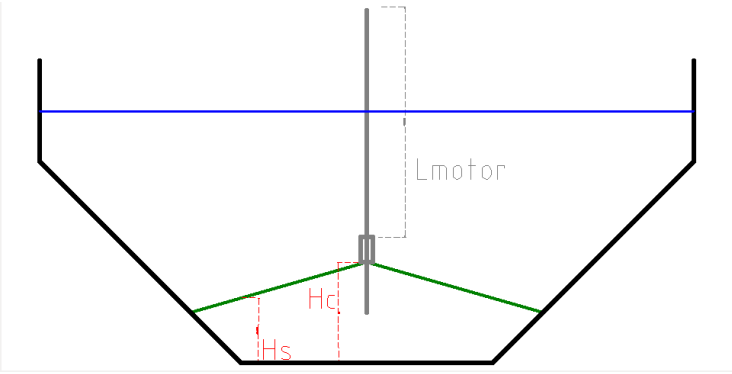

Figure 2: Heights used on Table 3.

h_c (cm)	h_s (cm)	L_{motor} (mm)
13.8	7	1000
15.8	9	960
17.8	11	940
19.8	13	920
21.8	15	900
23.8	17	880
25.8	19	860
27.8	21	840
29.8	23	820
31.8	25	800
33.8	27	780
35.8	29	760

Table 3: Positions used for laser layers

The water was shaken two hours before the experiment in order to spread the nanoscopic particles that remained from the previous experiment. No particles were added to the ambient water since the last experiment, but the inlet flow was mixed with particles. Bleach was dissolved in the solution before introducing it to the tank in order to prevent the late appearance of organism in the water, which compromises visibility and the quality of further experiments.

Among the high resolution cameras are 2 PCO, 1 JAI and 1 Nikon D850. The Nikon was positioned pointing to the center of the tank with a 14mm lens in order to cover most of the tank surface. Table 4 display the shooting frequency for each camera. Nikon images were compressed to jpg format in order to decrease dimensions of each image, and thus enable storing more images (5 times more) on the memory card.

Before starting injecting water, the layers were scanned twice in order to register the initial conditions of the fluid.

Camera	Freq (Hz)
PCO 1	1
PCO 2	1
JAI	1
Nikon D850	1

Table 4: Shooting frequency for each camera.

Surface water was removed at a similar rate as dense water was injected. The rotation period was increased from 120s to 130s half an hour before the experiment in order to remove the residual motion.

4 Field Observations

We observed a weak residual motion present in the beginning of the experiment. This residual motion is documented in the first two set of layer images.

Data obtained at the end of the experiment is shown in table 5:

Parameter	unit	value
h_f	m	0.390
Duration	min	134

Table 5: Data collected at the end of the experiment.

Density measured at the bottom in the end of the experiment, close to cp3, was 1006.4 $kg\ m^{-3}$.

5 Discussion and notes for next experiments

To prevent residual motion on next experiment, the level of the tank will be adjusted in the night before the experiment.

Cropex 2018 Grenoble
Daily report: Experiment 16

November 28, 2018

1 Initial conditions

The initial conditions used for the experiment are displayed in table 1.

Parameter	unit	value
Rotation period	s	60
Flow rate	$l\ s^{-1}$	0.8
ρ_{amb}	$kg\ m^{-3}$	999.5
ρ_{inlet}	$kg\ m^{-3}$	1020
h_i	m	0.39
Stratus		1 layer

Table 1: Initial conditions for the experiment

Table 2 shows the adimensional numbers computed for the experiment:

Rossby number	0.0381972
Rossby radius (R_D)	0.3144209
Burger number (Bu)	0.0314421
Nof	1.1886675
Γ	0.0794045

Table 2: Adimensional numbers for the experiment

2 Objectives

We expect to observe the formation of satellite cyclonic eddies close to the dense water inlet and the appearance of an anti-cyclonic gyre at the surface of the cental basin. Moreover, regarding the computed values for R_D and Γ, we expect the dynamics in the central gyre to suffer a noticeable influence from satellite gyres due to the increase in their shedding frequency and intensity when compared to experiments performed with a deeper basin - $h_i \approx 0.6\ m$.

3 Methodology

Data was collected using 3 conductivity probes (cp0, cp1 and cp3), one ADV profiler, one ADV - see Figure 2 - 2 gopro cameras tied to the metal structure on the top of the rotating table and 4 high resolution cameras for PIV analysis. More details about the tank configuration are documented in the file *one_geostrophic_source.dxf*.

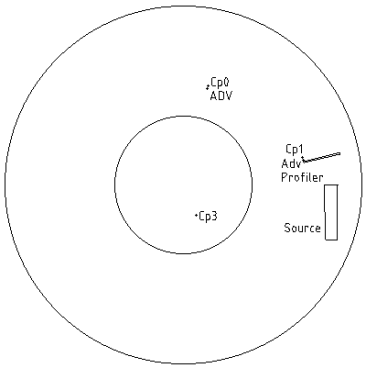

Figure 1: Experiment configuration.

Fluid motion was registered with a laser and high resolution cameras for posterior PIV analysis. The laser was configured to illuminate 12 layers, covering a total height of 24 cm with 2 cm gap between each level - except by the deeper gat which has a height of 4 cm - as detailed at Table 3. This table - along with Figure 2 - also documents an inclination of the laser sheet. The deepest level was located at 13.8 cm from the bottom in the center. The laser started from the higher level and moved downwards in 60s, stopping at each level to allow pictures to be taken. It took 30s to position the laser in the upper layer again and restart the acquisition. Three pictures are taken for each level. The laser rotating motor was powered with 3.00 V.

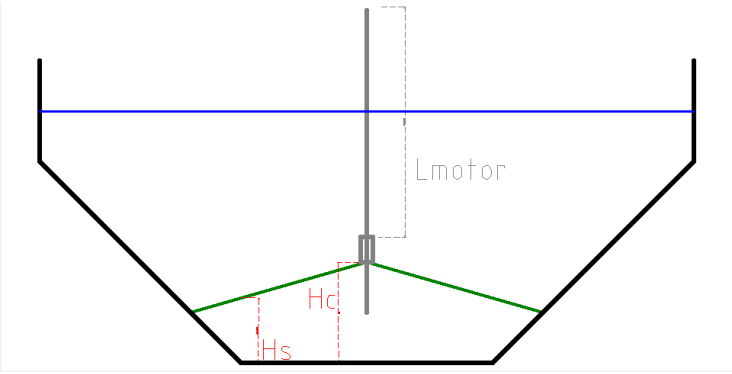

Figure 2: Heights used on Table 3.

h_c (cm)	h_s (cm)	L_{motor} (mm)
13.8	7	1000
15.8	9	960
17.8	11	940
19.8	13	920
21.8	15	900
23.8	17	880
25.8	19	860
27.8	21	840
29.8	23	820
31.8	25	800
33.8	27	780
35.8	29	760

Table 3: Positions used for laser layers

The water was shaken two hours before the experiment in order to spread the nanoscopic particles that remained from the previous experiment. Particles were added to the ambient water since the last experiment and the inlet flow was mixed with particles. Bleach was dissolved in the solution before introducing it to the tank in order to prevent the late appearance of organism in the water, which compromises visibility and the quality of further experiments.

Among the high resolution cameras are 2 PCO, 1 JAI and 1 Nikon D850. The Nikon was positioned pointing to the center of the tank with a 14mm lens in order to cover most of the tank surface. Table 4 display the shooting frequency for each camera. Nikon images were compressed to jpg format in order to decrease dimensions of each image, and thus enable storing more images (5 times more) on the memory card.

Before starting injecting water, the layers were scanned twice in order to register the initial conditions of the fluid.

Camera	Freq (Hz)
PCO 1	1
PCO 2	1
JAI	1
Nikon D850	1

Table 4: Shooting frequency for each camera.

Surface water was removed at a similar rate as dense water was injected.

4 Field Observations

We observed a weak residual motion present in the beginning of the experiment. This residual motion is documented in the first two set of layer images.

Data obtained at the end of the experiment is shown in table 5:

Parameter	unit	value
h_f	m	391
Duration	min	132

Table 5: Data collected at the end of the experiment.

Density measured at the bottom in the end of the experiment, close to cp3, was 1015.3 $kg\ m^{-3}$.

5 Discussion and notes for next experiments

Cropex 2018 Grenoble
Daily report: Experiment 17

November 29, 2018

1 Initial conditions

The initial conditions used for the experiment are displayed in table 1.

Parameter	unit	value
Rotation period	s	60
Flow rate	$l\ s^{-1}$	0.8
ρ_{amb}	$kg\ m^{-3}$	999.5
ρ_{bottom}	$kg\ m^{-3}$	1009.8
ρ_{inlet}	$kg\ m^{-3}$	1020
h_{bootom}	m	0.159
h_{amb}	m	0.231
h_i	m	0.39
Stratus		2 layer

Table 1: Initial conditions for the experiment

Table 2 shows the adimensional numbers computed for the experiment:

Rossby number	0.0381972
Rossby radius (R_D)	0.3144209
Burger number (Bu)	0.0314421
Nof	1.1886675
Γ	0.0794045

Table 2: Adimensional numbers for the source

2 Objectives

3 Methodology

Data was collected using 3 conductivity probes (cp0, cp1 and cp3), one ADV profiler, one ADV - see Figure 2 - 2 gopro cameras tied to the metal structure on the top of the rotating table and 4 high resolution cameras for PIV analysis. More details about the tank configuration are documented in the file *one_geostrophic_source.dxf*.

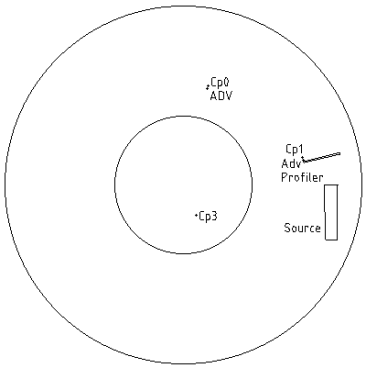

Figure 1: Experiment configuration.

Fluid motion was registered with a laser and high resolution cameras for posterior PIV analysis. The laser was configured to illuminate 12 layers, covering a total height of 24 cm with 2 cm gap between each level - except by the deeper gap which has a height of 4 cm - as detailed at Table 4. This table - along with Figure 2 - also documents an inclination of the laser sheet. The deepest level was located at 13.8 cm from the bottom in the center. The laser started from the higher level and moved downwards in 60s, stopping at each level to allow pictures to be taken. It took 30s to position the laser in the upper layer again and restart the acquisition. Three pictures are taken for each level. The laser rotating motor was powered with 3.00 V.

h_c (cm)	h_s (cm)	L_{motor} (mm)
13.8	7	1000
15.8	9	960
17.8	11	940
19.8	13	920
21.8	15	900
23.8	17	880
25.8	19	860
27.8	21	840
29.8	23	820
31.8	25	800
33.8	27	780
35.8	29	760

Table 3: Positions used for laser layers

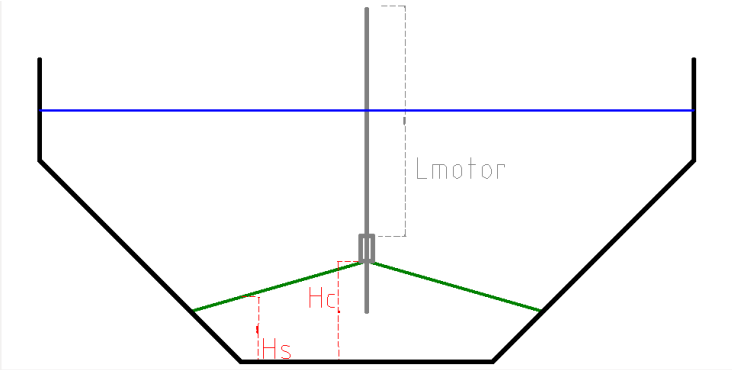

Figure 2: Heights used on Table 4.

Among the high resolution cameras are 2 PCO, 1 JAI and 1 Nikon D850. The Nikon was positioned pointing to the center of the tank with a 14mm lens in order to cover most of the tank surface. Table 5 display the shooting frequency for each camera. Nikon images were compressed to jpg format in order to decrease dimensions of each image, and thus enable storing more images (5 times more) on the memory card.

Before starting injecting water, the layers were scanned twice in order to register the initial conditions of the fluid.

Camera	Freq (Hz)
PCO 1	1
PCO 2	1
JAI	1
Nikon D850	1

Table 4: Shooting frequency for each camera.

Surface water was removed at a similar rate as dense water was injected.

The two layer system was built from the final configuration of the previous experiment. Particles were added to the ambient water through the surface and the inlet flow was mixed with particles. Bleach was dissolved in the solution before introducing it to the tank in order to prevent the late appearance of organism in the water, which compromises visibility and the quality of further experiments.

4 Field Observations

Data obtained at the end of the experiment is shown in table 6:

Parameter	unit	value
h_f	m	0.39
Duration	min	132

Table 5: Data collected at the end of the experiment.

Density measured at the bottom in the end of the experiment, close to cp3, was 1013.5 $kg\ m^{-3}$.

5 Discussion and notes for next experiments

The particles added at the surface layer were not evenly spread over the fluid. We will try to overcome this by adding particles to the surface in events separated by a few minutes in order to let the particles permeate different heights of the layer.

Cropex 2018 Grenoble
Daily report: Experiment 18

November 30, 2018

1 Initial conditions

The initial conditions used for the experiment are displayed in table 1.

Parameter	unit	value
Rotation period	s	120
Flow rate	$l\ s^{-1}$	0.8
ρ_{amb}	$kg\ m^{-3}$	999
ρ_{inlet}	$kg\ m^{-3}$	1020
h_i	m	0.39
Stratus		1 layer

Table 1: Initial conditions for the experiment

Table 2 shows the adimensional numbers computed for the experiment:

Rossby number	0.0763944
Rossby radius (R_D)	0.6365433
Burger number (Bu)	0.0636543
Nof	2.435922
Γ	0.0794045

Table 2: Adimensional numbers for the experiment

2 Objectives

We expect to observe the formation of satellite cyclonic eddies close to the dense water inlet and the appearance of an anti-cyclonic gyre at the surface of the central basin. Moreover, regarding the computed values for R_D and Γ, we expect the dynamics in the central gyre to suffer a noticeable influence from satellite gyres due to the increase in their shedding frequency and intensity when compared to experiments performed with a deeper basin ($h_i \approx 0.6\ m$) or a smaller density difference between the inlet and the ambient water. ($\Delta\rho \approx 10\ kg\ m^{-3}$).

3 Methodology

Data was collected using 3 conductivity probes (cp0, cp1 and cp3), one ADV profiler, one ADV - see Figure 2 - 2 gopro cameras tied to the metal structure on the top of the rotating table and 4 high resolution cameras for PIV analysis. More details about the tank configuration are documented in the file *one_geostrophic_source.dxf*.

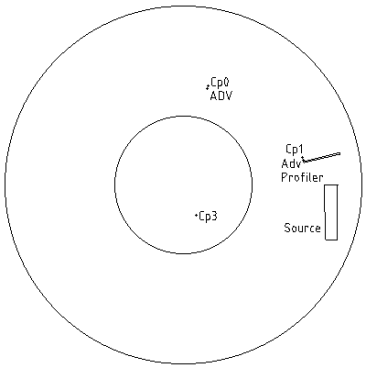

Figure 1: Experiment configuration.

Fluid motion was registered with a laser and high resolution cameras for posterior PIV analysis. The laser was configured to illuminate 12 layers, covering a total height of 24 cm with 2 cm gap between each level - except by the deeper gat which has a height of 4 cm - as detailed at Table 3. This table - along with Figure 2 - also documents an inclination of the laser sheet. The deepest level was located at 13.8 cm from the bottom in the center. The laser started from the higher level and moved downwards in 60s, stopping at each level to allow pictures to be taken. It took 30s to position the laser in the upper layer again and restart the acquisition. Three pictures are taken for each level. The laser rotating motor was powered with 3.00 V.

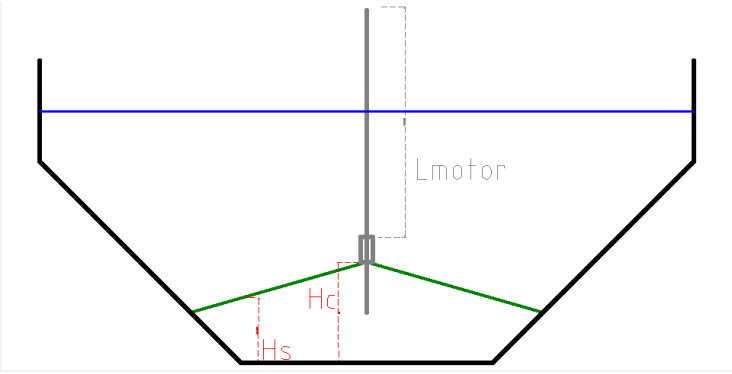

Figure 2: Heights used on Table 3.

h_c (cm)	h_s (cm)	L_{motor} (mm)
13.8	7	1000
15.8	9	960
17.8	11	940
19.8	13	920
21.8	15	900
23.8	17	880
25.8	19	860
27.8	21	840
29.8	23	820
31.8	25	800
33.8	27	780
35.8	29	760

Table 3: Positions used for laser layers

Among the high resolution cameras are 2 PCO, 1 JAI and 1 Nikon D850. The Nikon was positioned pointing to the center of the tank with a 14mm lens in order to cover most of the tank surface. Table 4 display the shooting frequency for each camera. Nikon images were compressed to jpg format in order to decrease dimensions of each image, and thus enable storing more images (5 times more) on the memory card.

Before starting injecting water, the layers were scanned twice in order to register the initial conditions of the fluid.

Camera	Freq (Hz)
PCO 1	1
PCO 2	1
JAI	1
Nikon D850	1

Table 4: Shooting frequency for each camera.

Surface water was removed at a similar rate as dense water was injected. The tank was drained and reffiled during the past night and particles were added to the ambient water. The inlet flow was mixed with particles and having bleach dissolved in the solution before introducing it to the tank in order to prevent the late appearance of organism in the water.

4 Field Observations

Data obtained at the end of the experiment is shown in table 5:

Parameter	unit	value
h_f	m	391
Duration	min	132

Table 5: Data collected at the end of the experiment.

5 Discussion and notes for next experiments

Cropex 2018 Grenoble
Daily report: Experiment 19

November 30, 2018

1 Initial conditions

The initial conditions used for the experiment are displayed in table 1.

Parameter	unit	value
Rotation period	s	110
Flow rate	$l\ s^{-1}$	0.8
ρ_{amb}	$kg\ m^{-3}$	999.5
ρ_{bottom}	$kg\ m^{-3}$	1006.2
ρ_{inlet}	$kg\ m^{-3}$	1004.2
h_{bootom}	m	0.2508
h_{amb}	m	0.1392
h_i	m	0.39
Stratus		2 layer

Table 1: Initial conditions for the experiment

Table 2 shows the adimensional numbers computed for the experiment:

Rossby number	0.0700282
Rossby radius (R_D)	0.2770961
Burger number (Bu)	0.0277096
Nof	0.5035667
Γ	0.0794045

Table 2: Adimensional numbers for the source

2 Objectives

3 Methodology

Data was collected using 3 conductivity probes (cp0, cp1 and cp3), one ADV profiler, one ADV - see Figure 2 - 2 gopro cameras tied to the metal structure on the top of the rotating table and 4 high resolution cameras for PIV analysis. More details about the tank configuration are documented in the file *one_geostrophic_source.dxf*.

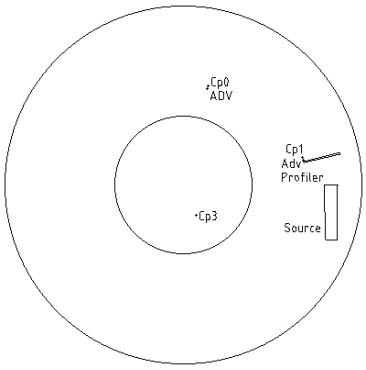

Figure 1: Experiment configuration.

Fluid motion was registered with a laser and high resolution cameras for posterior PIV analysis. The laser was configured to illuminate 12 layers, covering a total height of 24 cm with 2 cm gap between each level - except by the deeper gat which has a height of 4 cm - as detailed at Table 3. This table - along with Figure 2 - also documents an inclination of the laser sheet. The deepest level was located at 13.8 cm from the bottom in the center. The laser started from the higher level and moved downwards in 60s, stopping at each level to allow pictures to be taken. It took 30s to position the laser in the upper layer again and restart the acquisition. Three pictures are taken for each level. The laser rotating motor was powered with 3.00 V.

h_c (cm)	h_s (cm)	L_{motor} (mm)
13.8	7	1000
15.8	9	960
17.8	11	940
19.8	13	920
21.8	15	900
23.8	17	880
25.8	19	860
27.8	21	840
29.8	23	820
31.8	25	800
33.8	27	780
35.8	29	760

Table 3: Positions used for laser layers

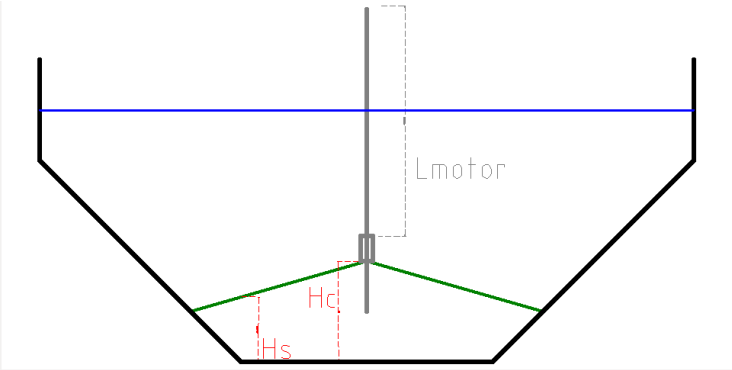

Figure 2: Heights used on Table 3.

Among the high resolution cameras are 2 PCO, 1 JAI and 1 Nikon D850. The Nikon was positioned pointing to the center of the tank with a 14mm lens in order to cover most of the tank surface. Table 4 display the shooting frequency for each camera. Nikon images were compressed to jpg format in order to decrease dimensions of each image, and thus enable storing more images (5 times more) on the memory card.

Before starting injecting water, the layers were scanned twice in order to register the initial conditions of the fluid.

Camera	Freq (Hz)
PCO 1	1
PCO 2	1
JAI	1
Nikon D850	1

Table 4: Shooting frequency for each camera.

Surface water was removed at a similar rate as dense water was injected.

The two layer system was built from the final configuration of the previous experiment. Particles were added to the ambient water through the surface and the inlet flow was mixed with particles. Bleach was dissolved in the solution before introducing it to the tank in order to prevent the late appearance of organism in the water, which compromises visibility and the quality of further experiments.

4 Field Observations

Data obtained at the end of the experiment is shown in table 5:

Parameter	unit	value
h_f	m	0.39
Duration	min	132

Table 5: Data collected at the end of the experiment.

5 Discussion and notes for next experiments

Cropex 2018 Grenoble
Daily report: Experiment 20

December 05, 2018

1 Initial conditions

The initial conditions used for the experiment are displayed in table 1.

Parameter	unit	value
Rotation period	s	120
Flow rate	$l\ s^{-1}$	0.8
ρ_{amb}	$kg\ m^{-3}$	999
ρ_{bottom}	$kg\ m^{-3}$	1009.1
ρ_{inlet}	$kg\ m^{-3}$	1018.7
h_{bootom}	m	0.16
h_{amb}	m	0.238
h_i	m	0.398
Stratus		2 layer

Table 1: Initial conditions for the experiment

Table 2 shows the adimensional numbers computed for the experiment:

Rossby number	0.0763944
Rossby radius (R_D)	0.6246127
Burger number (Bu)	0.0624613
Nof	2.2865991
Γ	0.0874045

Table 2: Adimensional numbers for the source

2 Objectives

3 Methodology

Data was collected using 3 conductivity probes (cp0, cp1 and cp3), one ADV profiler, one ADV - see Figure 2 - 2 gopro cameras tied to the metal structure on the top of the rotating table and 4 high resolution cameras for PIV analysis. More details about the tank configuration are documented in the file *one_geostrophic_source.dxf*.

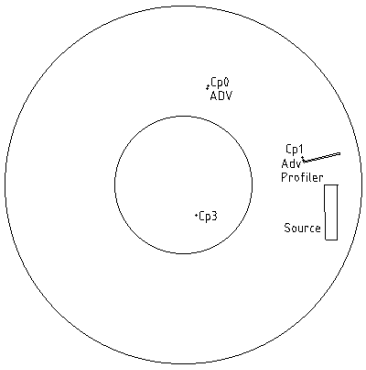

Figure 1: Experiment configuration.

Fluid motion was registered with a laser and high resolution cameras for posterior PIV analysis. The laser was configured to illuminate 12 layers, covering a total height of 24 cm with 2 cm gap between each level - except by the deeper gat which has a height of 4 cm - as detailed at Table 3. This table - along with Figure 2 - also documents an inclination of the laser sheet. The deepest level was located at 13.8 cm from the bottom in the center. The laser started from the higher level and moved downwards in 60s, stopping at each level to allow pictures to be taken. It took 30s to position the laser in the upper layer again and restart the acquisition. Three pictures are taken for each level. The laser rotating motor was powered with 3.00 V.

h_c (cm)	h_s (cm)	L_{motor} (mm)
13.8	7	1000
15.8	9	960
17.8	11	940
19.8	13	920
21.8	15	900
23.8	17	880
25.8	19	860
27.8	21	840
29.8	23	820
31.8	25	800
33.8	27	780
35.8	29	760

Table 3: Positions used for laser layers

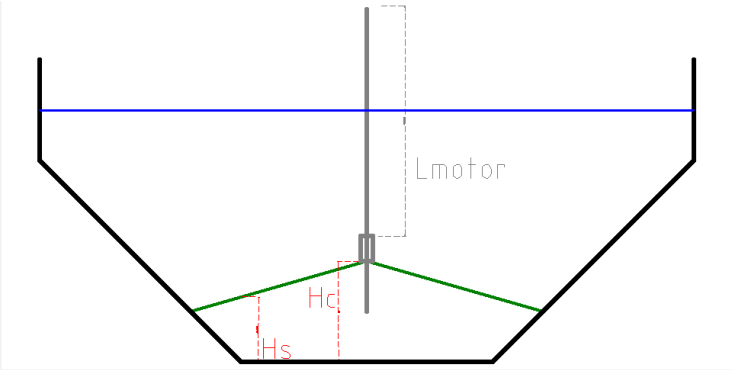

Figure 2: Heights used on Table 3.

Among the high resolution cameras are 2 PCO, 1 JAI and 1 Nikon D850. The Nikon was positioned pointing to the center of the tank with a 14mm lens in order to cover most of the tank surface. Table 4 display the shooting frequency for each camera. Nikon images were compressed to jpg format in order to decrease dimensions of each image, and thus enable storing more images (5 times more) on the memory card.

Before starting injecting water, the layers were scanned twice in order to register the initial conditions of the fluid.

Camera	Freq (Hz)
PCO 1	1
PCO 2	1
JAI	1
Nikon D850	1

Table 4: Shooting frequency for each camera.

A plastic plate was installed above the bottom inlet in order to prevent abrupt vertical currents to break the 2 layer interface. The stratification was then built by first injecting fresh water in the tank with a flow low enough to prevent the development of currents. After the injection was stopped, we waited 2 hour so the fresh water layer would achieve solid body rotation and then started to inject salt water with a density of 1010 $kg\ m^{-}3$. This process was done with a very small flow in order to create a interface between the two layers, but the flow was increased after the interface was already built. Then, after stopping the injection of salt water, floating inlets were added to the surface in order to complete the fresh water up to the desired level. Finally, the floaters were removed and the water was left to rest during the night in order to achieve solid body rotation.

Particles were added to the top and bottom layer and the inlet flow was mixed with particles. Bleach was dissolved in the solution before introducing it to the tank in order

to prevent the late appearance of organism in the water, which compromises visibility and the quality of further experiments. During the experiment, surface water was removed at a similar rate as dense water was injected.

4 Field Observations

Data obtained at the end of the experiment is shown in table 5:

Parameter	unit	value
h_f	m	.398
Duration	min	130

Table 5: Data collected at the end of the experiment.

Density measured at the bottom in the end of the experiment, close to cp3, was 1017.0 $kg\ m^{-3}$.

5 Discussion and notes for next experiments

After preparing the 2 layer stratification, we observed the bottom layer was static, but the surface layer had a very strong cyclone with a tryangular shape formed by three smaller cyclones. We belive the triangular shape was generated by the removal of the three floating inlets added to increase the thickness of the top layer. To prevent this condition, on the next experiment, instead of completing the volume of the surface layer with water at the surface, we will build the whole top layer at the first step.

Cropex 2018 Grenoble
Daily report: Experiment 21

December 06, 2018

1 Initial conditions

The initial conditions used for the experiment are displayed in table 1.

Parameter	unit	value
Rotation period	s	120
Flow rate	$l\ s^{-1}$	0.8
ρ_{amb}	$kg\ m^{-3}$	998.8
ρ_{bottom}	$kg\ m^{-3}$	1009
ρ_{inlet}	$kg\ m^{-3}$	1019
h_{bootom}	m	0.12
h_{amb}	m	0.447
h_i	m	0.567
Stratus		2 layer

Table 1: Initial conditions for the experiment

Table 2 shows the adimensional numbers computed for the experiment:

Rossby number	0.0763944
Rossby radius (R_D)	0.6935712
Burger number (Bu)	0.0693571
Nof	2.3445184
Γ	0.2564045

Table 2: Adimensional numbers for the source

2 Objectives

3 Methodology

Data was collected using 3 conductivity probes (cp0, cp1 and cp3), one ADV profiler, one ADV - see Figure 2 - 2 gopro cameras tied to the metal structure on the top of the rotating table and 4 high resolution cameras for PIV analysis. More details about the tank configuration are documented in the file *one_geostrophic_source.dxf*.

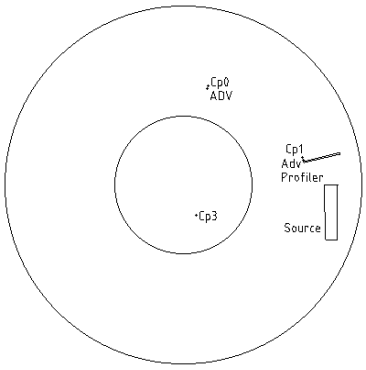

Figure 1: Experiment configuration.

Fluid motion was registered with a laser and high resolution cameras for posterior PIV analysis. The laser was configured to illuminate 12 layers, covering a total height of 44 cm with 4 cm gap between each level, as detailed at Table 3. This table - along with Figure 2 - also documents an inclination of the laser sheet. The deepest level was located at 13.8 cm from the bottom in the center. The laser started from the higher level and moved downwards in $60s$, stopping at each level to allow pictures to be taken. It took $30s$ to position the laser in the upper layer again and restart the acquisition. Three pictures are taken for each level. The laser rotating motor was powered with 3.00 V.

h_c (cm)	h_s (cm)	L_{motor} (mm)
13.8	7	1000
17.8	11	960
21.8	15	920
25.8	19	880
29.8	23	840
33.8	27	800
37.8	31	760
41.8	35	720
45.8	39	680
49.8	43	640
53.8	47	600
57.8	51	560

Table 3: Positions used for laser layers

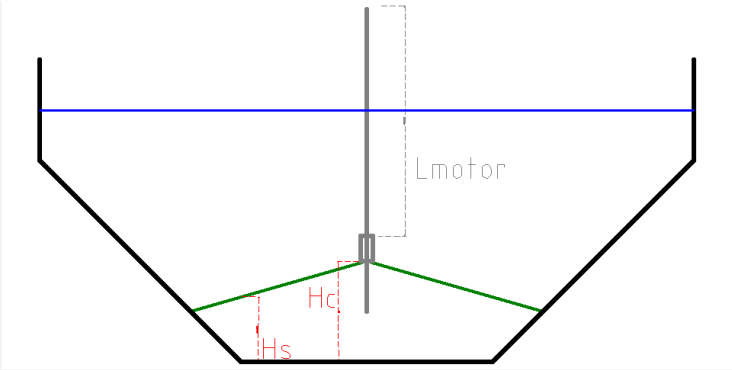

Figure 2: Heights used on Table 3.

Among the high resolution cameras are 2 PCO, 1 JAI and 1 Nikon D850. The Nikon was positioned pointing to the center of the tank with a 14mm lens in order to cover most of the tank surface. Table 4 display the shooting frequency for each camera. Nikon images were compressed to jpg format in order to decrease dimensions of each image, and thus enable storing more images (5 times more) on the memory card.

Before starting injecting water, the layers were scanned twice in order to register the initial conditions of the fluid.

Camera	Freq (Hz)
PCO 1	1
PCO 2	1
JAI	1
Nikon D850	1

Table 4: Shooting frequency for each camera.

A plastic plate was installed above the bottom inlet in order to prevent abrupt vertical currents to break the 2 layer interface. The stratification was then built by first injecting fresh water in the tank with a flow low enough to prevent the development of currents. After the injection was stopped, we waited 2 hour so the fresh water layer would achieve solid body rotation and then started to inject salt water with a density of 1010 $kg\ m^{-}3$. This process was done with a very small flow in order to create a interface between the two layers, but the flow was increased after the interface was already built. The system rested for the night until next day in order to achieve solid body rotation.

Particles were add at the free surface on the interval were the laser was moving upwards. Surface water was removed at a similar rate as dense water was injected.

4 Field Observations

Data obtained at the end of the experiment is shown in table 5:

Parameter	unit	value
h_f	m	0.567
Duration	min	138

Table 5: Data collected at the end of the experiment.

Density measured at the bottom in the end of the experiment, close to cp3, was 1016.0 $kg\ m^{-3}$.

5 Discussion and notes for next experiments

Cropex 2018 Grenoble
Daily report: Experiment 22

December 7, 2018

1 Initial conditions

The initial conditions used for the experiment are displayed in table 1.

Parameter	unit	value
Rotation period	s	120
Flow rate	$l\ s^{-1}$	0.8
ρ_{amb}	$kg\ m^{-3}$	998
ρ_{bottom}	$kg\ m^{-3}$	1018
ρ_{inlet}	$kg\ m^{-3}$	1008.7
h_{bootom}	m	0.108
h_{amb}	m	0.291
h_i	m	0.399
Stratus		2 layer

Table 1: Initial conditions for the experiment

Table 2 shows the adimensional numbers computed for the experiment:

Rossby number	0.0763944
Rossby radius (R_D)	0.4622588
Burger number (Bu)	0.0462259
Nof	1.2487679
Γ	0.0884045

Table 2: Adimensional numbers for the source

2 Objectives

3 Methodology

Data was collected using 3 conductivity probes (cp0, cp1 and cp3), one ADV profiler, one ADV - see Figure 2 - 2 gopro cameras tied to the metal structure on the top of the rotating table and 4 high resolution cameras for PIV analysis. More details about the tank configuration are documented in the file *one_geostrophic_source.dxf*.

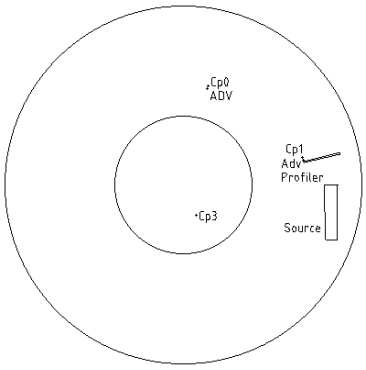

Figure 1: Experiment configuration.

Fluid motion was registered with a laser and high resolution cameras for posterior PIV analysis. The laser was configured to illuminate 12 layers, covering a total height of 24 cm with 2 cm gap between each level - except by the deeper gat which has a height of 4 cm - as detailed at Table 3. This table - along with Figure 2 - also documents an inclination of the laser sheet. The deepest level was located at 13.8 cm from the bottom in the center. The laser started from the higher level and moved downwards in 60s, stopping at each level to allow pictures to be taken. It took 30s to position the laser in the upper layer again and restart the acquisition. Three pictures are taken for each level. The laser rotating motor was powered with 3.00 V.

h_c (cm)	h_s (cm)	L_{motor} (mm)
13.8	7	1000
15.8	9	960
17.8	11	940
19.8	13	920
21.8	15	900
23.8	17	880
25.8	19	860
27.8	21	840
29.8	23	820
31.8	25	800
33.8	27	780
35.8	29	760

Table 3: Positions used for laser layers

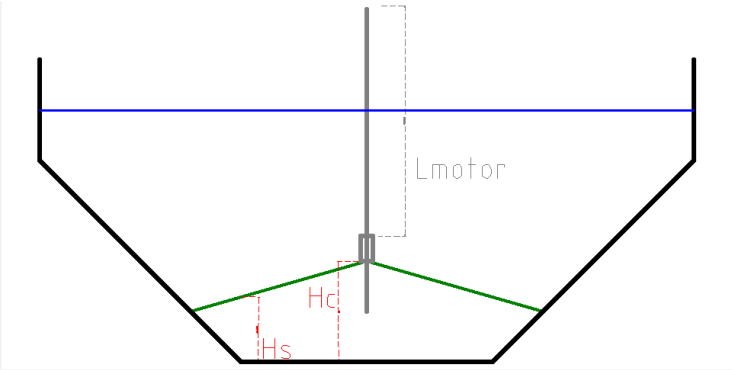

Figure 2: Heights used on Table 3.

Among the high resolution cameras are 2 PCO, 1 JAI and 1 Nikon D850. The Nikon was positioned pointing to the center of the tank with a 14mm lens in order to cover most of the tank surface. Table 4 display the shooting frequency for each camera. Nikon images were compressed to jpg format in order to decrease dimensions of each image, and thus enable storing more images (5 times more) on the memory card.

Before starting injecting water, the layers were scanned twice in order to register the initial conditions of the fluid.

Camera	Freq (Hz)
PCO 1	1
PCO 2	1
JAI	1
Nikon D850	1

Table 4: Shooting frequency for each camera.

A plastic plate was installed above the bottom inlet in order to prevent abrupt vertical currents to break the 2 layer interface. The stratification was then built by first injecting fresh water in the tank with a flow low enough to prevent the development of currents. After the injection was stopped, we waited 2 hour so the fresh water layer would achieve solid body rotation and then started to inject salt water with a density of 1020 $kg\ m^{-}3$. This process was done with a very small flow in order to create a interface between the two layers, but the flow was increased after the interface was already built. The system rested for the night until next day in order to achieve solid body rotation.

Particles were add at the free surface on the interval were the laser was moving upwards. Surface water was removed at a similar rate as dense water was injected.

4 Field Observations

There was air exiting from the boarder few minutes after starting the experiment. It creates some perturbations at the surface. Data obtained at the end of the experiment is shown in table 5:

Parameter	unit	value
h_f	m	0.397
Duration	min	132

Table 5: Data collected at the end of the experiment.

Density measured at the bottom in the end of the experiment, close to cp3, was 1017.0 $kg\ m^{-3}$.

5 Discussion and notes for next experiments

Cropex 2018 Grenoble
Daily report: Experiment 23

December 10, 2018

1 Initial conditions

The initial conditions used for the experiment are displayed in table 1.

Parameter	unit	value
Rotation period	s	120
Flow rate	$l\ s^{-1}$	0.8
ρ_{amb}	$kg\ m^{-3}$	999
ρ_{inlet}	$kg\ m^{-3}$	1020.3
h_i	m	0.4
Stratus		1 layer

Table 1: Initial conditions for the experiment

Table 2 shows the adimensional numbers computed for the experiment:

Rossby number	0.0763944
Rossby radius (R_D)	0.6510888
Burger number (Bu)	0.0651089
Nof	2.4703538
Γ	0.0894045

Table 2: Adimensional numbers for the experiment

2 Objectives

This experiment is a repetition of experiment 18 realized after reducing the leakage under the slope. We expect to access the interference of the leakage in previous experiments by comparing the results of both experiments.

We expect to observe the formation of satellite cyclonic eddies close to the dense water inlet and the appearance of an anti-cyclonic gyre at the surface of the central basin. Moreover, regarding the computed values for R_D and Γ, we expect the dynamics in the central gyre to suffer a noticeable influence from satellite gyres due to the increase in their shedding frequency and intensity when compared to experiments performed with a deeper basin ($h_i \approx 0.6\ m$) or a smaller density difference between the inlet and the ambient water. ($\Delta\rho \approx 10\ kg\ m^{-3}$).

3 Methodology

Data was collected using 3 conductivity probes (cp0, cp1 and cp3), one ADV profiler, one ADV - see Figure 2 - 2 gopro cameras tied to the metal structure on the top of the rotating table and 4 high resolution cameras for PIV analysis. More details about the tank configuration are documented in the file *one_geostrophic_source.dxf*.

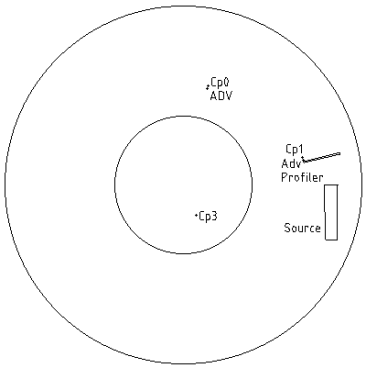

Figure 1: Experiment configuration.

Fluid motion was registered with a laser and high resolution cameras for posterior PIV analysis. The laser was configured to illuminate 12 layers, covering a total height of 24 cm with 2 cm gap between each level - except by the deeper gat which has a height of 4 cm - as detailed at Table 3. This table - along with Figure 2 - also documents an inclination of the laser sheet. The deepest level was located at 13.8 cm from the bottom in the center. The laser started from the higher level and moved downwards in 60s, stopping at each level to allow pictures to be taken. It took 30s to position the laser in the upper layer again and restart the acquisition. Three pictures are taken for each level. The laser rotating motor was powered with 3.00 V.

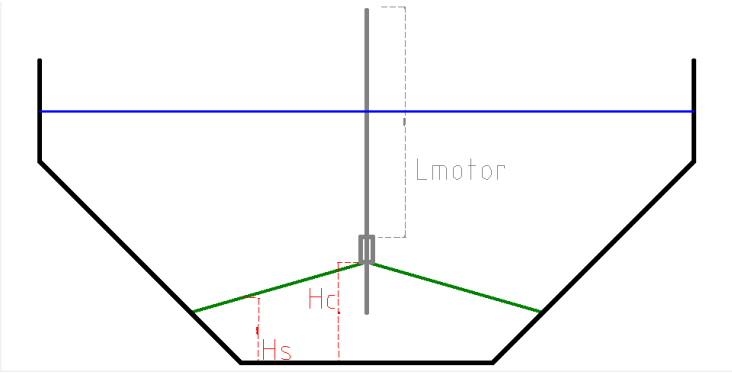

Figure 2: Heights used on Table 3.

h_c (cm)	h_s (cm)	L_{motor} (mm)
13.8	7	1000
15.8	9	960
17.8	11	940
19.8	13	920
21.8	15	900
23.8	17	880
25.8	19	860
27.8	21	840
29.8	23	820
31.8	25	800
33.8	27	780
35.8	29	760

Table 3: Positions used for laser layers

Among the high resolution cameras are 2 PCO, 1 JAI and 1 Nikon D850. The Nikon was positioned pointing to the center of the tank with a 14mm lens in order to cover most of the tank surface. Table 4 display the shooting frequency for each camera. Nikon images were compressed to jpg format in order to decrease dimensions of each image, and thus enable storing more images (5 times more) on the memory card.

Before starting injecting water, the layers were scanned twice in order to register the initial conditions of the fluid.

Camera	Freq (Hz)
PCO 1	1
PCO 2	1
JAI	1
Nikon D850	1

Table 4: Shooting frequency for each camera.

Surface water was removed at a similar rate as dense water was injected. The tank was drained and reffiled during the past night and particles were added to the ambient water. The inlet flow was mixed with particles and having bleach dissolved in the solution before introducing it to the tank in order to prevent the late appearance of organism in the water.

4 Field Observations

Data obtained at the end of the experiment is shown in table 5:

Parameter	unit	value
h_f	m	.402
Duration	min	130

Table 5: Data collected at the end of the experiment.

Density measured at the bottom in the end of the experiment, close to cp3, was 1016.9 $kg\ m^{-3}$.

There was a failure in the aquisition of images, conductivity and probes position data in the end of experiment

5 Discussion and notes for next experiments

Cropex 2018 Grenoble
Daily report: Experiment 24

December 11, 2018

1 Initial conditions

The initial conditions used for the experiment are displayed in table 1.

Parameter	unit	planned value	observed value
Rotation period	s	120	120
Flow rate	$l\ s^{-1}$	0.8	0.8
ρ_{amb}	$kg\ m^{-3}$	1000	999.2
ρ_{bottom}	$kg\ m^{-3}$	1015	1014.5
ρ_{inlet}	$kg\ m^{-3}$	see Figure 3	
h_{bootom}	m	.30	0.162
h_{amb}	m	.30	0.411
h_i	m	.60	0.573
Stratus		2 layer	

Table 1: Initial conditions for the experiment

Table 2 shows the adimensional numbers computed for the experiment:

Rossby number	0.0763944
Rossby radius (R_D)	0.5134974
Burger number (Bu)	0.0513497
Nof	1.2820551
Γ	0.2624045

Table 2: Adimensional numbers for the source

2 Objectives

This experiment was designed to reproduce the mesoscale features observed in the Ionean Sea thermohaline circulation during 2012 winter. We first expect to observe the development of a cyclonic surface circulation due to the injection of an intermediate water. Later, an increase in the inlet water density is expected produce a bottom layer and weaken the cyclonic gyre, eventually reversing its circulation. Afterwards, by ceasing the injection of dense water and restarting the injection of intermediate water, the circulation in expect to weaken again and the intensification of a cyclonic gyre shall be observed.

3 Methodology

3.1 Data gathering

Data was collected using 3 conductivity probes (cp0, cp1 and cp3), one ADV profiler, one ADV - see Figure 2 - 2 gopro cameras tied to the metal structure on the top of the rotating table and 4 high resolution cameras for PIV analysis. More details about the tank configuration are documented in the file *one_geostrophic_source.dxf*.

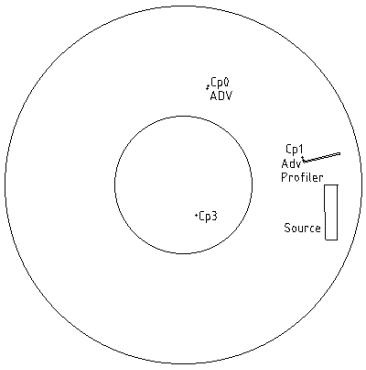

Figure 1: Experiment configuration.

Fluid motion was registered with a laser and high resolution cameras for posterior PIV analysis. The laser was configured to illuminate 12 layers, covering a total height of 44 *cm* with 4 *cm* gap between each level, as detailed at Table 3. This table - along with Figure 2 - also documents an inclination of the laser sheet. The deepest level was located at 13.8 *cm* from the bottom in the center. The laser started from the higher level and moved downwards in 60s, stopping at each level to allow pictures to be taken. It took 30s to position the laser in the upper layer again and restart the acquisition. Three pictures are taken for each level. The laser rotating motor was powered with 3.00 V.

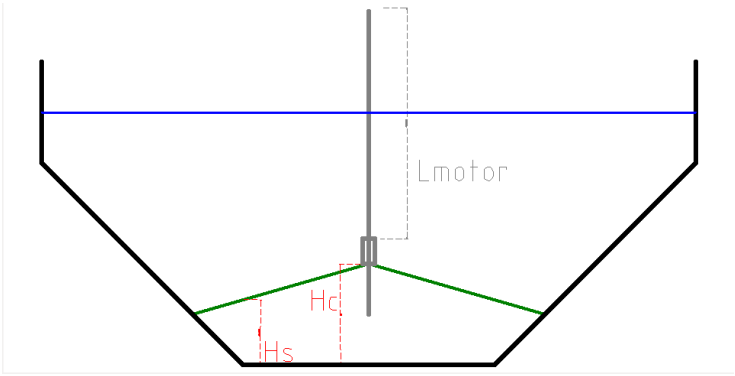

Figure 2: Heights used on Table 3.

h_c (cm)	h_s (cm)	L_{motor} (mm)
13.8	7	1000
17.8	11	960
21.8	15	920
25.8	19	880
29.8	23	840
33.8	27	800
37.8	31	760
41.8	35	720
45.8	39	680
49.8	43	640
53.8	47	600
57.8	51	560

Table 3: Positions used for laser layers

Among the high resolution cameras are 2 PCO, 1 JAI and 1 Nikon D850. The Nikon was positioned pointing to the center of the tank with a 14mm lens in order to cover most of the tank surface. Table 4 display the shooting frequency for each camera. Nikon images were compressed to jpg format in order to decrease dimensions of each image, and thus enable storing more images (5 times more) on the memory card.

Before starting injecting water, the layers were scanned twice in order to register the initial conditions of the fluid.

Camera	Freq (Hz)
PCO 1	1
PCO 2	1
JAI	1
Nikon D850	1

Table 4: Shooting frequency for each camera.

3.2 Tank preparation

A plastic plate was installed above the bottom inlet in order to prevent abrupt vertical currents to break the 2 layer interface. The stratification was then built by first injecting fresh water in the tank with a flow small enough to prevent the development of currents. After the injection was stopped, we waited 2 hour so the fresh water layer would achieve solid body rotation and then started to inject salt water with a density of 1015 $kg\ m^{-}3$. This process was initially done with a very small flow in order to create an interface between the two layers, but after the interface was formed the flow was increased. The system rested for the night until next day in order to achieve solid body rotation.

Particles were add at the free surface on the interval were the laser was moving upwards. Surface water was removed at a similar rate as dense water was injected.

3.3 Inlet density

For the first 90 minutes of experiment water is injected with a density of 1010 $kg\ m^{-3}$. After this period, density of the inlet water is increased to 1020$kg\ m^{-3}$ for more 90 minutes. Finally, the density of the inlet water is reduced again to 1010 $kg\ m^{-3}$ for 60 mintues. The flow rate is always the same.

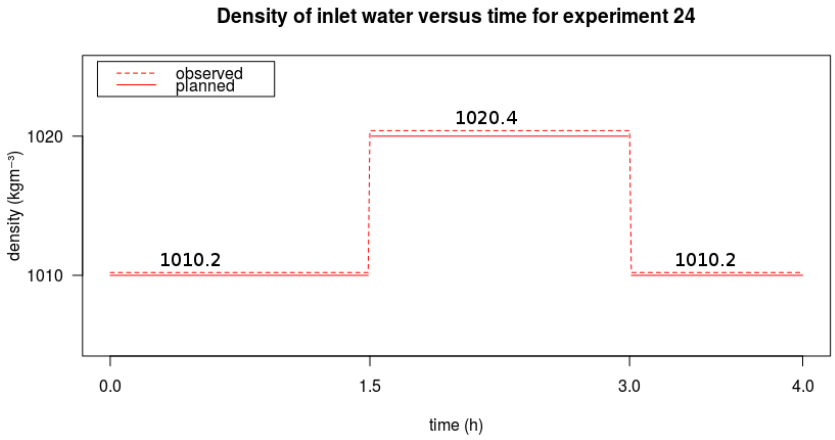

Figure 3: Experiment configuration.

4 Field Observations

Data obtained at the end of the experiment is shown in table 5:

Parameter	unit	value
h_f	m	0.572
Duration	min	242

Table 5: Data collected at the end of the experiment.

Density measured at the bottom in the end of the experiment, close to cp3, was 1016.2 $kg\ m^{-3}$.

5 Discussion and notes for next experiments

The expected cyclonic circulation in the beggining of the experiment was not observed.

Cropex 2018 Grenoble
Daily report: Experiment 25

December 12, 2018

1 Initial conditions

The initial conditions used for the experiment are displayed in table 1.

Parameter	unit	planned value	observed value
Rotation period	s	120	120
Flow rate	$l\ s^{-1}$	see section 3.3	
ρ_{amb}	$kg\ m^{-3}$	1000	999.4
ρ_{bottom}	$kg\ m^{-3}$	1015	1013.6
ρ_{inlet}	$kg\ m^{-3}$	see section 3.3	
h_{bootom}	m	.30	0.201
h_{amb}	m	.30	0.368
h_i	m	.60	0.569
Stratus		2 layer	

Table 1: Initial conditions for the experiment

Table 2 shows the adimensional numbers computed for the experiment:

Rossby number	0.0763944
Rossby radius (R_D)	0.6799067
Burger number (Bu)	0.0679907
Nof	2.2512199
Γ	0.2584045

Table 2: Adimensional numbers for the source

2 Objectives

3 Methodology

3.1 Data gathering

Data was collected using 3 conductivity probes (cp0, cp1 and cp3), one ADV profiler, one ADV - see Figure 2 - 2 gopro cameras tied to the metal structure on the top of the

rotating table and 4 high resolution cameras for PIV analysis. More details about the tank configuration are documented in the file *one_geostrophic_source.dxf*.

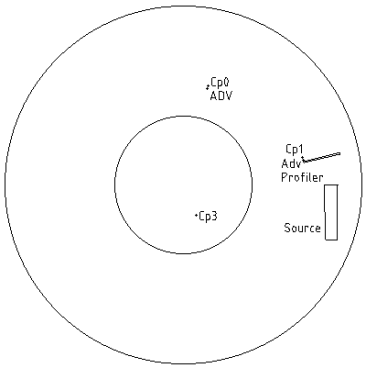

Figure 1: Experiment configuration.

Fluid motion was registered with a laser and high resolution cameras for posterior PIV analysis. The laser was configured to illuminate 12 layers, covering a total height of 44 cm with 4 cm gap between each level, as detailed at Table 3. This table - along with Figure 2 - also documents an inclination of the laser sheet. The deepest level was located at 13.8 cm from the bottom in the center. The laser started from the higher level and moved downwards in 60s, stopping at each level to allow pictures to be taken. It took 30s to position the laser in the upper layer again and restart the acquisition. Three pictures are taken for each level. The laser rotating motor was powered with 3.00 V.

h_c (cm)	h_s (cm)	L_{motor} (mm)
13.8	7	1000
17.8	11	960
21.8	15	920
25.8	19	880
29.8	23	840
33.8	27	800
37.8	31	760
41.8	35	720
45.8	39	680
49.8	43	640
53.8	47	600
57.8	51	560

Table 3: Positions used for laser layers

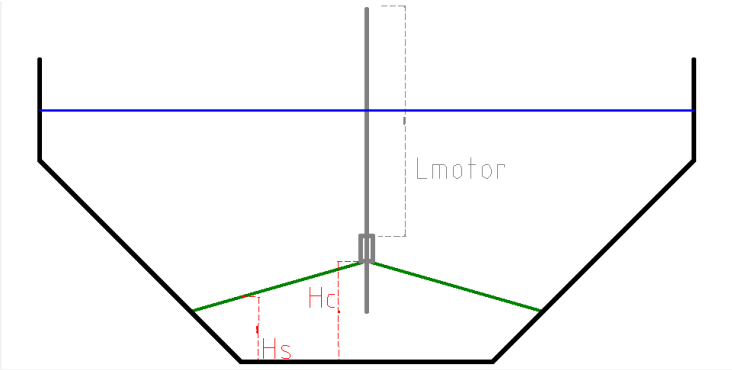

Figure 2: Heights used on Table 3.

Among the high resolution cameras are 2 PCO, 1 JAI and 1 Nikon D850. The Nikon was positioned pointing to the center of the tank with a 14mm lens in order to cover most of the tank surface. Table 4 display the shooting frequency for each camera. Nikon images were compressed to jpg format in order to decrease dimensions of each image, and thus enable storing more images (5 times more) on the memory card.

Before starting injecting water, the layers were scanned twice in order to register the initial conditions of the fluid.

Camera	Freq (Hz)
PCO 1	1
PCO 2	1
JAI	1
Nikon D850	1

Table 4: Shooting frequency for each camera.

3.2 Tank preparation

A plastic plate was installed above the bottom inlet in order to prevent abrupt vertical currents to break the 2 layer interface. The stratification was then built by first injecting fresh water in the tank with a flow small enough to prevent the development of currents. After the injection was stopped, we waited 2 hour so the fresh water layer would achieve solid body rotation and then started to inject salt water with a density of 1015 $kg\ m^{-}3$. This process was initially done with a very small flow in order to create an interface between the two layers, but after the interface was formed the flow was increased. The system rested for the night until next day in order to achieve solid body rotation.

Particles were add at the free surface on the interval were the laser was moving upwards. Surface water was removed at a similar rate as dense water was injected.

3.3 Inlet density

For the first 90 minutes, only the source corresponding to the Adriatic water injects water. After that, the two sources inject water togheter for more 90 minutes.

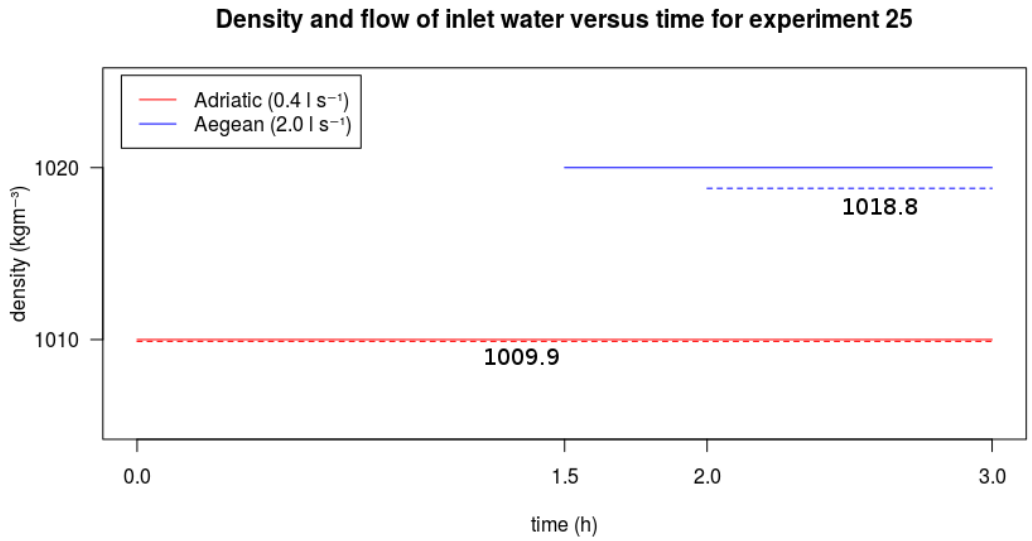

Figure 3: Experiment configuration.

4 Field Observations

There was air exiting from the boarder few minutes after starting the experiment. It creates some perturbations at the surface. At the start of the experiment, the pipe that feeds the Adriatic source was filled with water with a density of 1005 $kg\ m^{-3}$. This water was released in the tank during the first minutes of the experiment, as the water the 1010 $kg\ m^{-3}$ was filling up the tube. The injection of the Aegean water was delayed 30 minutes, as shown in the figure at section 3.3. Data obtained at the end of the experiment is shown in table 5:

Parameter	unit	value
h_f	m	0.568
Duration	min	192

Table 5: Data collected at the end of the experiment.

5 Discussion and notes for next experiments

A cyclonic circulation was observed when injecting intermediate water, followed by a reversal to anticyclonic when injecting bottom water.

Cropex 2018 Grenoble
Daily report: Experiment 26

December 13, 2018

1 Initial conditions

The initial conditions used for the experiment are displayed in table 1.

Parameter	unit	planned value	observed value
Rotation period	s	120	120
Flow rate	$l\ s^{-1}$	0.4	0.4
ρ_{amb}	$kg\ m^{-3}$	1000	999.5
ρ_{bottom}	$kg\ m^{-3}$	1015	1013.5
ρ_{inlet}	$kg\ m^{-3}$	see section 3.3	
h_{bootom}	m	.30	0.221
h_{amb}	m	.30	0.351
h_i	m	.60	0.572
Stratus		2 layer	

Table 1: Initial conditions for the experiment

Table 2 shows the adimensional numbers computed for the experiment:

Rossby number	0.0381972
Rossby radius (R_D)	0.5015804
Burger number (Bu)	0.050158
Nof	2.4474379
Γ	0.2614045

Table 2: Adimensional numbers for the source

2 Objectives

This experiment was designed to reproduce the mesoscale features observed in the Ionean Sea thermohaline circulation during 2012 winter. We first expect to observe the development of a cyclonic surface circulation due to the injection of an intermediate water. Later, an increase in the inlet water density is expected produce a bottom layer and weaken the cyclonic gyre, eventually reversing its circulation. Afterwards, by ceasing the injection of dense water and restarting the injection of intermediate water, the circulation in expect to weaken again and the intensification of a cyclonic gyre shall be observed.

3 Methodology

3.1 Data gathering

Data was collected using 3 conductivity probes (cp0, cp1 and cp3), one ADV profiler, one ADV - see Figure 2 - 2 gopro cameras tied to the metal structure on the top of the rotating table and 4 high resolution cameras for PIV analysis. More details about the tank configuration are documented in the file *one_geostrophic_source.dxf*.

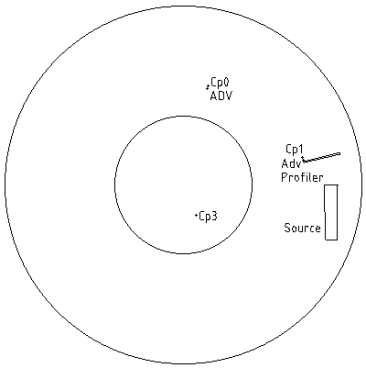

Figure 1: Experiment configuration.

Fluid motion was registered with a laser and high resolution cameras for posterior PIV analysis. The laser was configured to illuminate 12 layers, covering a total height of 44 *cm* with 4 *cm* gap between each level, as detailed at Table 3. This table - along with Figure 2 - also documents an inclination of the laser sheet. The deepest level was located at 13.8 *cm* from the bottom in the center. The laser started from the higher level and moved downwards in 60s, stopping at each level to allow pictures to be taken. It took 30s to position the laser in the upper layer again and restart the acquisition. Three pictures are taken for each level. The laser rotating motor was powered with 3.00 V.

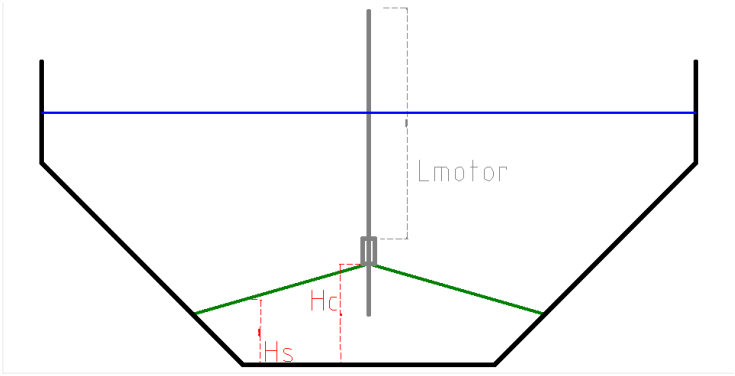

Figure 2: Heights used on Table 3.

h_c (cm)	h_s (cm)	L_{motor} (mm)
13.8	7	1000
17.8	11	960
21.8	15	920
25.8	19	880
29.8	23	840
33.8	27	800
37.8	31	760
41.8	35	720
45.8	39	680
49.8	43	640
53.8	47	600
57.8	51	560

Table 3: Positions used for laser layers

Among the high resolution cameras are 2 PCO, 1 JAI and 1 Nikon D850. The Nikon was positioned pointing to the center of the tank with a 14mm lens in order to cover most of the tank surface. Table 4 display the shooting frequency for each camera. Nikon images were compressed to jpg format in order to decrease dimensions of each image, and thus enable storing more images (5 times more) on the memory card.

Before starting injecting water, the layers were scanned twice in order to register the initial conditions of the fluid.

Camera	Freq (Hz)
PCO 1	1
PCO 2	1
JAI	1
Nikon D850	1

Table 4: Shooting frequency for each camera.

3.2 Tank preparation

A plastic plate was installed above the bottom inlet in order to prevent abrupt vertical currents to break the 2 layer interface. The stratification was then built by first injecting fresh water in the tank with a flow small enough to prevent the development of currents. After the injection was stopped, we waited 2 hour so the fresh water layer would achieve solid body rotation and then started to inject salt water with a density of 1015 $kg\ m^{-}3$. This process was initially done with a very small flow in order to create an interface between the two layers, but after the interface was formed the flow was increased. The system rested for the night until next day in order to achieve solid body rotation.

Particles were add at the free surface on the interval were the laser was moving upwards. Surface water was removed at a similar rate as dense water was injected.

3.3 Inlet density

For the first 90 minutes of experiment water is injected with a density of 1010 $kg\ m^{-3}$. After this period, density of the inlet water is increased to $1020kg\ m^{-3}$ for more 90 minutes. Finally, the density of the inlet water is reduced again to 1010 $kg\ m^{-3}$ for 60 mintues. The flow rate is always the same.

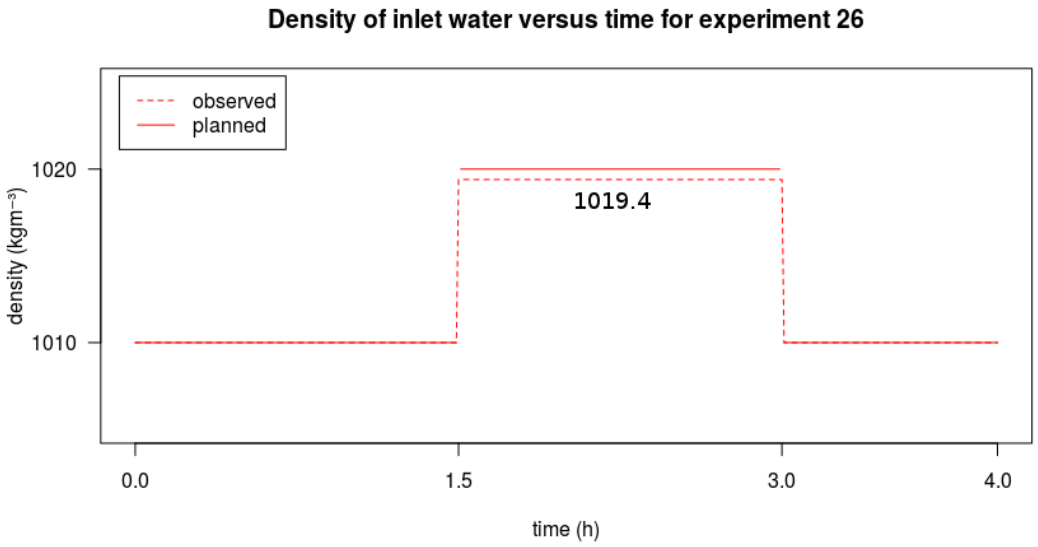

Figure 3: Experiment configuration.

4 Field Observations

Data obtained at the end of the experiment is shown in table 5:

Parameter	unit	value
h_f	m	0.572
Duration	min	253

Table 5: Data collected at the end of the experiment.

Density measured at the bottom in the end of the experiment, close to cp3, was 1016.2 $kg\ m^{-3}$.

The ADV profiler and the Vectrino were initiated only after 173 minutes of experiment.

Cropex 2018 Grenoble
Daily report: Experiment 27

December 14, 2018

1 Initial conditions

The initial conditions used for the experiment are displayed in table 1.

Parameter	unit	planned value	observed value
Rotation period	s	120	120
Flow rate	$l\ s^{-1}$	see section 3.3	
ρ_{amb}	$kg\ m^{-3}$	1000	999.5
ρ_{bottom}	$kg\ m^{-3}$	1015	1014.7
ρ_{inlet}	$kg\ m^{-3}$	see section 3.3	
h_{bootom}	m	.30	0.209
h_{amb}	m	.30	0.36
h_i	m	.60	0.569
Stratus		2 layer	

Table 1: Initial conditions for the experiment

Table 2 shows the adimensional numbers computed for the experiment:

Rossby number	0.0763944
Rossby radius (R_D)	0.5012809
Burger number (Bu)	0.0501281
Nof	1.223719
Γ	0.2584045

Table 2: Adimensional numbers for the source

2 Objectives

3 Methodology

3.1 Data gathering

Data was collected using 3 conductivity probes (cp0, cp1 and cp3), one ADV profiler, one ADV - see Figure 2 - 2 gopro cameras tied to the metal structure on the top of the

rotating table and 4 high resolution cameras for PIV analysis. More details about the tank configuration are documented in the file *one_geostrophic_source.dxf*.

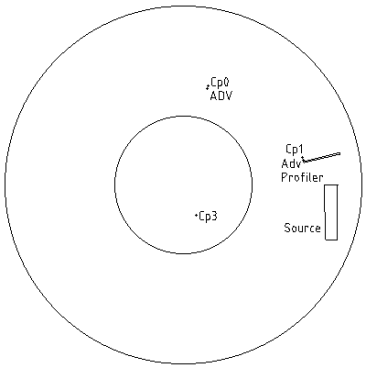

Figure 1: Experiment configuration.

Fluid motion was registered with a laser and high resolution cameras for posterior PIV analysis. The laser was configured to illuminate 12 layers, covering a total height of 44 cm with 4 cm gap between each level, as detailed at Table 3. This table - along with Figure 2 - also documents an inclination of the laser sheet. The deepest level was located at 13.8 cm from the bottom in the center. The laser started from the higher level and moved downwards in 60s, stopping at each level to allow pictures to be taken. It took 30s to position the laser in the upper layer again and restart the acquisition. Three pictures are taken for each level. The laser rotating motor was powered with 3.00 V.

h_c (cm)	h_s (cm)	L_{motor} (mm)
13.8	7	1000
17.8	11	960
21.8	15	920
25.8	19	880
29.8	23	840
33.8	27	800
37.8	31	760
41.8	35	720
45.8	39	680
49.8	43	640
53.8	47	600
57.8	51	560

Table 3: Positions used for laser layers

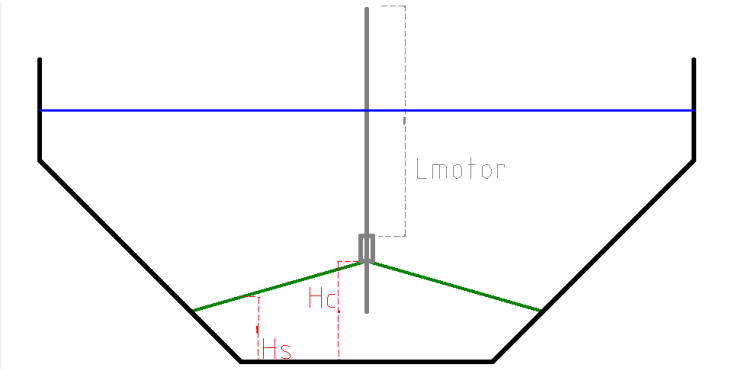

Figure 2: Heights used on Table 3.

Among the high resolution cameras are 2 PCO, 1 JAI and 1 Nikon D850. The Nikon was positioned pointing to the center of the tank with a 14mm lens in order to cover most of the tank surface. Table 4 display the shooting frequency for each camera. Nikon images were compressed to jpg format in order to decrease dimensions of each image, and thus enable storing more images (5 times more) on the memory card.

Before starting injecting water, the layers were scanned twice in order to register the initial conditions of the fluid.

Camera	Freq (Hz)
PCO 1	1
PCO 2	1
JAI	1
Nikon D850	1

Table 4: Shooting frequency for each camera.

3.2 Tank preparation

A plastic plate was installed above the bottom inlet in order to prevent abrupt vertical currents to break the 2 layer interface. The stratification was then built by first injecting fresh water in the tank with a flow small enough to prevent the development of currents. After the injection was stopped, we waited 2 hour so the fresh water layer would achieve solid body rotation and then started to inject salt water with a density of 1015 $kg\ m^{-}3$. This process was initially done with a very small flow in order to create an interface between the two layers, but after the interface was formed the flow was increased. The system rested for the night until next day in order to achieve solid body rotation.

Particles were add at the free surface on the interval were the laser was moving upwards. Surface water was removed at a similar rate as dense water was injected.

3.3 Inlet density

For the first 90 minutes, only the source corresponding to the Adriatic water injects water. After that, the two sources inject water togheter for more 90 minutes.

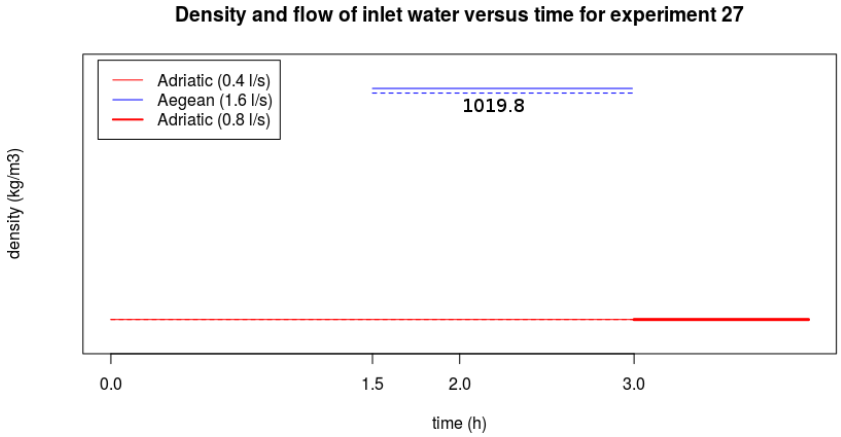

Figure 3: Experiment configuration.

4 Field Observations

There was air exiting from the boarder few minutes after starting the experiment. It creates some perturbations at the surface. At the start of the experiment, the pipe that feeds the Adriatic source was filled with water with a density of 1005 $kg\ m^{-3}$. This water was released in the tank during the first minutes of the experiment, as the water the 1010 $kg\ m^{-3}$ was filling up the tube.

The flow from the Aegean source was less deviated to the border when regarding exp 25 and it was observed to cross half the tank in 5 minutes.
Data obtained at the end of the experiment is shown in table 5:

Parameter	unit	value
h_f	m	0.568
Duration	min	279

Table 5: Data collected at the end of the experiment.

5 Discussion and notes for next experiments

This experiment confirmed the reversal observed at experiment 25 under similar conditions.